INVESTIGATION ON CYCLIC DEGRADATION OF THERMOPHYSICAL PROPERTIES OF PARAFFIN WAX AS A PHASE CHANGE MATERIAL AND THEIR IMPACT ON HEAT STORAGE PERFORMANCE

ANUSUIAH VASU

DOCTOR OF PHILOSOPHY

UNIVERSITI MALAYSIA PAHANG

UNIVERSITI MALAYSIA PAHANG

DECLARATION OF THESIS AND COPYRIGHT

Author's Full Name : ANUSUIAH VASU

Date of Birth : 07 MAY 1968

Title : INVESTIGATION ON CYCLIC DEGRADATION OF THERMOPHYSICAL PROPERTIES OF PARAFFIN WAX AS A PHASE CHANGE MATERIAL AND THEIR IMPACT ON HEAT STORAGE PERFORMANCE

Academic Session : SEMESTER I 2020/2021

I declare that this thesis is classified as:

☐	CONFIDENTIAL	(Contains confidential information under the Official Secret Act 1997)*
☐	RESTRICTED	(Contains restricted information as specified by the organization where research was done)*
☒	OPEN ACCESS	I agree that my thesis to be published as online open access (Full Text)

I acknowledge that Universiti Malaysia Pahang reserves the following rights:

1. The Thesis is the Property of Universiti Malaysia Pahang
2. The Library of Universiti Malaysia Pahang has the right to make copies of the thesis for the purpose of research only.
3. The Library has the right to make copies of the thesis for academic exchange.

Certified by:

V. Anusuiah

(Student's Signature)

680507-75-5026

New IC/Passport Number
Date:1 FEB 2021

(Supervisor's Signature)

Dr. Ftwi Yohaness Hagos

Name of Supervisor
Date: 1 FEB 2021

NOTE : * If the thesis is CONFIDENTIAL or RESTRICTED, please attach a thesis declaration letter

Universiti
Malaysia
PAHANG
Engineering • Technology • Creativity

SUPERVISOR’s DECLARATION

We hereby declare that we have checked this thesis and, in our opinion, this thesis is adequate in terms of scope and quality for the award of the degree of Doctor of Philosophy.

(Supervisor’s Signature)
Full Name : Dr. FTWI YOHANESS HAGOS
Position : SENIOR LECTURER
Date : 1 FEB 2021

(Co-supervisor’s Signature)
Full Name : Ts. Dr. MUHAMAD MAT NOOR
Position : SENIOR LECTURER
Date : 01 FEB 2021

Universiti
Malaysia
PAHANG
Engineering • Technology • Creativity

STUDENT’S DECLARATION

I hereby declare that the work in this thesis is based on my original work except for quotations and citations which have been duly acknowledged. I also declare that it has not been previously or concurrently submitted for any other degree at Universiti Malaysia Pahang or any other institutions.

V. Anusuiah
____
(Student’s Signature)

Full Name : ANUSUIAH VASU
ID Number : PMM 16007
Date : 1 FEB 2021

INVESTIGATION ON CYCLIC DEGRADATION OF THERMOPHYSICAL PROPERTIES OF PARAFFIN WAX AS A PHASE CHANGE MATERIAL AND THEIR IMPACT ON HEAT STORAGE PERFORMANCE

ANUSUIAH VASU

Thesis submitted in fulfillment of the requirements
for the award of the degree of
Doctor of Philosophy

College of Engineering
UNIVERSITI MALAYSIA PAHANG

FEBRUARY 2021

ACKNOWLEDGEMENTS

With profound appreciation and love, I would like to extend my heartfelt gratitude to a few among many who have helped make my dream and ambition come true.

First and foremost, my greatest appreciation goes to my supervisor Dr. Ftwi Yohaness Hagos. He has equipped me with valuable guidance, encouragement and advice throughout my time as his student. I am fortunate to have such a caring and wise supervisor.

I would also like to extend my gratitude to Ts. Dr. Mohamad Mat Noor, my co-supervisor, who has continuously supported and encouraged me to complete my study.

Next, my genuine thanks go to my friend, Muhammad Mukhtar Bin Noor Awalludin, who has given me a great deal of moral support throughout my PhD journey and has always encouraged me to get successfully complete this thesis.

I also wish to express my utmost gratitude to the backbone of my success, Vasu, my beloved husband. He has been continuously supporting, encouraging and extremely patient with me in order to make my childhood dream of completing my PhD come true. My wonderful daughters; Priyangah, Aisswarya and Kaviyahsri have tirelessly given me heartening words, and were always ready to help when I needed them. For that, I am so proud and thankful to have such understanding family members.

A quote by George Shinn goes “There is no such thing as a self – made man. You will reach your goals only with the help of others”. My success would not have been possible without the support of Mr. Nizam bin Abdullah from the Thermal Lab. He has been very supportive of my research work. I would also like to express my special thanks to the Faculty of Industrial Science & Technology, especially Mr. Khairul Affendi bin Yusof, the lab technician as well as Center of Excellence for Advanced Research in Fluid for helping me to process my samples.

I believe that the grace and prayers of my late parents, S.Venkitasamy and V.Subbulakshmi, are also prominent factors that helped me complete my study. Their eternal love has been my pillar of strength in giving me the courage and self- confidence to pursue my dreams of studying PhD after so many years. I believe their prayers are always with me.

Lastly, I would like to express my sincere appreciation to Universiti Malaysia Pahang and the Faculty of Mechanical Engineering now College of Engineering for financial assistance through the Doctoral Research Scheme.

ABSTRACT

Thermo-physical property study of the Phase Change Material (PCM) is necessary to build an efficient latent heat thermal energy storage system (LHTESS). The stability of thermophysical property due to repeated thermal cycling is an essential factor that has to be studied to find a promising latent heat storage material with a long-duration lifetime. Void formation during the solidification process in thermal cycling is an unwanted property in the PCM. This study concentrates on the void formation due to repeated thermal cycling and its impact on thermo-physical property degradation of paraffin wax. Paraffin wax with the melting temperature in the range of 58^{o}C to 62^{o}C is selected as PCM. Whereas Al_2O_3 and CuO nanoparticles of 20-40 nm size are selected as nanoparticle additive for this study. The nano-PCM composite and hybrid nano-PCM composite samples are prepared by mixing 5 wt% of Al_2O_3, 5 wt% of CuO and 2.5 wt% Al_2O_3+2.5 wt% CuO nanoparticles with paraffin wax by bottom heating and natural cooling at ambient temperature. Samples are made to undergo 1, 50, 100, 150, and 200 thermal cycles. Morphology of the samples is studied using a Scanning Electron Microscope (SEM). The thermal properties are analysed by Differential Scanning Calorimeter (DSC). Thermal Gravimetric Analyser (TGA) is used to analyse the thermal stability and reliability. Thermal conductivity is measured using KD2 Pro thermal properties analyser. Viscosity and density is also measured using Rheometer Kinexus Lab+ and Archimedes principle to observe the impact of void formation during solidification shrinkage. Void formation in samples is quantified with help of ImageJ software. Results have revealed that nanoparticles addition has reduced the void variation by 16.8% in the hybrid-PCM composite (2.5 wt% Al_2O_3+2.5 wt% Cuo-PCM) after 200 thermal cycles. The void ratio is fluctuated with the thermal cycle in all the samples and has an inverse relation with all the thermophysical properties measured. The percentage of void ratio variation after C200 compared to C1 in hybrid-PCM is -16.7%,which is the least value calculated among all the samples. CuO nanoparticle addition has shown 23.3%, 23.2% and 22.25% increment in latent heat of melting, solidification and peak degradation temperature, respectively. Hybrid–PCM has shown an improvement in thermal conductivity, viscosity and density by 5.43%, 9.58% and 4.07%, respectively. Peak degradation temperature value has increased by 13.4%, 22.25% and 6.43% compared to PCM by addition of Al_2O_3, CuO and hybrid nanoparticles, respectively. Compared to other samples, hybrid-PCM is more stable and has shown consistency in all the thermophysical properties throughout all the thermal cycles. Paraffin wax with 2.5 wt% Al_2O_3+2.5 wt% CuO nanoparticles is found to be a better energy storage material in LHTESS. An addition of surfactant is recommended to improve the stability of nanoparticle distribution in nanoparticle-PCM composites. Thermophysical property improvement and stability achievement in paraffin wax by the incorporation of 2.5 wt% Al_2O_3+2.5 wt% CuO nanoparticles have contributed to eliminating the limitations in the life span of paraffin wax usage in thermal energy storage applications.

ABSTRAK

Kajian sifat termo-fizikal Bahan Perubahan Fasa atau dikenali sebagai *Phase Change Material* (PCM) diperlukan bagi membina sistem penyimpanan tenaga haba pendam yang baik. Kestabilan sifat termofizik hasil kitaran termal yang berulang adalah faktor penting yang perlu dikaji untuk mendapatkan bahan penyimpan haba terpendam yang menjanjikan jangka hayat yang panjang. Pembentukan rompongan semasa proses pemejalan dalam kitaran termal adalah sifat yang tidak diingini dalam PCM. Kajian ini tertumpu pada pembentukan rompongan kerana kitaran termal yang berulang dan kesannya adalah pada kemerosotan sifat termo-fizikal lilin parafin. Lilin parafin dengan suhu lebur dalam lingkungan 58^{o}C hingga 62^{o}C dipilih sebagai PCM. Manakala partikel nano Al_2O_3 dan CuO dengan ukuran 20-40 nm dipilih sebagai bahan tambahan partikel nano untuk kajian ini. Sampel komposit nano-PCM dan komposit nano-PCM hibrid disiapkan dengan cara mencampurkan 5 wt% Al_2O_3, 5 wt% CuO dan 2.5 wt% Al_2O_3 + 2.5 wt% CuO partikel nano bersama lilin parafin dengan teknik pemanasan dari bawah dan dibiarkan sejuk secara semula jadi di suhu persekitaran. Sampel disiapkan bagi menjalani 1, 50, 100, 150, dan 200 kitaran termal. Morfologi sampel dikaji dengan menggunakan *Scanning Electron Microscope* (SEM). Sifat termal dianalisis dengan mengunakan *Differential Scanning Calorimeter* (DSC). *Thermal Gravimetric Analyzer* (TGA) telah digunakan bagi menganalisis kestabilan termal dan tahap kebolehpercayaan. Kekonduksian termal diukur dengan menggunakan penganalisis sifat termal KD2 Pro. Kelikatan dan ketumpatan juga telah diukur menggunakan prinsip Rheometer Kinexus Lab+ dan Archimedes untuk memerhatikan kesan pembentukan rompongan semasa pengecutan pemejalan. Pembentukan rompongan dalam sampel dinilai dengan bantuan perisian ImageJ. Hasil kajian mendapati penambahan partikel nano mengurangkan variasi rompongan sebanyak 16.8% pada komposit hibrid-PCM setelah 200 kitaran termal. Nisbah rompongan berubah-ubah dengan kitaran termal pada semua sampel dan mempunyai hubungan terbalik dengan semua sifat termofisik yang diukur. Peratusan variasi nisbah rompongan selepas C200 berbanding C1 di hibrid-PCM adalah -16.7%, yang merupakan nilai paling sedikit berbanding semua sampel. Penambahan nanopartikel CuO masing-masing telah menunjukkan kenaikan masing-masing sebanyak 23.3%, 23.2% dan 22.25% dalam haba laten lebur, pemejalan dan punck suhu penurunan. Hibrid – PCM telah menunjukkan peningkatan kekonduksian termal, kelikatan dan ketumpatan sebanyak 5.43%, 9.58% dan 4.07%. Nilai suhu degradasi puncak telah meningkat sebanyak 13.4%, 22.25% dan 6.43% berbanding PCM dengan penambahan nanopartikel Al_2O_3, CuO dan hibrid. Berbanding dengan sampel lain, PCM hibrid lebih stabil dan telah menunjukkan konsistensi dalam semua sifat termofizik sepanjang semua kitaran termal. Hibrid-PCM didapati merupakan bahan simpanan tenaga yang lebih baik dalam LHTESS. Penambahan surfaktan adalah disyorkan bagi meningkatkan kestabilan taburan partikel nano dalam komposit partikel nano-PCM. Peningkatan dan kestabilan sifat termofisik dalam lilin parafin dengan gabungan 2.5 wt% Al_2O_3 + 2.5 wt% partikel nano CuO telah mendapati menyumbang kepada mengatasi masalah jangka masa terhad penggunaan lilin parafin dalam aplikasi penyimpanan tenaga termal.

TABLE OF CONTENT

LIST OF TABLES

LIST OF FIGURES

LIST OF SYMBOLS

Ag	Argentum (Silver)
Al_2O_3	Aluminium oxide
$CaCO_3$	Calcium carbonate
CaO	Calcium oxide
$Ca(OH)_2$	Calcium hydroxide
$CaSO_4$	Calcium sulphite
CO_2	Carbon dioxide
Cu	Copper
CuO	Copper oxide
$C_4H_{10}O_2$	Butanediol
C_6H_{12}	Cyclohexane
$C_{18}H_{38}$	Octadecane
$FeCO_3$	Iron carbonate
FeO	Iron oxide
$Fe(OH)_2$	Iron II hydroxide
Fe_2O_3	Iron II oxide
Fe_3O_4	Iron III oxide
H_2O	Water
$MgSO_4$	Magnesium sulphate
n	Number of carbon atoms
NaOH	Sodium hydroxide
NO_2	Nitrogen dioxide
SiO_2	Silicon oxide
TiO_2	Titanium dioxide
2-D	2 Dimensional
ΔHm	Latent heat capacity of melting
ΔHs	Latent heat capacity of solidification
ºC	Degree celsius
°C/min	Degree celsius per minute

LIST OF ABBREVIATIONS

AD	“anno domini” – A latin phrase for “in the year of lord Jesus”
Al_2O_3+CuO-PCM	Aluminium oxide and copper oxide with phase change material
Al_2O_3-PCM	Aluminium oxide with phase change material
ASTM	American society for testing and material
BSED	Bla$_c$k scattered electron detector
C	cycles
CA	Capric acid
CA/LA	Capric acid/ lauric acid
CA/MA	Capric acid/myristic acid
CA/PA	Capric acid/ palmitic acid
CA/SA	Capric acid/ steraic acid
CB	Carbon black
C/C	Carbon/ carbon
CNT	Carbon nano tubes
C-H bond	Carbon- hydrogen bond
C_p	Specific heat of storage material
CPCM	Composite-PCM
C_s	Void ratio swing
CSP	Concentrated solar power
CuO-PCM	Copper oxide with phase change material
C1	After 1 thermal cycle
C50	After 50 thermal cycles
C100	After 100 thermal cycles
C150	After 150 thermal cycles
C200	After 200 thermal Cycles
C1 Al_2O_3-PCM	Al_2O_3-PCM after 1 thermal cycle
C50 Al_2O_3-PCM	Al_2O_3-PCM after 50 thermal cycles
C100 Al_2O_3-PCM	Al_2O_3-PCM after 100 thermal cycles
C150 Al_2O_3-PCM	Al_2O_3-PCM after 150 thermal cycles
C200 Al_2O_3-PCM	Al_2O_3-PCM after 200 thermal cycles
C1 Al_2O_3+CuO-PCM	Al_2O_3+CuO-PCM after 1 thermal cycle

C50 Al_2O_3+CuO-PCM	Al_2O_3+CuO-PCM after 50 thermal cycles
C100 Al_2O_3+CuO-PCM	Al_2O_3+CuO-PCM after 100 thermal cycles
C150 Al_2O_3+CuO-PCM	Al_2O_3+CuO-PCM after 150 thermal cycles
C200 Al_2O_3+CuO-PCM	Al_2O_3+CuO-PCM after 200 thermal cycles
C1-CuO	CuO-PCM after 1 thermal cycle
C50-CuO	CuO-PCM after 50 thermal cycles
C100-CuO	CuO-PCM after 100 thermal cycles
C150-CuO	CuO-PCM after 150 thermal cycles
C200-CuO	CuO-PCM after 200 thermal cycles
C1 PCM	Paraffin wax after 1 thermal cycle
C50 PCM	Paraffin wax after 50 thermal cycles
C100 PCM	Paraffin wax after f 100 thermal cycles
C150 PCM	Paraffin wax after 150 thermal cycles
C200 PCM	Paraffin wax after 200 thermal cycles
DCM	Di chloro methane
DSC	Differential scanning calorimeter
DTGA	Differential thermogravimetric analysis
EG	Extended graphite
EP	Extended perlite
ES	Energy storage
ESEM	Environmental scanning electron microscope
FESEM	Field emission scanning electron microscope
FSPCM	Form-stable phase change materials
FTIR	Fourier-transform infrared spectroscopy
GNPs	Graphite nano- platelets
Gnp	Graphite nano-particles
HDPE	High-density polyethylene
HTF	Heat transfer fluid
IRS	Infrared spectroscopy
KD2 Pro	Thermal property analyser
KOH	Potassium hydroxide
LA	Lauric acid
LDPE	Low-density polyethylene

LHS	Latent heat storage
LHTES	Latent heat thermal energy storage
LHTESS	Latent heat thermal energy storage system
MA	Myristic acid
MA/HDPE	Myristic acid/high-density polyethylene
MA/PA	Myristic acid/ palmitic acid
MCC	Microscale combustion calorimeter
MEPCM	Microencapsulated PCM
MMA	Methyl methacrylate
NAO	Nano aluminium oxide
NEPCM	N-Eicosane phase change materials
NMR	Nuclear magnetic resonance
NG	Nano graphite
np	Non-paraffin
p	paraffin
PA	Palmitic acid
PCM	Phase change materials
PE	Polyethylene
PEG	Polyethene glycol
PE/Al	Polyethylene/aluminium
PE/B	Polyethylene/boron
P/PE	Paraffin/polyethylene
P/PE/Al	Paraffin/polyethylene/aluminum
P/PE/B	Paraffin/polyethylene/boron
PET	Polyethylene terephthalate
REN21	Renewable energy policy network for the 21st century
rGO	Reduced graphene oxide
SA	Stearic acid
SBPWM	Simple boost pulse width modulation
SDG	Sustainable development goals
SDS	Sodium dodecyl sulphate
SHS	Sensible heat storage
SHTES	Sensible heat energy storage

SS	Sodium stearate
SSL	Sodium stearoy lactylate
TCES	Thermochemical energy storage
TCI	Topological crystalline insulator
TCS	Thermochemical heat storage
TEM	Transmission electron microscopy
TES	Thermal energy storage
TFA	Trifluro acetic acid
TGA	Thermal gravimetric analysis
TGA/DSC	Thermal gravimetric analysis / differential scanning calorimeter
T_m	Melting temperatures
T-max	Maximum decomposition temperature
T_{offM}	Offset temperature of melting
T_{offS}	Offset temperature of solidification
T_{onM}	Onset temperature of melting
T_{onS}	Onset temperature of solidification
TOS	Thermo-optical sensing
TPA	Thermal properties analyser
T-peak	Peak temperature
T_s	Solidification temperatures
TWy/Year	Terawatt year per year
USA	United States of America
vol. %	Volume percentage
Wt%	Weight percentage
XGNP	Graphene nanoplatelets
XRD	X- ray powder diffraction
ZSI	Z source inverter

CHAPTER 1

INTRODUCTION

1.1 Background

The world is working on its 2030 agenda for Sustainable Development Goals (SDGs). These goals can be achieved by social, economic and environmental fields. Out of 17 SDGs, five goals namely affordable clean energy (SDG7), responsible consumption and production (SDG12), climate action (SDG13), life below water (SDG14) and life on land (SDG15) are directly related to environmental issues. Whereas, three goals, namely zero hunger (SDG2), good health and wellbeing (SDG3) and decent work and economic growth (SDG8) is indirectly targeting the same environment-related problems (Economic Planning Unit, 2017). As so, more than 50% of SDGs are focused on energy crises and environmental issues.

Then again, the water, food and energy nexus also explains how these three are interrelated and take part in energy and environmental issues. Food production and water processing requires a substantial amount of energy (Reinhard et al., 2017). As result, this leads to unlimited usage of fossil fuels. Energy production to satisfy the needs of the growing population leads to greenhouse gas emissions and unwanted climate change. Due to the worldwide embracement of technology, more than one billion people have access to a continuous supply of electricity. Even though fossil fuel plays a vital role in the global energy mix, new technology development and renewable energy production can reduce the rapid depletion of fossil fuels (Economic Planning Unit, 2017). All the negative impacts caused by energy-related environmental could be alleviated by using renewable energy sources. World Energy Council has predicted that by 2060, the primary energy share in the energy mix will fall to 70%. Clean energy is the primary resource that requires development in the energy transition plan to fill the gap in the global energy mix (World Energy Council, 2018).

Solar energy is abundantly available heat energy that can be utilized to solve the current energy-related problems. Moreover, it is clean and free, but it is necessary to store the heat energy for future usage because of its intermittent nature. Systems that could store energy in the form of heat is called a Thermal Energy Storage System (TESS). Thermal Energy Storage (TES) is mainly classified into Sensible Heat Thermal Energy Storage (SHTES) and Latent Heat Thermal Energy Storage (LHTES). Among the two TES, LHTES using Phase Change Materials (PCM) can store a large amount of heat energy in a relatively small volume. PCMs are classified into organic, inorganic and eutectic. Organic PCMs, especially paraffin wax, plays a vital role to fill the gap between resource availability and energy demand. Paraffin wax has a wide range of applications where the heat energy is to be stored to be later utilised such as heating and cooling due to its wide range of melting temperature and high latent heat capacity. Even though PCMs have high energy density and the capacity to store more heat energy even for small temperature changes, they have poor thermal conductivity. Most of the research has concentrated on improving the structure and shape of the collectors and storage containers and adding nanomaterials with PCM to enhance the thermal conductivity of latent heat storage materials without compromising energy density (Agyenim et al., 2010; Cabeza et al., 2011; Khan et al., 2016; G. Li, 2015; Y. Lin et al., 2018; M. Liu et al., 2012)

Thermophysical properties of PCM such as latent heat capacity, thermal conductivity, density, viscosity and thermal stability are among the factors which decide TES performance. Furthermore, performance of TESS depends on energy loading and unloading time. Thus,the rate of loading and unloading of heat energy is mainly related to thermal conductivity of the material. Thermal conductivity of PCM could be improved by addition of nanomaterials (Kibria et al., 2015). Economic feasibility and thermal performance depend on the lifetime of thermophysical properties of storage materials. These thermophysical properties degrade due to dehydration or decomposition. This degradation takes place due to repeated heating and cooling (A. Sharma et al., 2002). Thus, thermophysical property studies and its deterioration due to repeated usage are equally essential to improve performance of the thermal energy storage system (TESS). Various studies concentrate on cyclic degradation of thermal stability and reliability of PCMs (Long & Jiankai, 2017; Mengjie et al., 2017; Rathod & Banerjee, 2013). During solidification shrinkage, voids are formed. These voids formation and growth have an impact on the thermophysical properties of PCM. However, few works have analysed thermophysical property degradation. Similarly, there is limited research that relates the void formation during solidification process in PCM and its impact on cyclic degradation of the thermophysical property.

Research works on LHTESS and SDGs are continuously done to address the greenhouse gases emission, environmental changes and need for thermal energy storage. This awareness encourages researchers to improve the performance of the material used in the TES after many cycles. Observing the void formation in paraffin wax after many thermal cycles and analysing the thermophysical property degradation due to repeated usage is an emerging topic to confirm its lifetime usage. This study also investigates the improvements in thermophysical properties of paraffin wax by adding nanomaterials.

1.2 Problem statement

Thermophysical properties of phase change materials (PCMs) and their thermal stability throughout their lifetime is vital to build efficient latent heat storage systems. Repeated heat loading and unloading (thermal cycle) of PCM several times result in degradation of thermophysical properties. Economic feasibility and long-term usage with high efficiency are the two main factors that depend on the stability of the thermophysical property of storage materials used in LHTESS. Void formation due to solidification shrinkage has a negative effect on the thermophysical properties of PCM. Thermophysical properties of many organic and inorganic PCMs are studied after many accelerated thermal cycles and additives are added to improve it but those studies have not concentrated on void formation. Degradation of thermophysical property due to repeated thermal cycling in paraffin wax and means to improve ithas not beenextensively studied. Nanomaterials are used by researchers to improve the thermal conductivity and thermal stability of PCM. However, those works did not focus on the effect of nanomaterials in the formation of voids and the degradation of thermophysical properties. Hence,, thermophysical property degradation due to void formation studies in paraffin wax and the effect of nanoparticle incorporation with paraffin wax in the void formation and thermophysical property stability are missing in the literature. Hence, that is the research gap found during the literature review.

1.3 Research objectives

The main objective of this research is to investigate the thermophysical property degradation in PCM due to heat loading and unloading for repeated cycles and its effect on thermal energy storage performance. The sub-objectives are:

1. To study the thermophysical property degradation due to repeated melting and solidification of PCM

2. To analyse the impact of thermophysical property degradation on the performance of thermal energy storage and

3. To enhance the thermal storage performance of base PCM by incorporation of nanoparticle

1.4 Scope of work

The scopes of this research are as stated below:

1. PCM, which is commonly used by researchers, namely paraffin wax with melting temperature in the range of 58-62°C and-with 99% purity, is selected

2. Commercially available and economically cheaper nanoparticles namely copper oxide (CuO) and aluminium oxide (Al_2O_3) are used in this research work

3. Changes in the thermophysical property of PCM–nanoparticle composites namely 5wt% Al_2O_3–PCM, 5wt% CuO-PCM, 2.5wt% Al_2O_3 + 2.5wt% CuO-PCM composites are observed after several charging/ discharging cycles

4. Thermophysical property of PCM and nanoparticle-PCM composites are analysed after 1, 50, 100, 150 and 200 thermal cycles

1.5 Significance of the study

Heat energy collection and storage can be improved by TES system. Among various TES systems, LHTES system using PCM has promising potential for high-performance heat energy storage. Among all the PCMs, organic PCM especially paraffin wax has high energy storing density. Many researchers have reviewed studies related to the thermophysical property of paraffin wax and other organic PCMs. Research has revealed that thermophysical property study is necessary to improve the performance of LHTESS. Void formation due to solidification shrinkage and distribution have an impact on the thermophysical property of energy storage material. Reduced thermal conductivity of paraffin wax could be improved by adding nano-additives. Repeated thermal cycling in Paraffin wax and other organic PCM results in significant thermophysical property changes.

There are limited studies focusing on thermophysical property degradation study in paraffin wax due to repeated usage in literature. Some studies concentrated on accelerated thermal cycling of paraffin wax. However, degradation in thermal conductivity and thermophysical properties based on void formation are yet to be studied. Hence, this work aims to investigate the thermophysical property degradation due to repeated thermal cycling and attempt to enhance the properties using nano-additives.

1.6 Thesis outline

This thesis consists of five chapters. including introduction, literature review, methodology, results and discussions and conclusions and recommendations. Chapter1 provides the background, problem statements, objectives and scope of the work, including motivation for this research work. Chapter 2 reviews the importance of TES and types of phase change materials. Recent research in enhancement techniques used to improve the thermo-physical property, void ratio, stability and reliability of PCM and nanoparticle-PCM composites are discussed. Chapter 3 explains the methodology to study the morphology of inner surface, thermal stability and reliability, thermal conductivity, viscosity, the density of paraffin wax and nanoparticle- paraffin wax composites (5wt% CuO-PCM, 5wt% Al_2O_3-PCM and 2.5wt% CuO + 2.5wt% Al_2O_3-PCM). This chapter includes methods used to analyse the raw results obtained. This study records the changes/ degradation in thermophysical and other properties mentioned above after many thermal cycles. In Chapter 4, collected data from experimental work is analysed in detail. Material characterisation of PCM and nanoparticle-PCM composites are done in the laboratory. The degradation of thermophysical property based on void formation and its impact on the efficiency of TES is discussed. Results are then compared with the work of other researchers. Chapter 5 reassesses the aim and objectives and briefs the research methods and results. Finally, this chapter concludes and shows the available opportunities for future research work.

CHAPTER 2

LITERATURE REVIEW

This chapter is focused on the necessity and types of energy storage systems in particular to LHTESS. Recent developments in techniques adopted in the enhancement of material property used in LHTESS are focused. A careful review of the application of paraffin wax in various fields and its importance is done. Drawbacks and methods followed by researchers to improve its performance are also carefully reviewed. Poor conductivity, instability at a higher temperature, degradation in thermo-physical properties due to repeated usage are the main problem faced by the paraffin wax users in LHTESS. Studies that investigate the degradation of thermophysical properties due to repeated thermal cycling are discussed. Various techniques adopted by researchers to improve the thermophysical properties are also given importance in this discussion.

2.1 Energy sources

Like food, cloth and shelter, energy is also one of the basic needs of humankind. As time passes on, humans need more power to help with their survival needs such as cooking, hunting and transportation. So, they have learned to use other forms of energy like wind and water. Primitive humans, either directly or indirectly, have used only renewable energy sources. After the industrial revolution, people have started using fossil fuels (coal, natural gas and petroleum) to satisfy their energy needs in domestic, agriculture and transportation fields. The two broad categories of available energy resources are non-renewable energy sources (fossil fuels) and renewable energy sources. Renewable energy sources include nuclear fission and fusion, hydropower, wind power, solar energy, biogas, tidal, geothermal energy and ocean thermal energy (Behl et al., 2010). According to Renewable Energy Policy Network for the 21st Century (REN21), it is evident that non-renewable energy sources are depleting. Furthermore, their usage pollutes the atmosphere by emitting CO_2 and NO_2, leads to the greenhouse effect (Zoundi, 2016). So, the world needs to find an alternative source of energy for future use and to slow down the depletion rate of fossil fuels (Alper & Oguz, 2016). Figure 2.1 clearly shows the depletion in the consumption rate of fossil fuels and the growing demand for renewable energy sources as time goes. More than half of the energy needs of the world is going to be satisfied through renewable energy sources by the year 2100.

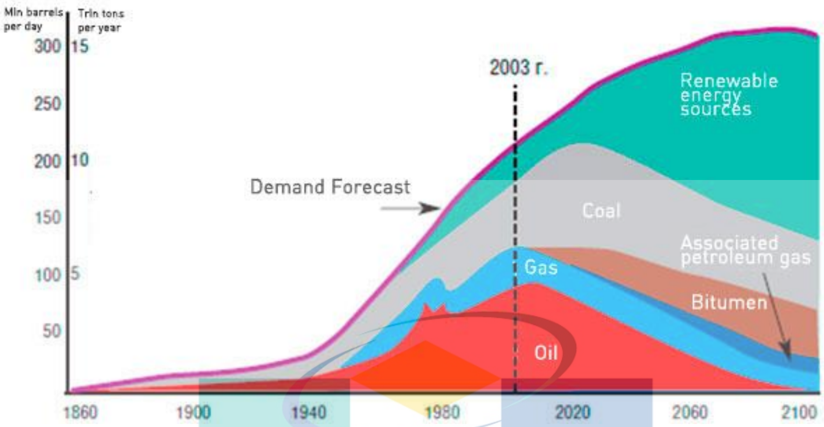

Figure 2.1 Forecast of world energy consumption

Source: Russia's energy industry. Problems and prospects. Nauka. – Moscow, (2006), Likhachev & Vladimir Likhachev, (2012)

Solar energy is a vast, clean and freely available renewable energy source. The amount of solar radiation that falls on a surface per unit area and per unit time is known as insolation or irradiance. According to the World Energy Council, solar irradiation on the earth surface per annum is approximately equal to 170 W/m^2. If this amount of irradiation is integrated throughout the year, then it results in 5.4 G J/m^2 on the ground. This energy collected per m^2 is approximately equal to energy extracted from one barrel of oil, 140 m^3 of natural gas, or 200 kg of coal. Energy from solar radiation can satisfy all the energy needs on the earth continuously, whether directly or indirectly (World Energy Council, 2018). However, solar flux changes daily and seasonally. Solar energy is available only in the day time, but, there is a necessity to use it in the night time also. This unavailability creates a gap between the waste heat energy availability and utility period. So, it is necessary to find a suitable way to store solar energy in an efficient manner.

From Table 2.1, it is clear that solar energy utilization is lesser than all the renewable energy sources listed except for geothermal energy source. The global potential of solar energy is high compared to other listed renewable energy sources. So, finding an efficient way of using solar energy could help solve many energy-related problems.

Table 2.1 The global energy potential and their current utilization of some renewable energy resources

Renewable Energy sources	**Global Potent (TWy/Year)**	**Global utilizati (TWy/Year)**	**Challenges**
Solar energy	23,000	0.0385	intermittent, high cost of production
Wind	25–70	0.0624	intermittent, high cost of production
Ocean Thermal Energy Conversion (OTEC) and Tides	3–11	1.248×10^{-4}	high initial cost, a few locations for installation
Biomass	2–6	1.9744	high cost of production, inefficient, requires more land
Hydro	3–4	0.608	high initial cost,
Geothermal	0.3–2	0.0176	reliability of supply

Source: Kukreja, (2009); Shahan, (2014)

2.2 Energy storage

Developing energy storage methods and finding a new energy source has equal importance. The challenge only starts when storing energy in a suitable form and converting it to the required form. Storing energy reduces wastage of various available energy sources that can be used when needed. There are several methods of Energy Storage (ES) systems available for, example mechanical, chemical, biological, hydrogen, and magnetic and thermal energy storage. Energy storage is possible using hydrogen as well. Even though there are many types of ES systems, they are limited by their cost, the volume of storage, low density and limited efficiency (A. Sharma et al., 2009). This world needs a low-cost and environmental-friendly abundant source with comfortable storage facilities. In solar thermal energy utilization, the most common energy storage system is the Thermal Energy Storage (TES) system which collects the excess heat energy during sunshine hours and stores it for off time usage.

2.3 Thermal energy storage system (TES)

TES has the potential to solve problems related to energy issues in the world. It is categorized into three groups, namely sensible heat storage (SHS), latent heat storage (LHS) and thermos-chemical heat storage (TCS) (S. A. Mohamed et al., 2016). The basic requirements of TES materials are namely high energy density, good thermal conductivity, good heat diffusivity, stable chemical properties, non-toxic, non-corrosive, long term charging and discharging without physical/chemical property degradation, the capability to recycle, easy handling, compatible with the container, easy manufacturing with cost-effectiveness and supporting to the green environment (Diaz, 2016).

2.3.1 Sensible heat thermal energy storage (SHTES)

In a sensible heat storage system, energy can be stored by changing the temperature of storage material. Specific heat capacity, mass and change in temperature of the storage material plays important roles to build an efficient storage system. Heat stored in the material is expressed in Equation 2.1 (Diaz, 2016) as:

$$Q = mCp\Delta T \tag{2.1}$$

where Q is the quantity of heat stored in J, m is mass of the heat storage medium in kg, C_p is the specific heat of storage material in J/kg K and, ΔT is the difference in temperature of storage material before and after the operation in K.

Water, aquifers, molten salts, rocks, concrete, and bricks are the storage materials used in SHS. Water is recommended for heat storage purposes in residential applications due to its high specific heat capacity. Care must be taken to prevent the mixing effect and heat loss during the storage process. It also needs ample space for storage. Aquifers are groundwater, and sometimes it contains gravel and sand due to geological formation. This type of storage system requires low investment and operating cost, but hydrogeological conditions make it complicated and conditional (G. Li, 2016). Molten salts are used as heat transfer fluid (HTF) and thermal energy storage system in concentrated solar power applications (CSP) (Guillot et al., 2012). The density of molten salt is comparably higher with other sensible heat storage liquids, but the main disadvantage of using that is oxidizing nature and corrosiveness. An antifreeze system is a big deal when using molten salts as HTF. Pure metals and alloys can also be used as TES because of its high thermal conductivity, high operating temperature and low vapour pressure but require oxidation free environment to avoid corrosion and are expensive (Alva et al., 2017). Solid storage mediums are low cost and readily available. There is no vapour pressure or leakage problem like a liquid storage medium. This storage medium can only be used as a passive heat storage system with air as HTF because it cannot be circulated. Rocks are advantageous for being non-toxic, non-flammable, cost-effective and readily available but require large air mass flow and heat loss occurrence during discharge (Tiskatine et al., 2016). Concrete is a solid material used in TES. It is known for its low cost, good thermal conductivity and good mechanical strength but the crack formation at high temperature and due to repeated usage requires proper characterization in the method of mixing (Salomoni et al., 2014). Bricks can be used for space heating, whereas sand can be used to store heat energy. The temperature of hot sand can go up to 700–1,000°C. Practically sand has the potential to store 550°C temperature (Alva et al., 2017).

Specific heat capacity and temperature variation play a vital role in SHS. The storage materials are non-toxic, non-flammable, non-corrosive (except molten salts) and have a long life. Since the specific heat capacity is high, SHS has high heat diffusivity. High thermal conductivity, low vapour pressure and cost-effectiveness are the attractive characteristics of SHS. Materials like concrete have mechanical strength, whereas sand can be used for high- temperature applications. Mostly all the materials could store heat energy without changing their structure, can operate without a reduction in storage capacity. Since the materials are non-toxic, secure handling and storing in simple containers is possible. Large space requirement, elevated weight (sand, rock, brick), heat loss during storage period because of the reduction in energy efficiency is a problem faced by this type of heat storage.

2.3.2 Latent heat thermal energy storage (LHTES)

Latent heat materials are also called phase change materials (PCM). PCM absorbs heat energy when it melts and is stored as its latent heat of fusion. Due to the heat absorption phase change of the material takes place. Thermal energy stored in PCMs is expressed in Equation 2.2 as:

$$Q = m.L \tag{2.2}$$

where m is mass of the material in kg and L denotes the latent heat of fusion in kJ/kg.

Heat energy is released during reverse phase transition (solidification). PCM undergoes a phase transition from solid-solid, solid-liquid, liquid - gas and solid-gas during the heating process. Solid-liquid phase transition during heating is commonly preferred because of its higher latent heat of fusion, less storage space complexity compared to solid-solid and liquid-gas transitions (Alva et al., 2017). Isothermal phase transformation, high storage density for a small change in temperature and compactness with container material of the phase change materials attracts the attention of the world and increase the application of PCM in various fields (Karaman et al., 2011). High capability of storing and releasing of a large amount of heat within a narrow temperature range involves application of PCM in space cooling, electronic cooling, waste heat recovery, smart housing, temperature control green-house and textiles, telecommunication and microprocessor, solar water heating and power generation (Z. Wang et al., 2015).

As mentioned in Table 2.2, Thermal Energy Storage (TES) materials are required to have thermal, physical, chemical and kinetic properties, to construct a highly efficient LHTESS. Thermal properties such as high latent heat of fusion on the basis of volume of the storage material plays an important role in minimizing size of the TESS. The rate of energy loading and unloading is decided by thermal conductivity of the storage material. Physical properties such as high energy density, small volume change during phase transition and low vapour pressure at the operating temperature could solve the energy-storing containment problems. The supercooling property is interrupted in the efficient heat extraction process. Degradation in PCM may take place due to dehydration, decomposition and interaction with the container materials due to repeated thermal cycling. So, it is necessary to select PCMs with corrosion-free container materials and chemically stable during long service. Commercial availability, abundancy and highly economical are other important factors that must be considered in selecting PCMs (S. A. Mohamed et al., 2016).

Table 2.2 Properties required for PCMs as thermal energy storage material

Thermal and Kinetic properties	**Physical properties**	**Chemical properties**
High thermal conductivity	Small volume change during phase transformation	Long term chemical stability
High latent heat per unit volume	Low vapour pressure	A completely reversible melt/freeze cycle
Melting temperature in the needed operating range	Suitable phase equilibrium	Compactibility with the container materials
High specific heat capacity	Congruent melting	
Lack of supercooling	High density	
High nucleation rate		
Sufficient rate of crystallization		

Source: Sharma et al., (2009)

2.3.3 Thermochemical energy storage (TCES)

Thermo-chemical heat storage is based on reversible chemical reaction shown in Equation 2.3 as:

$$C + heat \leftrightarrow A + B \tag{2.3}$$

where C is thermo-chemical material, A and B are two components formed during the chemical reaction.

During this reaction, heat energy is absorbed by the thermo-chemical material (C) and is converted chemically into two components (A and B). These components are stored separately. When materials A and B are combined, C is formed. Energy released during this reaction is the energy recovered from the TES. The storage capacity of this system is the heat of reaction when material C is formed. Charging is an endothermic process, whereas discharging is an exothermic process. Energy stored in thermo-chemical material is calculated using Equation 2.4 (Abedin & Rosen, 2011) as:

$$Q = n.\Delta H \tag{2.4}$$

where n is number of reactant in moles, and ΔH is reaction enthalpy in kJ mol^{-1}.

$MgSO_4 \cdot 7H_2O$, $FeCO_3$, Ca $(OH)_2$ CaO, Fe $(OH)_2$ FeO, $CaCO_3$, $CaSO_4 \cdot 2H_2O$ are promising materials used in thermo-chemical heat storage system. Component A and component B can be stored separately at ambient temperature. Thermo-chemical storage material is expected to have characteristics including complete reversibility of the reaction, cycling stability, desired operation temperature, high storage density, long term stability in thermophysical and mechanical properties, easy and high availability, low cost, supporting green environment, non-toxic and non-corrosive (Abedin & Rosen, 2011; André et al., 2016)

Energy stored in thermo-chemical storage is ten times higher than SHS and five times higher than LHS. In this type of storage, components are stored at the ambient temperature so, insulation is not required because there is a minimum/no heat loss is recorded during the storage period. This storage system is complex compared to SHS and LHS, but storage duration is unlimited. By avoiding the side reactions during exothermic reaction and reaction with the environment, it can have a high yield at the same time it can be environmentally friendly (Abedin & Rosen, 2011; Alva et al., 2017). Various performance factors of different TES are given in Table 2.3.

2.4 Classification of phase change materials

Over the past four centuries, different PCMs are used as thermal energy storage materials in a variety of applications. Depending on their phase transition temperature, they find applications in low (below 15°C), medium (15–90°C) and high temperature (above 90°C) applying fields. PCMs with low and medium phase transition temperature is used in space cooling and food industries, medical and electronic applications. In power production and aerospace applications, PCMs with high phase transition temperature is used. PCMs are classified as organic, inorganic and eutectic based on their chemical composition, which is given below in Figure 2.2 (Pielichowska & Pielichowski, 2014).

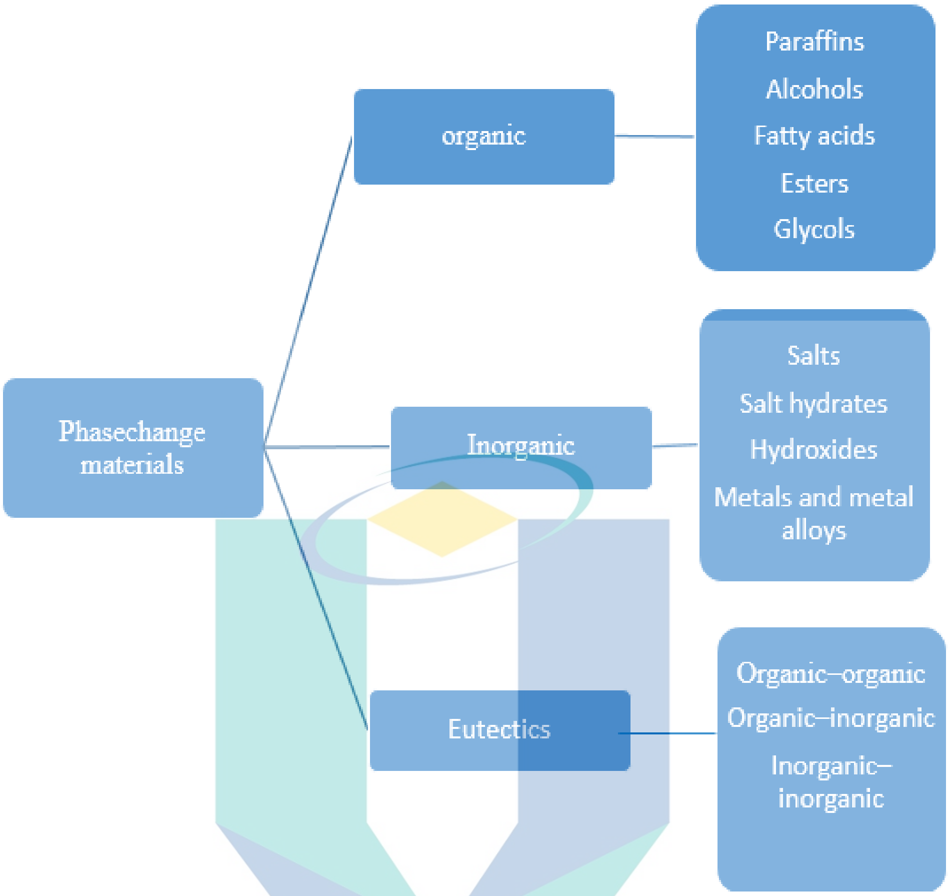

Figure 2.2 Classification of phase change materials

Source: Zalba et al., (2003)

Table 2.3 Comparison of different types of TES based on various performance factors

Performance Parameter	Type of Thermal Energy Storage		
	Sensible heat TES	**Latent heat TES**	**Chemical TES**
Temperature range	Up to 110°C (water tanks) 50°C (aquifers and ground storage) 400°C (concrete)	20-40°C (paraffin) 30-80°C (salt hydrates)	20-200°C
Storage density	Low (with high-temperature interval): 0.2 GJ/m^3 (for typical water tanks	Moderate (with low temperature interval): 0.3-0.5 GJ/m^3	Normally high: 0.5-3 GJ/m^3
Lifetime	Long	Often limited due to storage material Cycling	Depends on reactant degradation and side reactions
Technology status	Available commercially	Available commercially for some temperatures and materials	Generally, not available, but undergoing research and pilot project tests
Advantages	Low cost, reliable Simple application with available materials	Medium storage density Small volumes Short distance transport possibility	High storage density Low heat losses (storage at ambient temperatures) Long storage period Long-distance transport possibility Highly compact energy storage
Disadvantages	Significant heat loss over time (depending on level of insulation) Large volume needed	Low heat conductivity. Corrosiveness of materials Significant heat losses (depending on level of insulation)	High capital costs Technically complex

Source: Abedin & Rosen, (2011); Diaz, (2016)

2.4.1 Organic phase change materials

Organic PCMs include paraffin, fatty acids**,** alcohols, esters and glycols. Paraffin is chemically inert below 500°C. It is stable during thermal cycling, has no phase segregation and non-corrosive. It has very little subcooling, odourless, inexpensive, is an easily available, ecologically harmless and non-toxic material. Low thermal conductivity, super-cooling effect, the requirement of the nucleating agent to enhance solid crystallization and leakage in the containers are the main drawbacks of organic PCM (R.K Sharma et al., 2015). The low melting point of organic PCM limits its application in CSP (Alva et al., 2017). The melting point of fatty acids is higher compared to paraffin but is very expensive, mildly corrosive and has an unpleasant smell. All the other characteristics are the same as that of paraffin.

Applications of esters are suitable in smart clothing and polymer industries because they have phase transition at room temperature. Poly alcohols and Polyethene glycol (PEG) have all the functional characteristics of organic PCM. However, polyalcohols receive less attention from the researchers even though it has a high latent heat of fusion and PEG has thermal conductivity and super-cooling problem. Bio-based PCMs such as soybean oils, coconut oils, palm oils and beef tallow are used in thermal energy storage system for their higher latent heat and good thermal stability for thousands of melting/freezing cycles without oxidation (Sarier & Onder, 2012). In 1971, Hale et al. have listed the data regarding material properties of more than 500 PCMs needed by design engineers to build an effective thermal energy storage system. Many types of research followed this in organic PCM (Hale et al., 1971).

2.4.2 Inorganic phase change materials

Inorganic PCMs have very high latent heat density and double the heat storage capacity per unit volume compared to organic material. They have a high operating temperature, better stability, low cost and higher thermal conductivity compared to the organic PCMs. However, the drawbacks of inorganic PCMs are incongruent melting, phase segregation, sub-cooling, and corrosion on container material (Alva et al., 2017; S. A. Mohamed et al., 2016). Salt hydrates are mostly used in high-temperature applications in 300°C to 500°C range. During the phase transition, dehydration occurs due to weak bonding between the water molecules and the salt. This problem can be reduced by proper encapsulation (Pereira & Eames, 2016; Pielichowska & Pielichowski, 2014). Phase segregation and sedimentation of more massive phase can be reduced by adding gelling and thickening agents to increase the viscosity of salt hydrates, nucleating agents like carbon and borax are added to rectify the super-cooling problem. Inorganic salts (example: sodium nitrate, potassium nitrate) that are used in sensible heat storage can also act as latent heat storage material in CSP applications (M. Liu et al., 2015). Metal and metal alloys are well known for their high thermal conductivity, high latent heat of fusion per volume and high energy storage density. However, volume change during phase transition and their weight are the factors restricting its usage in latent heat thermal storage system (Cárdenas & León, 2013).

2.4.3 Eutectics

Eutectics are the combination of organic-organic, inorganic-inorganic or organic-inorganic phase change materials. When phase change materials having different melting and freezing temperature are mixed, they melt and freeze congruently, and this avoids separation of components (Alva et al., 2017).

The latent heat storage system has higher storage density compared to the sensible heat storage system of about five to ten times. The volume of storage of LHS is two times lower than SHS (Diaz, 2016). LHS has materials with a wide range of melting temperature so, can be used for all type of applications. Inorganic PCMs face many problems in commercialization includes the change of volume during phase transition, low thermal conductivity, super-cooling, corrosion with metal containers and not enough water molecules to dissolve the anhydrous salt (S. A. Mohamed et al., 2016). Thermal conductivity of phase change materials are high except organic PCMs even this problem could be rectified by using suitable nanoparticles (Babapoor & Karimi, 2015a; L. Colla et al., 2017; Lingkun Liu et al., 2016). PCM encapsulation prevents phase segregation and sedimentation, and it increases the surface area to heat transfer (Alva et al., 2017; Feczkó et al., 2016). The super-cooling problem faced by the PCM is reduced by making the heat transfer surface rough (Y. F. Fan et al., 2004) and adding nucleating agents (S. A. Mohamed et al., 2016).

2.5 Paraffin

Paraffin is saturated alkanes with an empirical formula of C_nH_{2n+2} where n stands for the number of carbon atoms. Paraffin with an odd number of alkane in the chain is isoparaffin whereas even number is n-paraffin. The carbon atoms number in the alkane chain decides the range of operating temperature, state of paraffin wax and thermophysical properties. Paraffin wax will be in the solid form if $20 \leq n \leq 40$. The melting temperature increases with several carbon atoms in the molecules. For example, the melting temperature of C_{14} is 4.5^{o}C, whereas C_{18} is 28^{o}C. Paraffin with 5 to 15 carbon atoms are in liquid form, have a melting temperature in the range of 23^{o}C to 67^{o}C. Commercial grade paraffin waxes are a mixture of hydrocarbons. They are derived from crude oil and are in solid form. Generally, paraffin waxes have a high melting point and latent heat of fusion. They can absorb and release a large amount of heat energy for many thermal cycles. They are excellent energy-storing materials having latent heat value between 200 – 220 kJ/kg, and the specific heat capacity is between 2.14 – 2.4 kJ/ kg. K. Some of the paraffin wax and blends with their thermophysical properties are listed in Table 2.4.

Paraffin waxes are comparably advantageous as it has a high latent heat of fusion, comfortable phase transition temperature, chemical stability, reliability non-toxicity, economical and easy availability. Paraffin wax has low thermal conductivity and density. Paraffin needs leak-proof containers because of its slow oxidative characteristics during oxygen exposure. These materials are compatible with metal containers except plastic (Abhat, 1983; Gulfam et al., 2019; R.K Sharma et al., 2015).

By referring to the literature of (Abhat, 1983); (Zalba et al., 2003); (Farid et al., 2004); (L.F; Cabeza et al., 2011); (Cárdenas & León, 2013); (Pielichowska & Pielichowski, 2014); (R.K Sharma et al., 2015); (Khan et al., 2016); (Alva et al., 2017) a detailed list of organic and other phase change materials can be obtained.

Table 2.4 Thermophysical properties of some paraffin, paraffin wax and blends for LHTESS

Substance	**T_{m}/ (°C)**	**H_f (kJ/kg)**	**K (W/mK)**	**P (kg/m^3)**	**Reference**
Decane	-29.65	202	-	726(l)	(Himran et al., 1994)
Undecane	-25.6	177	-	731(l)	(Himran et al., 1994)
Dodecane	-9.6	216	-	745(l)	(Himran et al., 1994)
Tridecane	-5.6	196	-	753(l)	(Himran et al., 1994)
Tetradecane	5.5	227	0.15	825(s) 994(l)	(Abhat, 1983)
Paraffin C14	4.5	165	-	-	(Abhat, 1983; R.K Sharma et al., 2015)
Paraffin C15-C16	8	153	-	-	(Abhat, 1983)
Paraffin C16-C18	20-22	152	-	-	(Abhat, 1983)
Paraffin C16-C18	20-22				
Paraffin C13-C14	22-24	189	-	790(l) 900(s)	(Abhat, 1983)
ParaffinC18	28	244	0.15	814	(Abhat, 1983)
Paraffin C20-C23	48-50	189	0.21	769(l) 912(s)	(Abhat, 1983)
Paraffin C22-C45	58-60	189	0.21	795(l) 920(s)	(Abhat, 1983)
Paraffin C23-C45	62-64	189	0.21	825(l) 915(s)	(Abhat, 1983)
Paraffin wax	64	173.9	0.167(l) 0.346(s)	790(l) 916(s)	(Lane, 1980; Ravi Kumar Sharma, 2016)
Paraffin C21-C50	66-68	189	0.21	830(l) 930(s)	(Abhat, 1983)

Table 2.4 Continued

Substance	**T_{m}/ (ºC)**	**H_f (kJ/kg)**	**K (W/mK)**	**P (kg/m^3)**	**Reference**
Biphenyl	71	119.2	-	994(l) 1166(s)	(Lane, 1980)
Propionamide	79	168.2	-	-	(Lane, 1980)
Naphthalene	80	147.7	0.132(l) 0.341(s)	976(l) 1145(s)	(Lane, 1980)
Tetradecane + Octadecane	-4.02-2.1	227.52	-	-	(Murat Kenisarin & Mahkamov, 2016)
91.67% Tetradecane + 8.33% Hexadecane	1.70	156.2	-	-	(L. F. Cabeza et al., 2011)
Tetradecane + Docosane	1.5-5.6	234.33	-	-	(L. F. Cabeza et al., 2011)
Paraffin blend (*n* = 14–16)	5-6	152	-	783(s)	(Lorsch et al., 1975)
Paraffin blend (*n* = 15–16)	5	147-153	-	751.6	(Lorsch et al., 1975)
Paraffin blend (*n* = 16–18)	20-22	152	-	-	(Lorsch et al., 1975)
Octadecane + Heneicosane	25.8-26	193.93	-	-	(L. F. Cabeza et al., 2011)
Octadecane + Docosane	25.5-27	203.8		-	(L. F. Cabeza et al., 2011)

Even though paraffin is more advantageous over other LHTESS, as mentioned above, they have low thermal conductivity. Thermal conductivity could be increased by adding highly thermally conductive materials and having fins in the storage containers. Stability of thermophysical property over the lifetime towards many thermal cycling is the preferable characteristics of phase change material.

2.6 Applications of paraffin wax

Paraffin wax is used in many fields where thermal energy is to be stored or used in other applications in different forms. Some of the promising applications of paraffin wax are summarised below and also listed in Table 2.5.

Xu et al. (2015) have investigated development of light-weighted thermal energy storage cement with paraffin and expanded vermiculite composite as aggregate. Vermiculite is calcined at 800°C to be a matrix for paraffin because of its desirable microstructure expansion and crystallization. Paraffin with expanded vermiculite composite is prepared in a 0.6:1.0 ratio by vacuum impregnation method. Results have revealed that paraffin is well impregnated in vermiculite, has high thermal stability and chemically inert. Low heat storage nature of the tested composite successfully reduced indoor temperature fluctuations and energy usage (Xu et al., 2015). Akeiber et al. (2016) have used paraffin wax with crude petrochemical feedstock waste of different ratios. Paraffin wax with melting and solidification temperature of 44°C and 19°C is used to test efficient thermal management in the buildings during hot weather. This new paraffin wax composite is tested in the prototype room resulted in remarkable energy-saving (Akeiber et al., 2016). Paraffin wax with expansion graphite composite with melting temperature of 41.9°C and latent heat value of 207.6 J/g is prepared by Liu et al., (2019). It is mixed with cement in different proportions and is tested for its chemical stability and thermal insulation. Results have shown that the temperature fluctuations inside the room are reduced (Lifang Liu, Qu, et al., 2019). Research in the same field is continued by mixing the novel composite prepared with cement to make a thermal insulation block. As the mass fraction of the PCM composite increases, their thermal storage capacity is also increased. Temperature fluctuation is controlled (Lifang Liu, Chen, et al., 2019).

Table 2.5 Some of the applications of paraffin wax

Year	Materials	Field of application	Key findings	Reference
2015	paraffin/expanded vermiculite composite	Building -concrete	• Develop lightweight concrete composite • Reducing indoor air temperature fluctuations	(Xu et al., 2015)
2016	Encapsulated paraffin wax	Building – roof structure	• Remarkable electricity saving • Good temperature management under the roof	(Akeiber et al., 2016)
2019	Paraffin/ expansion graphite composite	Building- Foamed cement	• Lightweight and high heat preservation capacity • Can create efficient thermal insulation walls	(Lifang Liu, Qu, et al., 2019)
2019	Paraffin/Expanded graphite	Building- foamed cement blocks	• Foamed blocks with 30% cement content have a good thermal energy performance • Lowest indoor temperature • Can develop energy insulation walls	(Lifang Liu, Chen, et al. 2019)
2016	Paraffin wax	Solar drier- shell and tube latent heat storage	• LHTES can supply hot air to dry food products • Discharging time 10 hrs (Temperature range 17°C-5°C)	(Agarwal & Sarviya, 2017a)
2017	Commercial grade paraffin wax	Solar drier	• Suitable thermal storage material for driers	(Agarwal & Sarviya, 2017b)
2017	Paraffin wax/ Graphite foam matrices	Low-temperature thermal energy storage	• Paraffin wax/ Graphite foam composite is a promising thermal energy storage material.	(Karthik et al., 2017a)
2018	Paraffin wax as stainless steel capsule	Packed bed Thermal Energy Storage	• Rate of charging is directly proportional to HTF mass flow rate • Maximum thermal efficiency for 100 kg/h	(Senthil et al., 2018)

Table 2.5 Continued

Year	Materials	Field of application	Key findings	Reference
2018	paraffin wax/expanded graphite/nickel particle composite	phase change microactuator	• No wire-no electrodes • Nickel particle improved the magnetic permeability • Attractive for braille display	(B. Liu et al., 2018)
2019	Palm oil and Paraffin	Solar air heater	• Palm oil can replace paraffin in the future	(Ojike & Okonkwo, 201
2019	Encapsulated paraffin wax	water thermocline storage tank	• Performance of PCM water tank is not good • Outlet water temperature is near phase transition temperature of PCM for a long time	(He et al., 2019)
2019	Paraffin wax	Solar air heater	• High thermal performance • Thermal efficiency variation of 12% to 65%	(SunilRaj & Eswaramoorthy, 2019)
2015	paraffin wax/low density polyethene blends	Solid fuel - Rocket application	• The high concentration of low-density polyethene with a low concentration of paraffin wax showed good performance	(Kim et al., 2015)
2018	paraffin wax/ Aluminium particle	Hybrid rocket fuel	• Addition aluminium increase the strength of the fuel • Strain rate dependence is strong in material	(Veale et al., 2018)
2019	Paraffin/Polyethylene (P/PE), Paraffin/Polyethylene/ Boron (P/PE/B) and Paraffin/Polyethylene/ Aluminum (P/PE/Al)	Rocket fuel	• Tensile strength of Paraffin/Polyethylene (P/PE) is increased • Boron addition enhance the tensile strength	(Pal & Ravikumar, 201
2010	paraffin wax, carbon nanotubes (CNTs), and C/C composites	Thermal control system over pulsed power in electronics	• CNTs addition with paraffin wax improved performance of thermal control unit • Extend protection against pulsed heat loading in electronics	(Shaikh & Lafdi, 2010)

Table 2.5 Continued

Year	Materials	Field of application	Key findings	Reference
2012	paraffin wax/ CNF composites	Electric thermal storage	• Thermal storage capacity is five times greater than traditional thermal storage	(K. Zhang et al., 2012)
2014	Paraffin wax/ recycled materials	Solar energy accumulator	• Thermal conductivity is doubled by adding aluminium wool from drink cans • Can be used as calefaction system in the houses	(Alejandro Reyes et al., 2014)
2015	Paraffin wax/ soft drink cans	Solar energy accumulator	• With 1260 cans an accumulator with more than 13,000 kJ, is obtained • The addition of aluminium strips increases the thermal efficiency of the accumulator • Can be used as calefaction system in the houses	(A. Reyes et al., 2015)
2018	Paraffin-wax hosting carbon fillers	Thermo-optic switching	• Paraffin with graphene reduces optic switching time by 54% • Promising thermo-optical sensing materials in TOS device applications	(Said et al., 2018)
2019	Paraffin wax	Heat exchanger	• Reynolds number of air is directly proportional to the heat transfer rate • Paraffin wax enhances the thermal performance of the heat exchanger	(Abdulrahman et al., 2019)
2020	Paraffin wax /water	Thermal energy accumulator	• Energy storing time is short • Energy removal is high • For 25% of paraffin wax addition, only 12% of accumulated energy is recorded	(A. Reyes et al., 2020)

Paraffin is used as a heat storage material in solar driers by Agarwal and Sarviya (2016). In this research, the heat transfer fluid is air. Test results confirm that hot air could be released even during non-sunshine hours for nearly 10 hrs in the temperature range of 17^{o}C to 5^{o}C (Agarwal & Sarviya, 2017a). The same authors have continued their research in commercial paraffin wax that is produced by Indian Oil Company in 2017. It is characterized to design latent heat storage. At the end of the research, paraffin wax is found to be a suitable material for solar drier applications (Agarwal & Sarviya, 2017b). SunilRaj and Eswaramoorthy (2019), have added Al_2O_3 nanoparticles with paraffin wax to improve moister removal. Efficiency of the solar drier with a mass fill ratio of 0.90 reaches at most 65% (SunilRaj & Eswaramoorthy, 2019). Thermophysical properties of paraffin wax-graphite foam composite are tested for low thermal energy storage applications by Karthik et al. (2017). Thermal conductivity value has increased by 980% (11 W/mK). From the results, it is confirmed that the mentioned composite has potential in thermal energy storage applications (Karthik et al., 2017a). Ojike et al. (2019) have used both palm oil with paraffin wax for solar heater applications. Flat plate collector type is coupled with the thermal storage system. Evaluation of the system has shown 57.3% and 46% efficiency at the peak time for palm oil and paraffin wax respectively. Both are good energy storage materials for future use (Ojike & Okonkwo, 2019).

Expanded graphite and nickel particles are added with paraffin wax. This increases thermal conductivity and magnetic permeability. Liu et al. (2018) have investigated this material to make a phase change microactuator. Results have revealed that with 1.42 W input power supply 140 μm actuation is obtained in 5 s. This PCM-composite-based microactuator is found to be useful in Micro-Electro-Mechanical Systems (MEMS) (B. Liu et al., 2018).The study of He et al. (2019) has combined water TES and encapsulated paraffin wax packed bed to cultivate higher performance and efficiency in TES. Performance of TES with PCM packed bed is better when operating at low flow rates compared to TES without PCM packed. Outlet water temperature is maintained near melting temperature of the phase change material for a longer time (He et al., 2019).

Paraffin is shown in application as rocket fuel. Kim et al. (2015) to increase the combustion performance of paraffin wax solid. Low-density polyethylene (LDPE) is doped with paraffin wax in two different concentration. Results have concluded that melting temperature has decreased with an increase in paraffin wax concentration. At the same time, latent heat capacity has decreased with the decrease in paraffin wax concentration. Low concentration of polyethylene with paraffin wax is a promising latent heat material that can be used as a solid fuel (Kim et al., 2015). Paraffin wax with aluminium particles is tested as a solid fuel for the large-scale launch vehicle. This research is focussed on the structural property study for pure and aluminium doped fuel. Aluminium addition has increased the strength of the solid fuel. Thermal propagation inside the material has an effect on structural performance. Tensile strength failure is recorded for increasing strain (Veale et al., 2018). Mechanical properties of hybrid rocket fuels are based on paraffin wax that is studied by Pal and Ravi Kumar (2019). Samples are prepared with Polyethylene (PE), Polyethylene/Boron (PE/B) and Polyethylene/aluminium (PE/Al) additives are mixed with paraffin wax as a base material. Polyethylene and stearic acid addition have increased the tensile strength and elastic modulus (Pal & Ravikumar, 2019). An investigation is carried out by Shaikh and Lafdi (2010) to provide thermal protection in electronics using paraffin wax doped with carbon nanotubes and C/C (Cabon/Carbon). Thermal control systems with different combinations of CNTs with paraffin wax are prepared and subjected to a non-uniform and uniform power supply. Results have revealed that CNTs addition with paraffin wax TCs has improved the thermal performance and gives thermal protection (Shaikh & Lafdi, 2010). Electrical thermal storage (ETS) is studied by Zang et al. (2012), using paraffin wax with carbon nanofibers (CNFs). CNFs acted as a conductive filler. As a result of thermal performance analysis, thermal energy storage capacity is increased by five times compared to the traditional way of storing (K. Zhang et al., 2012).

Heat exchanger,is designed as; a solar energy accumulator and evaluated by Reyes et al. (2014). Authors have achieved this using paraffin wax filled soft drink cans and aluminium wools from recycled cans (5%). This has behaved as a solar energy accumulator, and the amount of energy accumulated is 3,000 kJ. Output heat energy could be used for drying and calefaction systems in houses (Alejandro Reyes et al., 2014). Same authors in 2015, have tried with 300 paraffin filled disposable cans and 7.5% aluminium strips to form the same. The energy accumulated in this trial is about 13,000 kJ. In 2020, heterogeneous paraffin wax and water mixture is examined for thermal energy accumulator. This trial has included both sensible and latent heat energy in the laboratory scale. Storage time reduction and increment in heat removal are recorded (A. Reyes et al., 2020). Paraffin wax has extended its application in thermo-optic switching . This concept is examined by Said et al. (2018), with paraffin wax with carbon fillers. Thermal property analysis has revealed that the paraffin wax- graphene composite has decreased the thermo-optical switching time for an increase in graphene concentration (Said et al., 2018).

Recent applications from Table 2.5 concludes that paraffin wax is a promising thermal energy storage material for LHTESS. It finds application from the buildings to rockets. It is necessary to confirm the long-term usage of paraffin wax without degradation in the thermophysical property for efficient and economical usage. So, thermal conductivity enhancement, thermophysical property study due to repeated usage and finding ways to improve a longer lifetime of the material is necessary to be further studied.

2.7 Thermal conductivity enhancement in paraffin wax

Thermal conductivity of the Phase Change material is to be improved to enhance efficiency of a thermal energy storage system. This improvement will help to enhance the rate of charging and discharging; hence, improve the performance of LHTESS. As shown in Table 2.3, over two decades, many techniques are investigated by researchers to enhance thermal conductivity of paraffin wax.

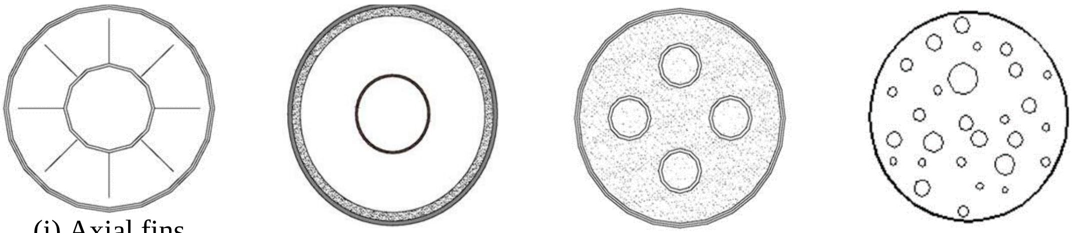
(i) Axial fins

(ii) Circle shaped fins

(iii) Shell or multitube

(iv) Bubble disturbance

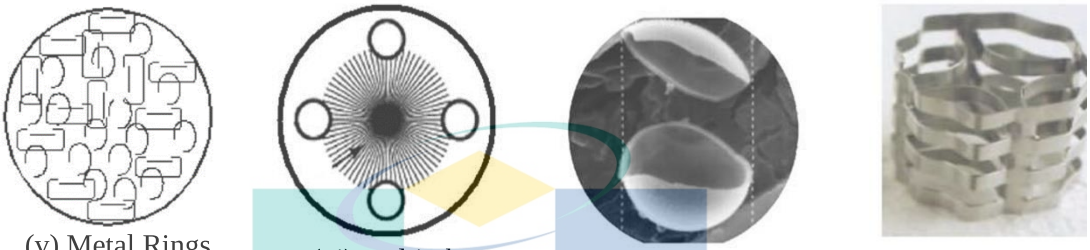
(v) Metal Rings

(vi) multitube with Carbon brushes

(vii) Micro encapsulation

(viii) Metal Matrix

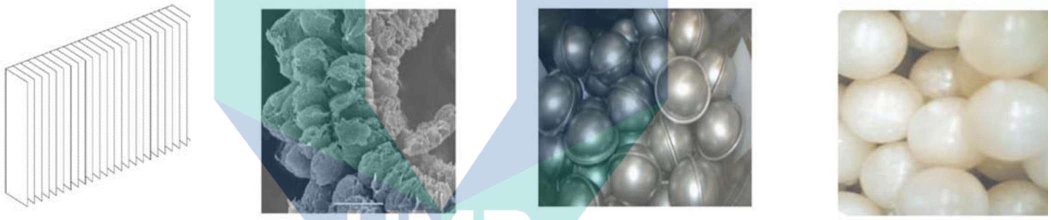
(ix) Finned Container

(x) Flakes of graphite

(xi) Hallow metal balls

(xii) Polyolefin balls


(xiii) Polypropylene panel

(xiv) Module beam

(xv) PCM+Graphite

(xvi) Flat panel

Figure 2.3 Enhancement techniques used to increase the rate of heat transfer
Source:Agyenim et al., (2010)

Examples of configurations proposed by researchers in the heat exchanger are shell with dimpled finned tube (Morcos, 1990), rectangular uniformly spaced axial spins on the inner tube (Padmanabhan.P.V & Murthy Krishna.M.V, 1986), longitudinal fins inside the vertical storage tube (Velraj et al., 1999). shell and tube exchanger at the different operating conditions with nanoparticle- PCM (Khan & Ahmad Khan, 2018) and finned tube heat exchanger (Kabbara et al., 2016). Enhancement of thermal conductivity of 2-D concentric horizontal annulus configuration with different shaped inner tubes is investigated in this work. In this numerical study, a team of researchers has considered two circular, one elliptical, and one finned cylindrical design. Both melting and solidification are enhanced by using fins. Fins usage is efficient in the case of solidification due to the reduction of natural convectional movement (Rabienataj et al., 2016). Heat transfer performance of stable and rotating latent heat storage tanks are compared. Results have revealed that PCM in a slowly rotating storage tank has higher heat transfer characteristics compared to the fast rotating one (Kurnia et al., 2017).

Adding high conductivity particle is another way of enhancing heat transfer in PCM. Different nanoparticle composites with various mass fractions of Al_2O_3, Fe_2O_3 and Si_2O_3 are added with PCM to enhance the thermal conductivity and efficiency (Babapoor & Karimi, 2015a). Colla et al., (2016) have selected Rubitherm RT20 and Rubitherm RT25 as the base PCM and alumina (Al_2O_3) and carbon black (CB) nano-powders as additives to improve the thermal conductivity of nanoparticle PCM. (L. Colla et al., 2017). Manganese oxide nanowires and nanotubes (Liang et al., 2018), copper nanoparticle of different weight ratio (S. C. Lin & Al-kayiem, 2016), copper foam (C. Wang et al., 2016), copper, aluminium, zinc and iron nano-additives (Owolabi et al., 2016) are some of the researches that have handled metal nano-materials to improve heat transfer in paraffin wax.

Adding exfoliated graphite nano-platelets (Xiang & Drzal, 2011), long multi-walled carbon nanotubes, carbon nano-fibers and graphite nano-platelets (GNPs) (L. W. Fan et al., 2013), reduced graphene oxide (rGO) with different diameters (S. C. Lin & Al-kayiem, 2016), graphite foam (P-wax/G-foam) as an interpenetrating matrix (Karthik et al., 2017b), expandable graphite namely Fire carb TEG-315 and Fire carb TEG-160(M. Kenisarin et al., 2019), are some of the carbon-based nano-additives used by the researchers to improve the heat transfer in the paraffin wax.

Jiang et al. (2015) have selected paraffin wax-Al_2O_3 composite as PCM, encapsulated using methyl methacrylate (MMA) and sodium dodecyl sulphate (SDS) to improve the thermal conductivity and stability (Jiang et al., 2015). Microencapsulated paraffin wax with nano-Al_2O_3 in poly (methyl methacrylate-co-methyl acrylate) shell has shown improvement in thermal conductivity (Jiang et al., 2015). Different ratios of paraffin wax – SiO_2 composite encapsulated in SiO_2 spherical balls synthesised by sol-gel method have retained a large amount of latent heat of fusion (Belessiotis et al., 2018). Thus micro and macro encapsulation also have helped to enhance the performance of LHTESS.

Most of the researches concentrates on thermal conductivity improvement of paraffin wax by making changes in the geometry of the experimental set up. This is achieved by using fins or increasing the surface of contact, using more than one PCMs, by micro or macro encapsulation and by incorporating nano-materials. However, few studies focus on the stability of phase change materials in long-term usage. It is necessary to extend the study on the effect of thermo-physical properties due to thermal cycling.

2.8 Accelerated thermal cycling in organic PCMs

Latent heat thermal energy storage system undergoes at least one thermal cycle per day, and that is called a normal thermal cycle. However, such type of thermal cycle test can be conducted in the laboratory using an oven to study the behaviour of a PCM after a repeated number of thermal cycles. This type of heating and cooling manually is called accelerated thermal cycling. Accelerated thermal cycling test is conducted on many organic and inorganic PCMs in the laboratory to check the stability and thermophysical property degradation. Researches related to organic PCMs are listed in Table 2.6. In the table below 'np' represents non –paraffin organic PCM whereas 'p' represents paraffin wax.

Sharma et al. (2002) have investigated the changes in the latent heat of fusion and melting temperatures of a few fatty acids upon 1,500 thermal cycles. For repeated thermal cycling hot plate is maintained at the temperature above the melting temperature of the materials. Acetamide, stearic acid and paraffin wax are characterised using DSC. Results have shown no regular degradation in melting temperature. By observing the degradation of latent heat of fusion, acetamide and paraffin wax are recommended for LHTESS.

Absorption of moisture from the surrounding is noted in acetamide (A. Sharma et al., 2002).

Sari & Karaipekli, (2007) have studied the thermal reliability of capric acid and palmitic acid mixtures. Characterisation of samples using DSC and FTIR after 1,000, 2,000, 3,000, 4,000 and 5,000 cycles are studied. Authors have reported that the melting temperature of eutectic is 21.85°C while the freezing temperature is 22.15°C. Latent heat value of melting and freezing are 171.22 J/g and 173.16 J/g,. CA/PA (Capric acid / Palmitic acid) mixture has shown excellent thermal reliability and chemical stability (Sari & Karaipekli, 2008b). Authors have continued their research in 2008 regarding capric acid in the extended graphite of 10 wt% to study its reliability and stability after 5,000 cycles. This composite has shown good thermal conductivity increment by 64% (Sari & Karaipekli, 2008a). The research is extended in 2009 using palmitic acid with EG (Extended Graphite) of 5wt%, 10wt%, 15wt% and 20wt% after 3,000 cycles. This novel form stable eutectic has a melting point of 60.88°C and a freezing point of 60. 81°C. Latent heat of melting is recorded as 148.36 J/g and latent heat of freezing as 149.66 J/g. A mass fraction of 80% is left even after 3,000 thermal cycles. Thermal conductivity is recorded at 2.5% higher than pure PA. Palmitic acid/ EG also has good thermal reliability and chemical stability (Sari & Karaipekli, 2009). In the same way, they have carried out another study on the chemical stability of lauric acid with 10wt% EP (Extended Perlite) upon thermal 1,000 cycles. The characterisation is followed in the same way as discussed earlier for other fatty acids. Results have recorded the thermal conductivity increment of 86%. Latent heat of melting and freezing is 93.36 J/g and 94.87 J/g, respectively. Melting and solidifying temperatures is 44.13 °C and 40.97 °C, respectively. This fatty acid in EP has shown good thermal reliability (Sari et al., 2009).

Table 2.6 Some performance studies of organic PCM based on accelerated thermal cycling

Year	Material	Type	No. of cycles	Key findings	Research gap	Reference
2002	Acetamide Stearic acid Paraffin wax-6106, P116, 5838, 6035, 403, 6499	**p**	1500	• Latent heat of fusion degrades • Does not show any regular degradation	Thermophysical properties other than latent heat capacity is not studied	(A. Sharma et al., 2002)
2007	Capric acid (CA)/ Palmitic acid (PA) mixture	np	5000	• CA/ PA of (76.5% / 23.5%) shows high thermal stability and reliability	Only thermal stability and latent heat is studied	(Sari & Karaipekli, 2008b)
2008	Capric acid/EG (10 wt%)	np	5000	• Increase in thermal conductivity (64%) • Good chemical stability and thermal stability	Thermal conductivity and stability is concentrated	(Sari & Karaipekli, 2008a)
2008	Paraffin wax Inorganic PCMs	p	1000	• Inorganic PCMs- Unsuitable for LHTES • Erythritol has a high energy density • Paraffin wax is suitable for LHTES	Stability and latent heat is the centre of attention	(Shukla et al., 2008)
2009	Lauric acid + Extended Perlite EP 10 wt%)	np	1000	• Increment of thermal conductivity 86% • Latent heat: melting 93.3, Freezing 94.87	Latent heat value is measured, but the degradation study is missing	(Sari et al., 2009)
2009	Palmitic acid/ EG (EG: 5%, 10%, 15%, 20%)	np	3000	• Mass fraction left- 80% • Thermal conductivity- 2.5% higher than pure PA • High thermal reliability and chemical stability	Thermal stability is highly considered. Thermophysical property study is missing	(Sari & Karaipekli, 2009)

Table 2.6 Continued

Year	**Material**	**Type**	**No. of cycles**	**Key findings**	**Research gap**	**Reference**
2010	Capric acid (CA)/ Lauric acid (LA), CA/PA, CA/ Stearic acid (SA) within expanded vermiculate	np	5000	• Mass fraction left- 40% • Increase in thermal conductivity- 104% to 150% • Good thermal reliability and chemical stability	Thermal conductivity and stability is mainly done	(Karaipekli & Sari, 2010)
2013	Micro-encapsulated paraffin wax: 23% and 49% / Polyaniline	p	200, 400,600,800 and 1000	• Little change in latent heat of fusion • Melting and freezing temperature changes negligible • High thermal reliability	Latent heat value changes are noted, but means to improve is not tried	(Silakhori et al., 2013)
2015	Palmitic acid (MA)/PA (70/30 wt %) MA/PA /SS (70/30/5 wt.%)	np	200, 500, 1000, 1500	• Melting temperature, latent heat of fusion is less after 1500 cycles	Latent heat degradation is noted. Improving methods are not studied	(Fauzi et al., 2015)
2015	Paraffin wax/ EG various concentration)	p	60	• Latent heat decrement- 2% • PCM with EG has high thermal performance	EG/PCM composite is tested only 60 cycles	(Jin et al., 2015)
2015	Paraffin wax RT 100 + EG	p	200	• Mass fraction left- 80% • The high thermal conductivity increases with packing density • High thermal reliability and chemical stability	Mainly concentrated in thermal conductivity and reliability.	(Q. Zhang et al., 2015)

Table 2.6 Continued

Year	**Material**	**Type**	**No. of cycles**	**Key findings**	**Research gap**	**Reference**
2016	Polyethene glycol (PEG 600)	np	1500	• Latent heat degrades • Melting temperature is stable until 500 cycles • Has compositional stability	Latent heat degrades and melting temperature is unstable after 500 cycles	(R. K. Sharma et al., 2016)
2017	Paraffin mixtures XBL-22	p	1-3200 - Increment-800 4000-10000 Increment-1000	• Degradation in latent heat of fusion- 9.1%	Thermophysical property study other than latent heat is missing	(L. Zhang & Dong, 2017a)
2017	Capric acid (CA)/LA (1: 9), CA/MA (4:6), CA/PA (11:9)	np	2000	• No change in Phase Change temperature • Latent heat value decreased by 4.5%	Latent heat value degradation is mentioned	(Mengjie et al., 2017)
2017	TiO_2 / Paraffin wax composite TiO_2 / Paraffin wax + sodiumStearoyl lactylate (SSL) 0.5, 0.7, 1, 2, 3, 4 wt% nanoparticles	p	180	• Latent heat melting temperature is appreciable • Composite with surfactant has high • thermal stability	By adding nanomaterials, appreciable changes can be identified	(Sami & Etesami, 2017)

Table 2.6 Continued

Year	Material	Type	No. of cycles	Key findings	Research gap	Reference
2018	Glutaric acid Container material: - Aluminium - Copper - Stainless steel	np	2000	• Melting temperature degradation: 0.47% • Latent heat degradation: 0.45% • Stainless steel has less corrosion effect	Both melting temperature and latent heat degrade. Other properties are not studied	(Dheep & Sreekumar, 2018)
2018	CA-LA/ Diatomite EG- 3%, 5%, 7%, 10%	np	200	• Excellent thermal reliability • Thermal conductivity increment- 39.7%, 61.6%, 77.6% and 114.2%	Nanoparticle addition shows increment thermal conductivity, but latent heat value is not concentrated	(Wen et al., 2018)
2019	LA, MA, PA, SA	np	10 000	• Phase transition temperature and latent heat decreased • Supercooling- 4.15^0C • Negligible change in thermal conductivity and specific heat • High chemical stability and thermal reliability	Latent heat value degrades but has high thermal stability. Other thermophysical study is missing	(Yang et al., 2019)
2019	Beeswax (size:1.53 cm^3)	np	0, 500, 1000	• The heat of fusion degrades with increasing thermal cycles • Minimal sample requirement	The heat of fusion degrades. Means to improve it is not tried.	(Putra et al., 2019)

Meanwhile, in 2010, binary mixtures of fatty acids of Capric acid (CA)/)/ Lauric acid (LA), CA/ Palmitic acid (PA), CA/ Stearic acid (SA) within expanded vermiculate is tried after 500 cycles. In this research, mass fraction left is recorded as 40%. Latent heat of melting and freezing is 61.3 J/g and 72.05 J/g respectively. Melting and freezing temperatures are recorded as 19.09^{o}C, and 25.64^{o}C increment of thermal conductivity is recorded as 104 to 155%. These binary mixtures have shown adequate thermal reliability and chemical stability (Karaipekli & Sari, 2010).

At the same time, paraffin wax and a few inorganic PCMs are tested by Shukla et al. for their suitability as storage material in LHTES. After 1,000 thermal cycles, thermal characterisation is carried out for the samples using DSC. Authors have concluded that inorganic PCMs are not suitable for LHTES upon repeated thermal cycles. Paraffin wax and erythritol have shown excellent thermal reliability. The authors highly recommend paraffin wax at the end of the experiment (Shukla et al., 2008).

Meanwhile, one thousand accelerated thermal cyclic tests are conducted on microencapsulated paraffin wax (73% and 49%) /polyamine by Silakori et al., (2013). Samples are characterised by DSC, TGA, FTIR and FESEM. A stainless steel strip heater (24VDC), deep cooler (12VDC) is used to conduct thermal cycling. Microencapsulated paraffin wax has shown reliability upon thermal cycling. FESEM pictures have shown that there is no structural change in encapsulation hence confirm the stability of encapsulated material also. Melting and freezing temperature changes is negligible (Silakhori et al., 2013).

A dual mixture of fatty acids, with and without surfactant, is tested after 200, 500, 1,000 and 1,500 cycles by Fauzi et al. (2015). MA/PA (70/30 wt%) and MA/PA/SS (70/30/5 wt%) are the composites used as PCM without and with sodium stearate as surfactants. (Fauzi et al., 2015). The thermal performance of paraffin wax in expanded graphite of various concentration is examined upon 60 thermal cycles. Paraffin wax has shown high thermal performance with EG, but latent heat value has decreased by 2% (Jin et al., 2015). Paraffin wax RT100 with extended graphite is studied for 200 thermal cycles in the same year (Q. Zhang et al., 2015). The thermal characterisation is carried out with SEM, TGA, and DSC. Thermal conductivity is measured by the transient heat source method. Mass fraction left is recorded as 80%. Thermal conductivity is high, and that increased with packing density. It has structural stability and thermal reliability. Latent heat capacity value on melting and solidification are recorded as 163.6 kJ/kg and 161.5 kJ/kg, respectively (Q. Zhang et al., 2015).

Chemical stability and accelerated thermal cycle tests are conducted by Sharma et al. (2016), on polyethylene glycol (PEG) of 6,000 molecular weight. It is characterised using FTIR and DSC after 1,500 thermal cycles. Results have shown that the tested material has high compositional stability and the melting temperature lied in the range of 55-60^{o}C, however latent heat of fusion degradation is noted. Authors have recommended five years as an adequate period for usage provided that the material can undergo 300 thermal cycles per year (R. K. Sharma et al., 2016). Experimental study on stability and reliability of paraffin wax mixtures (XBL- 22) with the melting point of 22^{o}C and the latent heat capacity of 198.6 KJ/kg are studied by Zang et al. (2017). Accelerated thermal cycling is carried out up to 10,000 times. Position of PCM in the heat source and heat sink change its position automatically in a particular time interval in the testbed. Thermal cycling took place automatically and periodically. This study has revealed that changes in melting temperature are not notable, but degradation in latent heat is recorded as 9.1% after 10,000 cycles (L. Zhang & Dong, 2017a).

Mengjie et al. (2017) have investigated the thermal stability of organic binary PCMs. DSC analysation is conducted after 4,000 thermal cycles. Results have revealed that CA/MA composite PCM has shown adequate thermal performance with no change in phase change temperature. Latent heat value has decreased by 8.88 Joule/g after 2,000 thermal cycles (Mengjie et al., 2017). Thermal stability and reliability of TiO_2 / Paraffin wax composite of different wt% from values 0.5% to 4% is investigated with and without sodium stearoyl lactylates (SSL) by S. Sami & N. Etesami, (2017). Characterisation has been done with DSC, TGA, and FESEM. Results have shown that the maximum latent heat capacity has occurred with the nanoparticle composite of 1 wt% with SSL. The thermal conductivity is higher with the addition of surfactant compared to the pure paraffin wax. These composites have shown high chemical stability and reliability after several thermal cycles (Sami & Etesami, 2017).

Glutaric acid with a transition temperature of 94.97 ^{o}C to 99.20 ^{o}C range is studied for its reliability and corrosive nature after 2,000 accelerated thermal cycles by Ram Dheep & Sreekumar, (2018). Analysis revealed that the melting temperature and latent heat value have shown 0.47% and 0.48% changes respectively compared to the uncycled glutaric acid. It has promising reliability and is compactable with a stainless steel container. Conclusively, the authors have recommended glutaric acid as a storage material in LHTESS (Dheep & Sreekumar, 2018). Furthermore, Wen et al. (2018) have investigated CA-LA (Capric acid/Lauric acid) / diatomite of different wt% upon 200 thermal cycles. The sample is prepared by the vacuum impregnation method. Characterisation after 200 thermal cycles is done using DSC, TGA, FTIR and XRD. Results have shown excellent thermal reliability after several cycles, and the thermal conductivity has increased by 39% - 114%. Increasing EG concentration has resulted in an increase in thermal conductivity (Wen et al., 2018).

Thermal property and chemical stability changes are examined due to repeated usage by Yang et al. (2019) upon 10,000 thermal cycles. Fatty acids of LA, MA, PA and SA are selected and allowed to undergo several thermal cycles. DSC and FTIR are used to characterise the samples. Thermal property analyser (LFA 457, NETZSOH) is used to measure thermal conductivity of the samples. Results have shown that the phase transition and latent heat values have decreased by -0.37^{o}C and -7.57% respectively. There are no notable changes in the thermal conductivity and specific heat capacity. However, super-cooling is noted as 4.15^{o}C (Yang et al., 2019).

On the other hand, Putra et al. (2019) have designed a thermoelectric module, which is a new method for thermal cycling. In this, thermoelectric polarity is changed according to the sample temperature. Thus thermal cycling is achieved. Bee wax of minimal amount (1.53 cm^3) is exposed to 0, 500, 1,000 thermal cycles. As a result of characterization using DSC, degradation in the latent heat value is recorded with an increasing number of thermal cycles (Putra et al., 2019).

The literature review above signifies that many studies concentrate on non-paraffin organic PCMs. Just a few studies on accelerated thermal cycling have been carried out in using paraffin but the applications of paraffin wax is wide in low and medium temperature thermal energy storage requirement areas. Even those few studies have missed out on monitoring the thermophysical properties. Thermophysical properties have their impact on the efficiency of LHTESS. Addition of nanoparticle has shown improvement in thermal conductivity, stability and latent heat capacity of PCM. The thermal cyclic test proves the degradation in thermophysical properties of paraffin wax.

This study mainly concentrates on the detailed investigation of all the thermophysical properties after many thermal cycles and means to improve it by adding nanoparticles.

2.9 Void analysis

The voids formation during solidification shrinkage affects the heating process. So, it should be regulated in the distribution aspect. If it is heterogeneous in such a way big voids are created near the wall of the container that could cause damage to it so, Sulfredge et al. (1990) have studied the ways of distributing voids using organic materials. Authors believe that this knowledge could help to use metallic salts in the LHTESS. The experiment is conducted with degassed and gassed organic liquids. Cyclohexane (C_6H_{12}) and butanediol ($C_4H_{10}O_2$) are filled in the glass tube and closed tightly to avoid atmospheric contact and then are cooled in a constant temperature bath using ethylene glycol. Void initialisation depends on viscosity and heat removal rate of the liquid. Void patterns of both liquids are different. Liquid with soluble gases have shown void distribution in the material (C.D; Sulfredge et al., 1990)

The same team (1992) has investigated organic PCMs to understand the fundamental reason for void formation during solidification shrinkage in the cylindrical form of containers and ways to distribute it. From the literature reviewed, the authors have observed that void formation could affect the melting process of the material. Cyclohexane (C_6H_{12}) with a freezing point of 6.5°C and butanediol ($C_4H_{10}O_2$) with solidification temperature of 19°C is considered for this study. Vacuum distillation process is followed to remove the dissolved gases to the maximum extent from the experimental liquid. Bothliquids are allowed to solidify inside the glass tubes in the hanging position (0 gravity) to accurately examine void patterns. Liquids are cooled in constant temperature bath using ethylene glycol. As the cooling rates are higher, less time is available to form a connection between voids so, closer spacing is observed. Viscosity of the liquid and the cooling rate are highly connected. Very little difference is observed between the lightly and heavily gassed samples. Soluble gases seem to regulate the void formation in phase change materials. Void formation in degassed samples depends on the location and pattern of initial shrinkage(C.D; Sulfredge et al., 1993).

If voids are formed at the time of solid shrinkage, then further heating cycles are affected. If the voids are formed away from the wall, then during melting process liquid does not reach voids, and that damages the capsule wall. Sulfredge et al. (1992) have continued their research in this concept to find a method to distribute voids in high shrinkage material like metallic salts. Cyclohexane is filled in the cylindrical Pyrex. The method reviewed in Section 2.9 is followed to collect the results. Results have revealed that voids are nucleated while solidification has started. The number of voids formation depend on surface area required for heat diffusion at low temperature. At higher temperature, pressure communication and the density decides the number of voids. Pressure communication plays a vital role in the distribution of voids (C. D. Sulfredge et al., 1992).

Tagawai et al. (1992) have considered density change during solidification. In this study, the cylindrical tube of 1.36 mm inner diameter and 12 mm thickness is used. Acrylic plastic with height of 102 mm is selected to fill the experimental liquid. Cyclohexane (C_6H_{12}) and butanediol ($C_4H_{10}O_2$) are selected for this experimental work. The experiment is conducted in the same way that Sulfredge et al. (1992) have followed in their previous work. Method of experimenting is reviewed in Section 2.9. Void formation and growth while solidification shrinkage is noted by freezing both liquids from the top and bottom separately. In both cases the void free solid area is formed. Voids are nucleated and grew longitudinally like worms. If the liquid is being frozen from the bottom, then voids are at the top, but it moved towards the hot liquid area and spread when it is being frozen from the top. Dissolved gases in the liquid have a tendency to distribute the voids (Tagavi et al., 1990). Thus, solidifying method also decides the void distribution.

Void formation and growth due to unidirectional freezing from the top is carried out by Sulfredge et al. (1993). Cyclohexane is selected, and the experiment is conducted in the same way as the authors followed earlier. Results revealed that initiation of voids is due to the cavity nucleation or liquid shrink if the cooling rate is high. Freeze over is formed near the top of the container. Void migration depends on sublimation (C. D. Sulfredge et al., 1993).

Chala et al. (2014) have investigated void formation in statically cooled crude oil to solve the gelled crude oil formation inside the pipeline that is stopped for a period of time. Results have concluded that void formation depends on cooling temperature and rate of cooling. Void formation analysis could help to avoid oversizing of the pipeline.

This confirms the yield strength, gel compressibility and restarts ability (Chala et al., 2014a). Researchers team have continued their research in analysing the effects of void formation at different cooling conditions. From the investigation, it is confirmed that the widest cooling regime has caused maximum voids in all the regions of the pipe. Reducing the cooling regime has not reduced the voids at lower end temperature. Higher temperature has shown lower voids near the pipe wall but higher voids around the pipe core. The work is continued to study the effect of cooling rate on voids in waxy crude oil. In this research mode of cooling is quiescent. There is no definite trend obtained for both slow and fast cooling rate. The volume of voids is unpredictable, with the rate of cooling (Chala et al., 2015a).

From the 1950s, research related to void formation in PCM is in progress. Those researches deal with the impact of soluble gases in void distribution, controlling nucleated wormholes by the dissolved gasses and interaction of bubbles in the solidification interface. Some studies have concentrated on the movement of bubbles. In the absence of a gravitational field, the movement of bubbles is due to the temperature gradient. For the past 20 years, there is no research work carried out in this area. Somehow, voids are undesirable in LHTESS as well as in all the fields where solidification is involved, including crystal growth, welding, casting, glass technology and engineering (Tagavi et al., 1990). These works highlight possibility of analysing chemical-physical property changes in PCM. Analysing the void formation during solidification could help to identify the degradation in chemical-physical properties of PCM. Doping nano-material is also another aspect to improve the thermophysical property. It also helps to spot out its effect on thermal performance in a thermal storage system during thermal cycling on a long-term basis.

2.10 Nanoparticle –paraffin wax performance enhancement and characterization techniques

Nanoparticles are microscopic particles with dimensions less than 100 nm. The nanoparticle has a very high surface area to volume ratio. Copper is a metal that can be bent. However, copper nanoparticles of size smaller than 50 nm are considered super hard material. Copper nanoparticles does not exhibit the same ductility, malleability as bulk copper. This nature can help PCM to improve its thermal conductivity and stability. The information in Table 2.7 shows the research work related to performance enhancement in PCMs due to the addition of nano-materials.

Li et al. (2013) have tested the thermal conductivity enhancement and microstructure of nano-graphite paraffin composite. For this research, paraffin is used as a base PCM, and nano-graphite (NG) is the nanoparticle used. Paraffin is placed in the water bath of 60°C then NG is added, the mixture is dispersed by agitation and cooled to 20°C to get the nano-graphite/paraffin sample. Heat conduction is tested by a hot disk thermal analyser, and the morphology is examined by environmental scanning microscope (ESEM). DSC analyses the phase change properties. The experimental results have revealed that the addition of NG increases the thermal conductivity, improve the performance in energy storage. The main advantage of using NG is that it is very cheap and easily prepared from exfoliated graphite and expanded graphite. The phase change temperature of the nano-graphite composite slightly decreases compared to paraffin. As the thermal conductivity increases, the latent heat gradually decreases (M. Li, 2013).

Improvement in thermal properties of paraffin wax doped with TiO_2 nanoparticles was experimentally analysed by Wang et al. (2014). Industrial grade paraffin wax with melting temperature in the range of 48- 50°C is selected for this research. TiO_2 nanoparticle preparation is clearly explained in this journal. TiO_2 nanoparticle and TiO_2 paraffin wax composite are analysed using DSC, FTIR, XRD, SEM and TEM. Thermal conductivity of nano-composite is measured by transient short hot wire method. Results reveal that in the low loading level of nanoparticle phase change temperature is reduced. Latent heat capacity value increased by 1% after the addition of nanoparticle but further increased as nanoparticle loading concentration decrease the latent heat capacity value. Thermal conductivity is recorded as high at solid-state compared to the liquid-state (J. Wang et al., 2014).

Table 2.7 Research works on performance enhancement of nano- Paraffin wax composites

Year	Type of study	Material	Instruments	Key findings	Reference
2013	Thermal conductivity enhancement and microstructure of nano-graphite paraffin	Paraffin, graphite (NG)	• Hot disc thermal analyser • ESEM • DSC	• Thermal conductivity increases • Exfoliated graphite and expanded graphite can be used to prepare nanoparticles • The phase temperature decreases • As the temperature increases latent heat decreases	(M. Li, 2013)
2014	Thermal property improvement in paraffin wax by the addition of TiO_2 nanoparticle	Paraffin wax, TiO_2	• FTIR • DSC • XRD • SEM and TEM	• Latent heat capacity increased by 1% nanoparticle addition • Thermal conductivity is high in solid-state	(J. Wang et al., 2014)
2014	Thermal conductivity enhancement of magnetic nanoparticles with paraffin wax	Paraffin wax, nanoFe_3O_4	• FTIR • DSC • XRD	• Latent heat capacity increased by 20% for 10% addition of nano-magnetic particle • Thermal conductivity enhancement was recorded	(Sahan & Paksoy, 2014)
2015	The effect of Al_2O_3 on morphology and thermal properties, of microencapsulated PCM (MEPCM)	Paraffin Wax, nanoAl_2O_3, Methyl methacrylate (MMA), Sodium dodecyl sulphate(SDS)	• Ultrasonic vibrator • SEM • DSC • TGA • FTIR • Hot Disc	• Thermal conductivity increases • MEPCM has good phase change properties and high encapsulation efficiency • Good stability • Potential cooling agent in building application with cost-effective	(Jiang et al., 2015)

Table 2.7 Continued

Year	Type of study	Material	Instruments	Key findings	Reference
2016	Chemical stability and thermal reliability of PCM with life span in Latent heat storage. Economic feasibility is also discussed.	Paraffin wax in a glazing system	• DSC • DTA • GA • FTIR • NMR • X-ray diffraction analyser	• Solar irradiation has no impact on reliability and durability of the material • Melting point decreases • High stability for thermal properties that a change may occur in the chain structure	(Goia & Boccaleri, 2016a)
2016	Thermal conductivity of Paraffin wax- Al_2O_3 nano-composite stabilized with (SSL)	Paraffin wax, nanoAl_2O_3 (2, 5, 7.5 & 10 wt %), SSL	• Transient hot wire technique • DSC	• The highest value of thermal conductivity - 10 wt % of nano-Al_2O_3 at 35°C • Nanoparticle addition reduces the latent heat	(Nourani et al., 2016)
2017	Study of enhanced energy storage and passive cooling (refrigeration) using nano-PCM	Rubitherm RT20, Rubitherm RT25, nanoAl_2O_3, hydrophIliano powder, carbon black	• Hot disc thermal analyser • DSC	• Thermal conductivity of nano-PCM increased • Latent heat enhancement for Al_2O_3-PCM and CB – PCM • Both Al_2O_3 nano-PCM is unstable due to the deposition • CB based nano-PCM is extremely stable	(L. Colla et al., 2017)

Table 2.7 Continued

Year	**Type of study**	**Material**	**Instruments**	**Key findings**	**Reference**
2018	Melting enhancement of paraffin wax by the addition of Cu, CuO, Al_2O_3 nanoparticles	Paraffin wax, 5% nanoCu, 5% nanoCuO and 5% nanoAl_2O_3	• Simulation -®COMSOL Multiphysics 4.3a	• Addition of 5% of nanoparticles has shown improvement in the rate of melting • Rate of charging and discharging increased by 10 and 8 times, respectively with Cu addition • Specific and latent heat value decreased • Density, viscosity and thermal conductivity are increased	(Gunjo et al., 2018)
2019	Effect on thermophysical properties of Iraqi paraffin wax due to the addition of nanoparticle	Paraffin wax, 5% nanoAl2O3, nanoZnO2 and nanoSiC	• Not mentioned	• 5% nanoAl2O3, nanoZnO2 and nanoSiC addition show the improvement in density and viscosity. • 1% nanoSiC addition has increased thermal conductivity compared to others. • SiC nanoparticle in recommended with paraffin wax.	(A. H. Ali et al., 2019)
2019	Nanographine with paraffin wax in industrial helmet application	Paraffin, nano graphene	• Ultrasonicator, DSC, TGA	• Nano-PCM shows good heat transfer rate • Thermal conductivity improvement is noted in NG/paraffin composite	(M. A. Ali et al., 2019)
2020	Stability test on TiO_2-Ag embedded paraffin wax with and without different surfactant	Paraffin wax, TiO_2-Ag, surfactants SDBS, SDS and SSL	• SEM, DSC, XRD	• TiO_2-Ag with paraffin shows thermal conductivity and latent heat of fusion enhancement • SDS helps in a homogeneous distribution of nanoparticles before and after 100 thermal cycles	(Prabhu & ValanArasu, 2020)

Magnetic nanoparticles tested for cancer treatment shows favourable condition due to high magnetic density and thermal conductivity. Thermal conductivity enhancement of magnetic nanoparticles with paraffin wax as PCM is tested by Shan and Palsory (2014). Paraffin wax with melting temperature in the range of 46- 48^oC is selected for this research. Liquid PCM is mixed with nano-magnetic prepared by sol-gel method in 1%, 5%, 10%, 15% weight concentration. The mixture is prepared using an ultrasonic water bath for 2 hours. The sample is characterised with FTIR, XRD and DSC. Results conclude that latent heat capacity is increased by 20% for 10% addition of nano-magnetic particle. Thermal conductivity enhancement of 50% is recorded in nano-PCM composite compared to pure paraffin wax (Sahan & Paksoy, 2014).

The effect of metallic nanoparticle on morphology, thermal properties of microencapsulated PCM (MEPCM) is experimentally investigated in this work. Jiang et al. (2015) selected paraffin wax with melting temperature of 28^oC as PCM, methyl methacrylate (MMA) and sodium dodecyl sulphate (SDS) is the raw materials used for the encapsulation. Al_2O_3 is the nanoparticle used in this work. The nanoparticle is dissolved in C_2H_2OH with magnetic stirring for 15 minutes, kept in ultrasonic vibrator for three hours and dried with vacuum drier ended with white powder. By polymerization reaction, microencapsulated paraffin wax with nano-Al_2O_3 is prepared. Morphology and chemical characteristics are analysed with, SEM, FTIR. Thermal conductivity is measured using the Hot Disc thermal conductivity meter, Sweden. Thermal conductivity improvement is observed in Al_2O_3 addition. MEPCM has high encapsulation efficiency and good phase change properties. It has good thermal conductivity and can be used as a cooling agent in cooling applications as it is cost-effective (Jiang et al., 2015).

The comparative study of composite PCMs with different nanoparticles the different mass fraction is the main focus of the study by Babapoor et al. (2015). Various metal oxide nanoparticles are added with paraffin-based PCM. Al_2O_3, Fe_2O_3 and Si_2O_3 with sizes 11 nm and 20 nm are the nanoparticles used in this research. Paraffin wax is heated to the temperature above melting point, and nanoparticles of desired mass are added. Then, the mixture is kept in sonicator bath for 45 minutes to get a uniformly mixed sample. DSC analysis is conducted to find the influence of nanoparticles in phase change and latent heat storage capacity. Morphology studies are carried out with the help of SEM. Thermal conductivity is tested with a digital conductivity meter based on the transient hot-wire method. The results show that adding five nanoparticles together shows improvement in onset temperature. An optimum amount of nanoparticle addition increases thermal conductivity and efficiency. Nanoparticle addition records the drop in latent heat during melting and solidification. PCM composite with high thermal conductivity is obtained with sample containing Al_2O_3 (Babapoor & Karimi, 2015b).

Chemical stability and thermal reliability of phase change materials are the main focus of this study. Economic feasibility is also considered by Goia et al. (2016) in the latent heat storage system. Paraffin wax of commercial-grade in a glazing system is exposed to sunlight then thermophysical properties of paraffin wax are checked in 0, 3, 6 and 12 months' time interval. Ageing of physical properties is investigated by DSC, TGA, FTIR, vibrational spectroscopy (Raman spectroscopy), Nuclear magnetic resonance and X-Ray powder diffraction analysis. By analysing all the data, the authors concluded that solar irradiation has no impact on the reliability and durability of the material. After ageing melting temperature decreases by 1.5°C but a decrease in the transition temperature is agreed with literature available in the different applications of PCM. PCM used for this analysis is commercial grade so one can get it quickly. Results show that paraffin wax has excellent stability of thermal properties. Vibrational spectra analysis highlights the possibility of chain structural change occurrence (Goia & Boccaleri, 2016a).

Nourani et al. (2016) have tested Paraffin wax- Al_2O_3 composite stabilized using sodium stearoyl lactylate (SSL) for thermal conductivity enhancement. Paraffin wax with melting temperature in the range of 54-58°C, Al_2O_3 nanoparticle and SSL is selected for this research. Nano-composite is prepared by mixing PCM and Al_2O_3 of a different mass fraction (2 wt%, 5 wt%, 7.5 wt% & 10wt%). SSL is also mixed with nano-composite in the ratio of 35:1. Mixing is done with the help of a magnetic stirrer for one hour to disperse the nanoparticle provided that the sample is in the melting state. To avoid bubble formation vacuum pump is used. Then, ultra-sonication was done for 2 hrs at 80 w and 50 kHz to confirm the uniform distribution of nanoparticle. Small amount of petroleum ether is added in the sample to keep it in liquid form. Samples are analysed using DSC. Thermal conductivity is carried out using transient hot-wire method. Results have shown thermal conductivity enhancement and have a nonlinear relation with the mass fraction of nano-Al_2O_3. The highest value of thermal conductivity is recorded for 10.0 wt% of Al_2O_3 addition at 35°C and heating and melting time reduction by 27%. Reduction in latent heat value is noted in 7.5 wt% and 10 wt% addition of Al_2O_3 but has thermal stability (Nourani et al., 2016).

This research is performed to find nano-PCM for improved energy storage for passive cooling applications. Colla et al. (2017) select Rubitherm RT20 (Paraffin wax with melting temperature 20°C) and Rubitherm RT25 (Paraffin wax with melting temperature 25°C), as a base PCM and new alumina (Al_2O_3) and carbon black (CB) nano-powders for this research. Samples are prepared by mixing nanoparticles of mass fraction 1wt% with base PCM and stirred mechanically for 20 min in 600 rpm then ultra-sonicated by immersing in 30°C thermostatic bath for 150 minutes. Thermal properties are analysed using DSC, and thermal conductivity is measured by a hot disc technique. Improvement in the thermal conductivity is observed in PCM. Both nanoparticle PCM record the improvement in latent heat. Both Al_2O_3 based nanoparticle PCM is unstable at a higher temperature because a deposition is observed at the same time, while CB-based nanoparticle PCM is exceptionally stable (L. Colla et al., 2017).

Melting enhancement study is carried out in paraffin wax by the addition of Cu, CuO and Al_2O_3 nanoparticles by Gunjo et al. (2018). ®COMSOL Multiphysics 4.3a is used to generate a -3D numerical model of shell and tube LHTESS with regenerative nature. Nano-paraffin fluid is prepared by adding 5% Cu, 5% Cuo and 5% Al_2O_3 nanoparticles with paraffin wax in the liquid form. Rate of energy loading and unloading is investigated. The results reveal that rate of melting is enhanced due to addition of nanoparticles with paraffin wax. Rate of energy charging and discharging is increased by 10 and 8 times respectively in 5%Cu-paraffin wax. Other nano-particle CuO and Al_2O_3 addition shows increment of 3.46 and 2.25 times in rate of charging and 3% and 1.7% in discharging,. Even though there is an increment in charging and discharging rate specific and latent heat of fusion is reduced (Gunjo et al., 2018).

Thermophysical property study of Iraqi paraffin wax is carried out after addition of 0%, 1%, 2%, 3%, 4% and 5% of Al_2O_3, ZnO_2 and SiC nanoparticles by Ali et al. (2019). Ultrasonicator is used to mix the nanoparticle with paraffin wax. During the mixing time, paraffin wax is maintained in the liquid stage with help of a hot water bath. Solidified nanoparticle-paraffin wax is tested to collect the thermophysical property to analyse the enhancement. Results of 5% addition of ZnO_2, Al_2O_3 and SiC nanoparticles addition shows the highest density increment of 6.84% ,6.5% and 5.8% and viscosity improvement of 10.2%, 9% and 4.5%, respectively. Compared to other nano-paraffin wax composites 1% addition of ZnO_2, Al_2O_3 and SiC nanoparticles addition have shown an increment of 1.8%, 3.3% and 4.2%, respectively. Nano SiC is recommended as a suitable energy-storing material (A. H. Ali et al., 2019).

Ali et al. (2019) has worked on testing the heat transfer enhancement in paraffin wax by the addition of nanographene (NG). Samples are prepared with the help of ultrasonicator. Nanoparticle addition ratio is maintained as 1%, 2% and 3%. Samples are tested for heat transfer characteristics. The rate of heat transfer is high for NG/paraffin compared to pure paraffin. High thermal conductivity is observed in NG/paraffin composite. NG with 3% ratio shows good heat transfer nature and comfortable in the helmet for four hours in an ambient temperature of 35ºC. A slight reduction in the latent heat value is noted with a high concentration of NG compared to other ratios of NG (M. A. Ali et al., 2019).

Thermal stability of TiO_2-Ag-paraffin wax composite is tested for stability to be a energy-storing material for thermal energy storage system by Prabhu and ValanArasu (2020). TiO_2-Ag with and without different SDBS(Sodium Dodecyl Benzene Sulphonate), SDS (Sodium Lauryl Sulphate) and SSL(Sodium Stearytol lactylate) is prepared for stability testing. Different concentration of nanoparticle and surfactant of 1:0.25, 1:1 and 1:2.ratio is prepared for the test. Accelerated thermal cycling and physical settlement study are conducted. Accelerated thermal cycling is carried out 100 times by heating using constant temperature hot water bath and cooled by the cold-water bath at room temperature. By SEM analysis, a sample with SDS has shown homogeneous distribution of nanomaterials even after 100 thermal cycles. Authors have concluded that nanoparticle addition has improved thermal conductivity, increased the latent heat capacity of both melting and solidification. Melting and solidification temperature is reduced. TiO_2-Ag with SDS surfactant is found to be a promising energy-storing material for a thermal energy storage system (Prabhu & ValanArasu, 2020).

Investigation on thermophysical property enhancement by addition of nanoparticles with paraffin wax has been carried out for many years. Mostly all the researchers found that there is an improvement in thermal conductivity. Some works have recorded reduction in latent heat value of paraffin wax due to addition of nanoparticles but, few works have noted the increment as well. This nanoparticle-paraffin composite property investigation is mostly carried out just one time. But, this work should be continued for many thermal cycles to confirm the enhancement in thermophysical properties even after repeated thermal cycling. This work concentrates on the investigation of nano-paraffin wax property degradation due to many thermal cycling.

2.11 Chapter summary

This chapter has reviewed the applications of paraffin wax in various research areas. Paraffin wax applications are seen in low and medium-temperature solar energy storage usage fields from floor to space. Study on paraffin wax concentrated on improving its thermal conductivity and tensile strength. Few studies concentrated thermal conductivity degradation due to accelerated thermal cycling of organic PCMs, but this type of work in paraffin wax is yet to be studied. Research related to void formation due to solidification shrinkage faced a long break for the past four decades. Since paraffin wax application is seen in various fields, studies related to thermo-physical property degradation due to repeated thermal cycling based on voids must be encouraged. This study will help to build an efficient LHTESS. The following chapter explains the methodology adopted to analyse the thermo-physical properties of PCM and nanoparticle-PCM composites.

CHAPTER 3

METHODOLOGY

This chapter concentrates on methods adopted in preparation and analysis of samples to achieve the objectives stated in Chapter 1. From the literature review, it is clear that paraffin wax with melting temperature in the range of 40 – 70°C is used in many fields like water heating and drying. This chapter explains the methods followed to find the thermophysical properties, density and porosity formation during solidification of PCM. Justification for selecting PCM and nano-PCM composite for this research is given in the following section.

3.1 Materials

Materials used in this study are given in Section 3.1.1 and 3.1.2 in detail. Purity, thermal and physical properties of the materials, namely paraffin wax, nanoAl_2O_3, nano CuO are listed in the corresponding sections. Information on place of purchase is also provided for future reference.

3.1.1 Paraffin wax

Paraffin wax is selected as PCM because it is widely used in many fields where heat energy storage is required. For any thermal storage applications paraffin wax is prefered due to its favourable thermodynamic, kinetic, chemical, and economic properties., Therefore, commercial paraffin wax with available thermophysical data is selected for this research. Thermophysical properties of paraffin wax are given in Table 3.1. Commercial paraffin waxes and paraffin are mostly used in the application of solar heating systems. Hence, these materials were produced in bulk and widely used elsewhere then, paraffin is selected for this work. Paraffin wax has melting temperature in the range of 58–62°C with 99% purity is used as a sample in this study (ASTMD 87, Sigma-Aldrich, USA).

Table 3.1 Thermophysical properties of the PCM selected for the research

PCM	Melting Temperature (°C)	Specific HeatCapacity (kJ/kg/K)	Latent Heat Capacity (kJ/kg)	Thermal conductivity (W/m/K)	Density (kg/m^3)
Parrafin wax	58-62	0.9	189	0.21	795 (l) 920 (s)

Source: Abhat, (1983)

3.1.2 Nanoparticles

From the literature, it is observed that in many applications, Al_2O_3 and CuO nanoparticles are doped with paraffin wax to improve the thermophysical properties. Considering the economic and performance point of view, these nanoparticles are selected for this research. Thermo-physical properties of Al_2O_3 and CuO nanoparticles are given in Table 3.2. Al_2O_3 Np (Nanoparticle) with a molecular weight of 101.96 g/mol is purchased from Bendosan Laboratory chemicals, Malaysia. CuO Np with 79.55 g/mol molecular weight is purchased from ASTMD 87, Sigma-Aldrich, USA.

Table 3.2 Thermo-physical properties of selected nanoparticles

Nanoparticle	Melting Temperature (°C)	Thermal conductivity (W/m/K)	Density (kg/m^3)	Specific heat capacity (J /kg/ K)	Size range (nm)
Al_2O_3	2977	36	3600	765	20 -40
CuO	1201	18	6510	540	20-40

Source:Gunjo et al., (2018)

3.2 Material preparation and thermal cycling

3.2.1 Paraffin wax

Paraffin wax is filled in ceramic containers of 9 cm height and 7.5 cm in diameter. Ceramic material is selected as a container due to its desirable melting temperature (600–4,000°C) and thermal expansion in the range of 1–15 ppm/°C. Ceramics generally have excellent chemical resistance even for weak acids and weak bases. Paraffin wax of 220g is filled in a ceramic container heated using a constant temperature heat source using FAVORIT stirring hot plate (model: HS0707V2). The bottom face of the ceramic container is heated to simulate bottom charging and top discharging of phase change material (PCM). Temperature of the sample and heater is measured using an infrared thermometer (DT-1100B with temperature measuring range from −50 to 1,100°C). Maximum temperature of the heater is maintained at 125°C so that the bottom of the container temperature can be maintained at 100°C. It is observed that the sample took nearly 2 hours to completely melt. The ceramic container with a liquefied (Molten) sample is carefully placed in a cement container of 15.5 cm diameter and 15.5 cm height for a transient solidification process. The thickness of the wall and the bottom of the container is 2 cm and 6.5 cm, respectively. As a result, thermal dissipation is allowed to take place in one direction. The sample is cooled until it has reached the room temperature. The ceramic container is then carefully broken down to get the solidified paraffin wax in a cylindrical form. The sample has completed one complete cycle of liquefaction and solidification (named as C1) which is further investigated. By following the same procedure, samples with completion of 50 cycles of liquefaction and solidification (C50), 100 thermal cycles (C100), 150 thermal cycles (C150) and 200 thermal cycles (C200) are prepared and stored at room temperature. The same heating and cooling methods are utilised each time by controlling the heating temperature. Cylindrical form of the solid sample is cut longitudinally at the top and then broken down manually without disturbing the inner surface in order to get two pieces. While one half of the sample is stored for thermal analysis, the other half is sliced down carefully using a hacksaw blade from the outer curved surface to obtain an appropriate size with a dimension of 5 cm × 3.5 cm × 0.5 cm. Inner surface of the sample is carefully preserved to be studied. Ceramic container and cement container that are used to cool the container with the melted samples are shown in Figure 3.1.

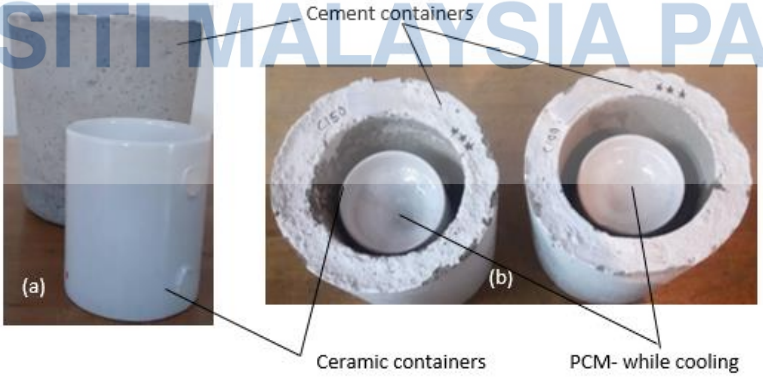

Figure 3.1 (a) Ceramic and cement containers (b) cooling method

3.2.2 Nanoparticle-paraffin wax composites

Paraffin wax of 220 g is filled inside the ceramic container and is allowed to melt by bottom heating method using a stirring hot plate (FAVORIT stirring hot plate (model: HS0707V2). Temperature of the heater is maintained in such a way that the sample can remain in liquid form. After that, 5wt% (11 g) of the nanoparticle is added with the liquid paraffin, and the mixture is allowed to mix in the magnetic stirrer. Mixing rate of rotation is fixed at 1,000 rpm for forty minutes so that the nanoparticles are uniformly distributed in the PCM (Tang et al., 2016).

In total, 15 nanoparticle-PCM composites are prepared in the ceramic containers. Among them, five are 5wt% Al_2O_3-Paraffin wax composite, five are 5wt% CuO-paraffin wax composite, and the rest are 2.5wt% (5.5 g) Al_2O_3 + 2.5wt.% (5.5 g) CuO–paraffin wax composites (hybrid-PCM composite). All the samples are allowed to undergo several thermal cycles of 1, 50, 100, 150, and 200. Samples are heated and cooled in the same way as pure paraffin wax. For melting, samples need a minimum of two hours but for cooling it requires nearly eight hours. The experiment is carried out for nearly eight months. The experimental set up for heating and cooling of both PCM and nanoparticle-PCM is shown in Figure 3.2.

Sample preparation method for nanoparticle- paraffin wax composite is followed as mentioned in Section 3.2.1. Samples that are prepared in this way are ready for further studies. Prepared samples and their notations used in this work for the samples are mentioned in Table 3.3. For material testing, the same methodology is followed for both nanoparticle–paraffin wax composite and pure paraffin wax. The designation of the samples is given in Table 3.4. Methodology for property analysis is explained in the following session.

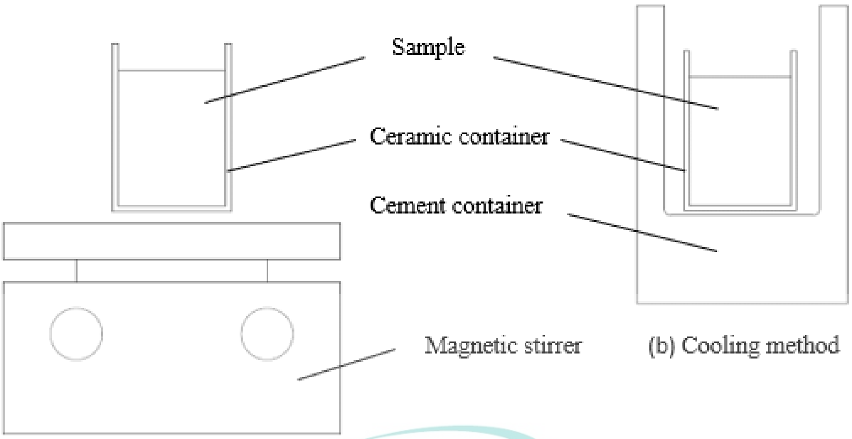

(a) Heating method

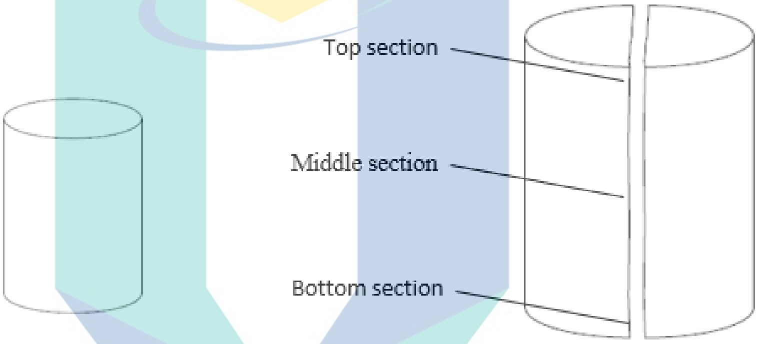

(c) Solidified sample in cylindrical form

(d) Sectioned sample

Figure 3.2 Sample preparation (a) heating, (b) cooling, (c) solidified sample and (d) sectioned sample

Table 3.3 Pure and nano-enhanced paraffin wax samples

	Pure samples	**Nano-enhanced samples**		
	Paraffin wax	Paraffin wax+5 wt.% Al_2O_3	Paraffin wax+5 wt.% CuO	Paraffin wax+2.5 wt.% Al_2O_3+2.5 wt% CuO
Noations	PCM	Al_2O_3-PCM composite	CuO-PCM composite	Al_2O_3+CuO-PCM composite
	Base PCM	Al_2O_3-PCM Al_2O_3+PCM	CuO-PCM CuO+PCM	Al_2O_3+CuO-PCM Al_2O_3+CuO+PCM Hybrid-PCM

Table 3.4 Designation of the samples

Sample notation	Representation
C1 PCM	Paraffin wax after one thermal cycle
C50 PCM	Paraffin wax after 50 thermal cycles
C100 PCM	Paraffin wax after 100 thermal cycles
C150 PCM	Paraffin wax after 150 thermal cycles
C200 PCM	Paraffin wax after 200 thermal cycles
C1 Al_2O_3-PCM	Al_2O_3-PCM after one thermal cycle
C50 Al_2O_3-PCM	Al_2O_3-PCM after 50 thermal cycles
C100 Al_2O_3-PCM	Al_2O_3-PCM after 100 thermal cycles
C150 Al_2O_3-PCM	Al_2O_3-PCM after 150 thermal cycles
C200 Al_2O_3-PCM	Al_2O_3-PCM after 200 thermal cycles
C1-CuO	CuO-PCM after one thermal cycle
C50-CuO	CuO-PCM after 50 thermal cycles
C100-CuO	CuO-PCM after 100 thermal cycles
C150-CuO	CuO-PCM after 150 thermal cycles
C200-CuO	CuO-PCM after 200 thermal cycles
C1 Al_2O_3+CuO-PCM	Al_2O_3+CuO-PCM after one thermal cycle
C50 Al_2O_3+CuO-PCM	Al_2O_3+CuO-PCM after 50 thermal cycles
C100 Al_2O_3+CuO-PCM	Al_2O_3+CuO-PCM after 100 thermal cycles
C150 Al_2O_3+CuO-PCM	Al_2O_3+CuO-PCM after 150 thermal cycles
C200 Al_2O_3+CuO-PCM	Al_2O_3+CuO-PCM after 200 thermal cycles

3.3 Material morphology

Figure 3.3 shows method of characterisation of PCM and nanoparticle-PCM. Standard methods that are followed by other researchers are adopted in this study when measuring the thermophysical properties of paraffin and nanoparticle-paraffin wax composites. Thermal cycling is done on the materials during sample preparation and is explained in Section 3.2.

3.3.1 Voids measuring method

Scanning Electron Microscope (SEM) is used to study void formation in the current research work. Electrons are accumulated on the surface of the specimen when poor conductivity samples are observed under high-vacuum SEM. This accumulation leads to the charge-up phenomenon. This charging phenomenon results in unclear images. This situation commonly occurs with hydrocarbon samples. A thin layer of metal is coated on the sample before the observation to avoid the charging problem. The current sample has low thermal conductivity; therefore, the samples are coated with a thin layer of platinum to enable good interaction between the surfaces of the sample with the electrons for a clear image formation in SEM.

Morphology of the platinum-coated sample is examined in a Benchtop Scanning Electron Microscope (SEM), EQPCRO88, HITACHI/TM3030 PLUS, Japan. This is shown in Figure 3.4. ASTM E 2298 standard of measurement is followed during the sample analysis. The magnification used in this instrument is in the range of 15x–60 kx. The spatial resolution is 2 nm at 5 kV. This instrument is operated using the secondary electron detector of tungsten at 15 kV. The back-scattered electron detector (BSED) is used to reduce beam damage to the sample. Field of view of the sample is 11 mm from the working distance. The analysis is carried out, and images are observed for sample C1, C50, C100, C150 and C200 with 100 times(x) magnification. The focus area for each sample is at the bottom, centre, and top. The half-cylindrical PCM and a sample prepared for SEM analysis are shown in Figure 3.5.

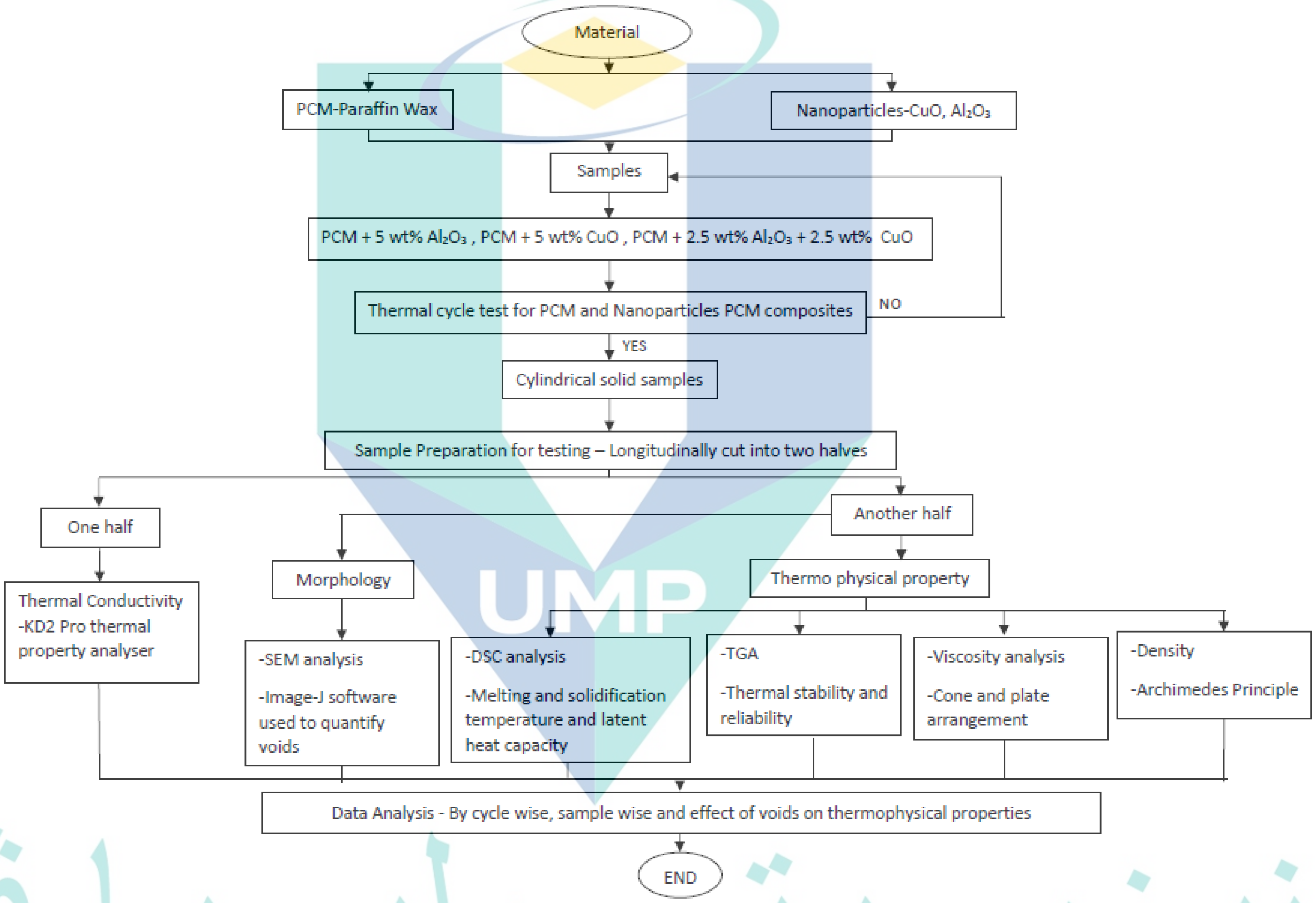

Figure 3.3 Flow chart on the experimental process of analysing the characteristics of PCM and nanoparticle-PCM composite

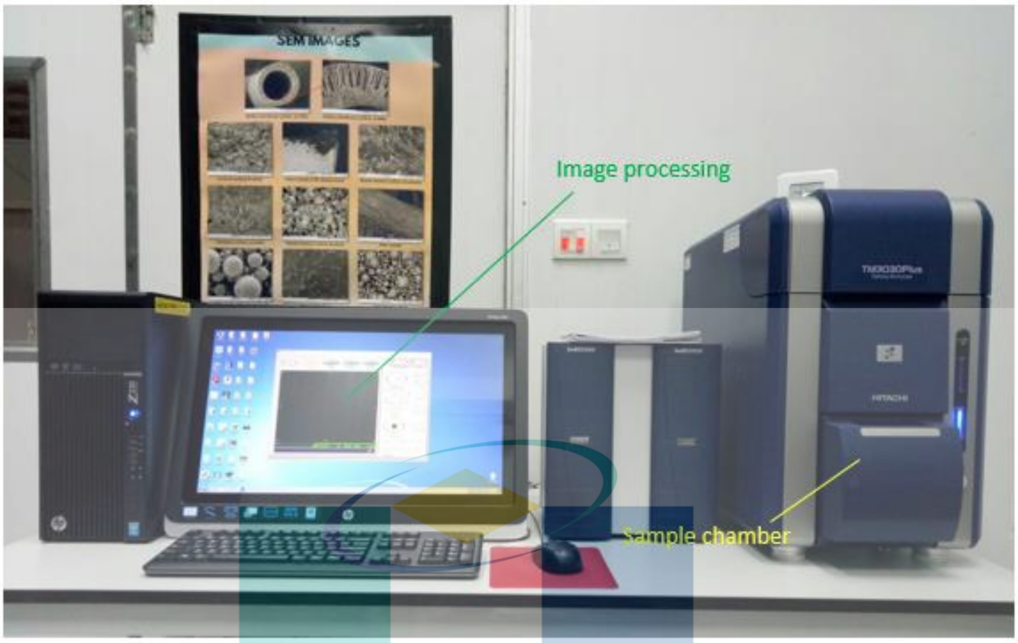

Figure 3.4 Scanning electron microscope (EQPCRO88, HITACHI/TM3030 PLUS)

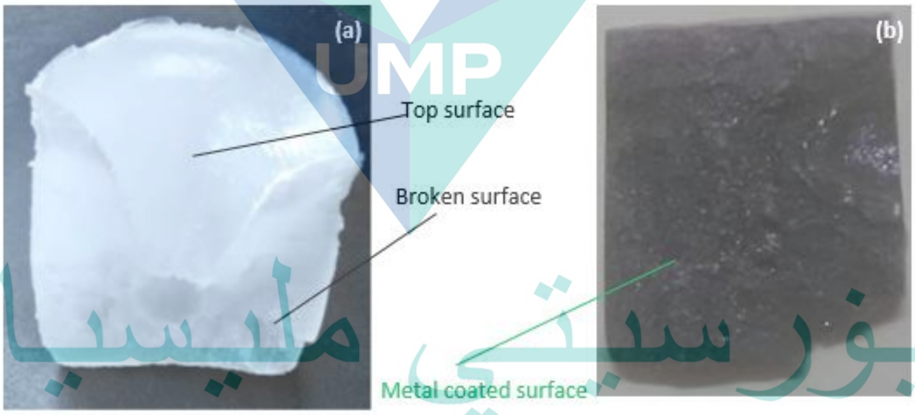

Figure 3.5 Nanoparticle- PCM composite (a) sample after breaking into half and (b) sample with metal coating

3.3.2 Void analysis

The SEM images are further treated with image processing software for analysis of voids in the sample. The image analysis method is commonly used to compute the porosity of different materials (Buckman et al., 2017). It is a universal application span from biomedical (bone and tissue void scan), material and metallurgy. It converts photomicrographs into two phases. In addition to porosity, it can also provide quantitative pore system information, such as pore sizes and shapes. The standard image analysis workflow is mainly used by researchers is porosimetry techniques. Those are He-porosimetry and mercury injection capillary pressure porosimetry (MICP) and point count analysis. In this analysis, SEM photograph is systematically threshold to produce binary images. In the binary images, the greyscale value is zero (minimum) for pores (black) and (maximum) 255 for flat surface (white). This greyscale is worked on a light intensity basis.

Quantifying voids can give more information about the changes that took place in thermal and physical properties. For each sample, a total of six images are taken at six different places. Two images from each bottom, centre and top of all the samples are considered. Voids formed on the inner surface of the samples could be quantified using ImageJ software. SEM images are converted to binary pictures using ImageJ software. Binary pictures with the original SEM image are as shown in Figure 3.6.

In Figure 3.6 (b), the black colour represents pores formed during the solidification process (K. Liu et al., 2019). From these binary images, it is seen that the porosity is heterogeneous, and the pore sizes are not uniform. So, by image analysis, void ratio is calculated for scanned images (Schneider et al., 2012). Magnification of the pore system image is an important parameter to be controlled in porosity quantification in image analysis. It can change according to the magnification and leads to drastic error, especially in comparative studies. Magnification is maintained as X100 in the current work. The magnification corresponds to 756 pixels for 1 mm length. Void measurement is repeatedly done five times for each image. Average of ten measurements is done for each bottom, centre and top of every sample.

The ratio of pore area to the total area of the sample material gaves rise to total porosity. Porosity of the sample is calculated by using Equation 3.1 (Haines et al., 2015) as;

$$Pore\ system\ image\% = \frac{Total\ area\ of\ black\ pixels}{Total\ area\ of\ pixels} \times 100 \qquad 3.1$$

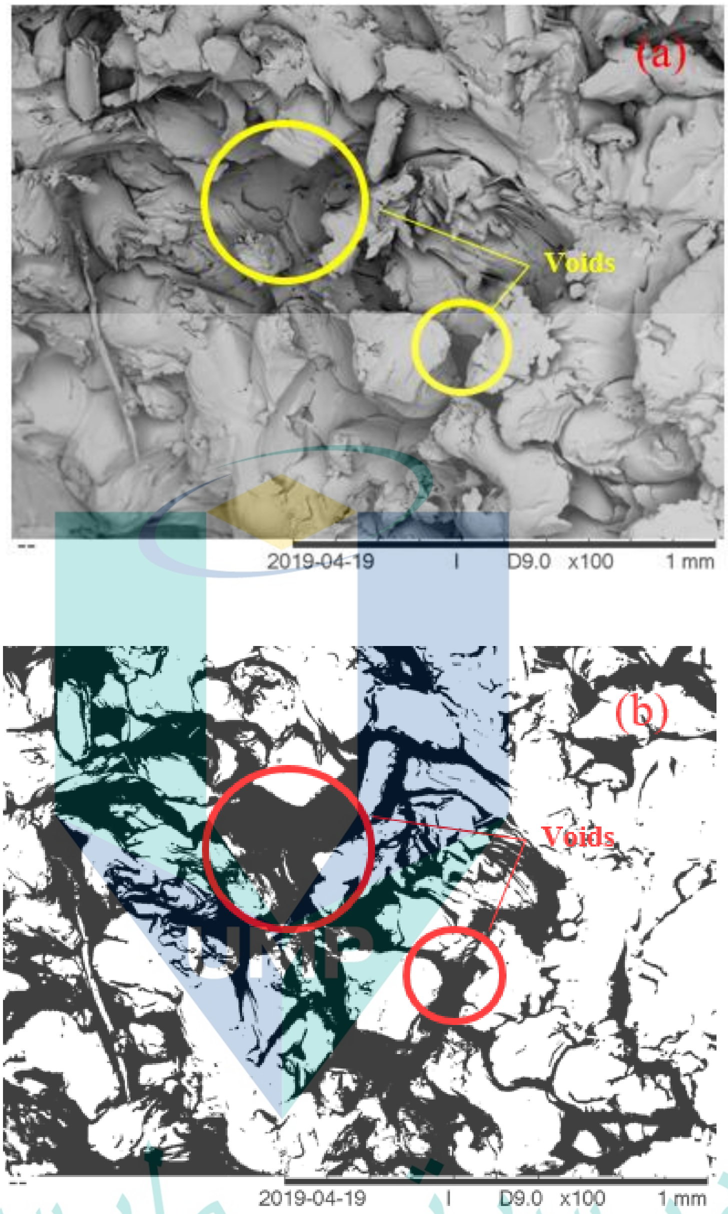

Figure 3.6 (a) original and (b) binary image of Al_2O_3+ CuO- PCM,C200, bottom

3.4 Thermophysical property measurement

Thermophysical properties of the paraffin wax is measured using Differential Scanning Calorimetry (DSC), Thermogravimetric Analyser (TGA), KD2 Pro thermal property analyser and Rheometer Kinexus Lab+. Density is measured conventionally by following a standard, namely ASTM C693 methods. The methodology of measuring and analysing the thermophysical properties, is explained in the following sections.

3.4.1 Differential scanning calorimetry (DSC)

Thermal properties such as melting temperature and latent heat capacity of paraffin wax after several thermal cycles are investigated using a Differential Scanning Calorimeter (NETISCH DSC 214 Polyma), which is shown in Figure 3.7. This instrument has followed the ASTM 3148 standard for measurement.

The methodology is adapted from other research works (L. Colla et al., 2017; Hosseini et al., 2014). Temperature calibration is made using an empty crucible. Samples of 0.8–1 mg mass range are used for this analysis. Initially, these samples are placed in the crucible, pressed, and then the crucible is covered with a lid. This action has helped to increase the thermal contact between the sample and crucible. All these preparations are done at room temperature. Crucibles containing the samples are placed into the DSC instrument, and nitrogen gas atmosphere with 40–60 ml/min flow is maintained inside. DSC measurements are carried out in a temperature range of 30–100°C with a 5°C increment for every minute. Liquid nitrogen coolant is used to bring temperature of the samples down to room temperature.

Figure 3.7 Differential Scanning Calorimeter (NETISCH DSC 214 Polyma)

Graphs obtained for heating and cooling during DSC analysis are shown in Figure 3.8. Peak of graph represents the phase change behaviour of the latent heat material. Peak temperature value in the heating graph gives the melting temperature (61°C) whereas, in the cooling curve, it gives the solidification temperature (55.52°C). The smaller peak near the main peak is due to the solid-solid transition. Area under the solid-liquid transition peak gives the latent heat capacity value of heating. In the heating and cooling graphs, latent heat values are between 145.9 J/g and -147.4 J/g. Onset temperature and endpoint of heating and cooling curves of DSC are the Phase change temperatures (Drahansky et al., 2016), which represents the starting and completion of melting and solidification process. This could be generated directly through the software that is used to draw the graph in system.

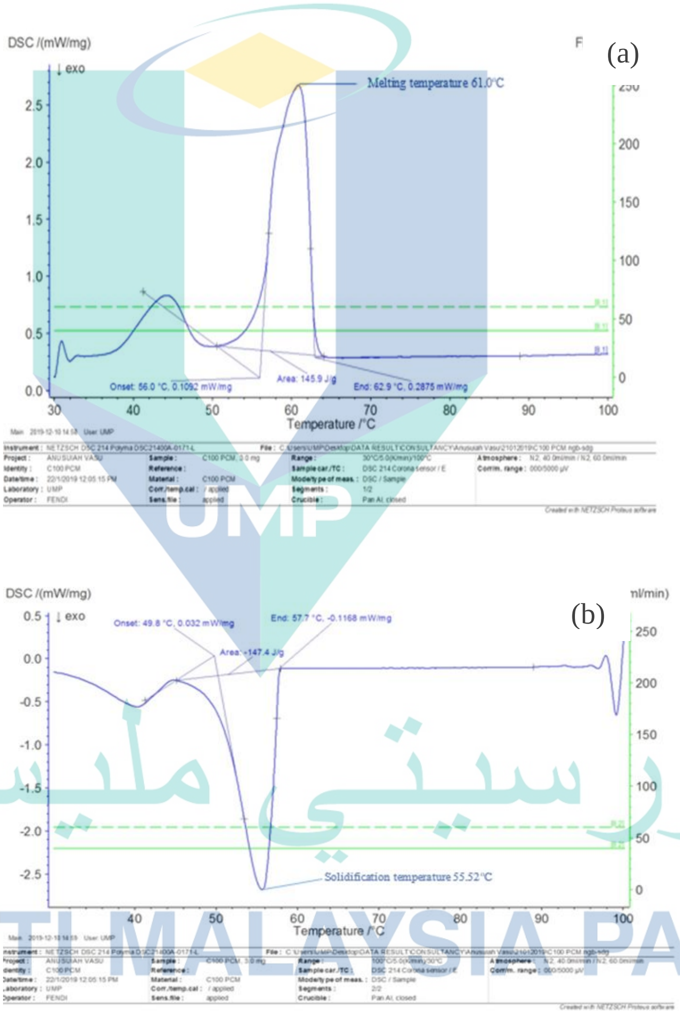

Figure 3.8 DSC graphs (a) heating and (b) cooling process of paraffin wax

3.4.2 Thermogravimetric analysis (TGA)

Thermal stability of samples, including degradation temperature and percentage of weight loss as a function of temperature, is recorded using Metler Toledo, TGA/DSC1. The instrument is shown in Figure 3.9 (Goia & Boccaleri, 2016b; Jiang et al., 2015; Yu et al., 2014). This instrument has followed the ASTM 6375 standard for measurement. Operating temperature range of the instrument is from −25 °C to 800°C. In this study, 0.4–9 mg samples are tested at the heating rate of 10°C/min from room temperature to 600°C. Nitrogen gas is purged with a flow rate of 30 ml/min. Calibration is done with the help of STARe software. By measuring the difference between weight of the sample and the reference pan, thermal decomposition characteristics of the sample are examined. Cooling is carried out by refrigeration using water.

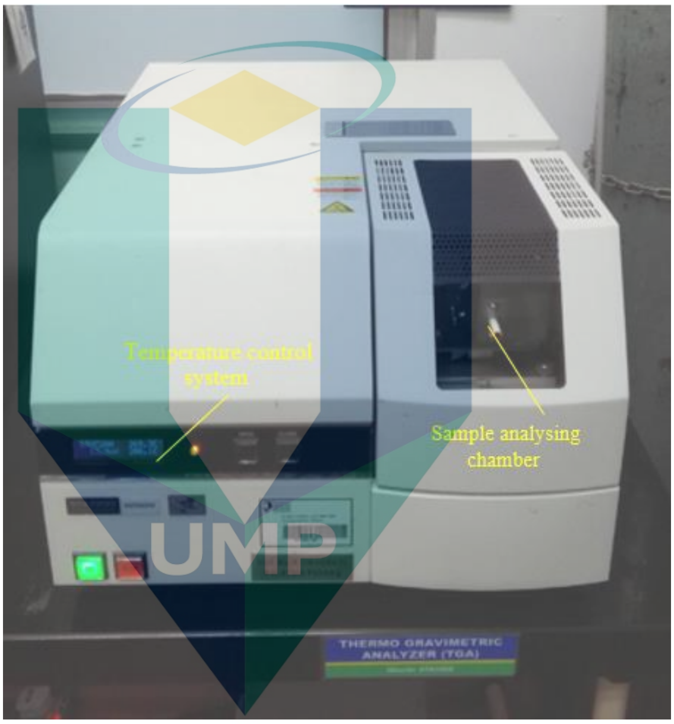

Figure 3.9 Metler Toledo, TGA/DSC 1 instrument

3.4.3 Thermal conductivity measurement

Thermal conductivity of the solid sample is measured using KD2 Pro (30 mm dual needle (SH-1)) Thermal Properties Analyzer (TPA), Decagon Devices (M. Kenisarin et al., 2019). The standard method of ASTM D 5334 is followed in the instrument. KD2 Pro instrument is shown in Figure 3.10.

This instrument is based on transient hot-wire method. The meter used has a probe with a heating element and a thermal resistor, which is inserted vertically into the test sample, as shown in Figure 3.10. Thermal conductivity of the sample is measured at room temperature (28.14°C). The measurement is made at least five times, and average value is taken for analysis. To avoid errors due to temperature rise, sample is allowed to cool for two to three minutes to make sure that the temperature of the sample is nearly 28.14°C.

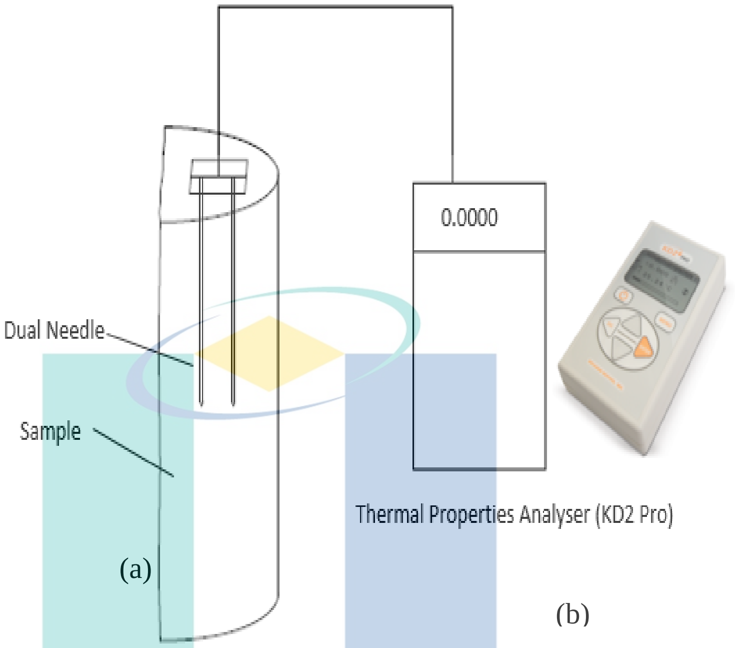

Figure 3.10 (a) Schematic diagram of thermal conductivity measurement (b) KD2 Pro

The instrument is calibrated using glycerine, and the allowed error of this instrument is 0.0032 at 28.14°C. During the measurement, the error value should be below this optimum value to obtain accurate results. Accuracy of this instrument is ±0.01 W/m·K. Table 3.5 shows the specification of KD2 Pro thermal conductivity testing setup. The same method is followed to experiment with all other samples.

Table 3.5 Specification of KD2 Pro thermal conductivity testing

Specification	**Operation condition**
Sensor used	30mm dual needle (SH-1) for solid 60 mm single needle (KS-1) for liquid
Measurement range	0.02–2.00 W/mK
Accuracy	±5% from 0.2 to 2 W/mK ± 0.01 W/mK from 0.02 to 0.2 W/mK
Operating environment	−50°C to 150°C

3.4.4 Viscosity measurement

Rheometer Kinexus Lab+ (MAL 1135931), DKSH Technology Sdn. Bhd. is the instrument used to measure viscosity of all the samples.The rheometer used is shown in Figure 3.11. Temperature range and resolution of the instrument are −40°C to 300°C and 0.01°C. Torque and normal force range is 5 nNm to 200 mNm, and 0.001 N to 50 N. Temperature control system in the instrument is maintained over the melting temperature the of sample (T > 62°C). Viscosity is measured between temperature range of 65–100°C with an increase of 5°C/min under the shearing stress of 1 Pa using cone and plate arrangement. Up to 2 mg sample is used in this measurement (Drahansky et al., 2016).

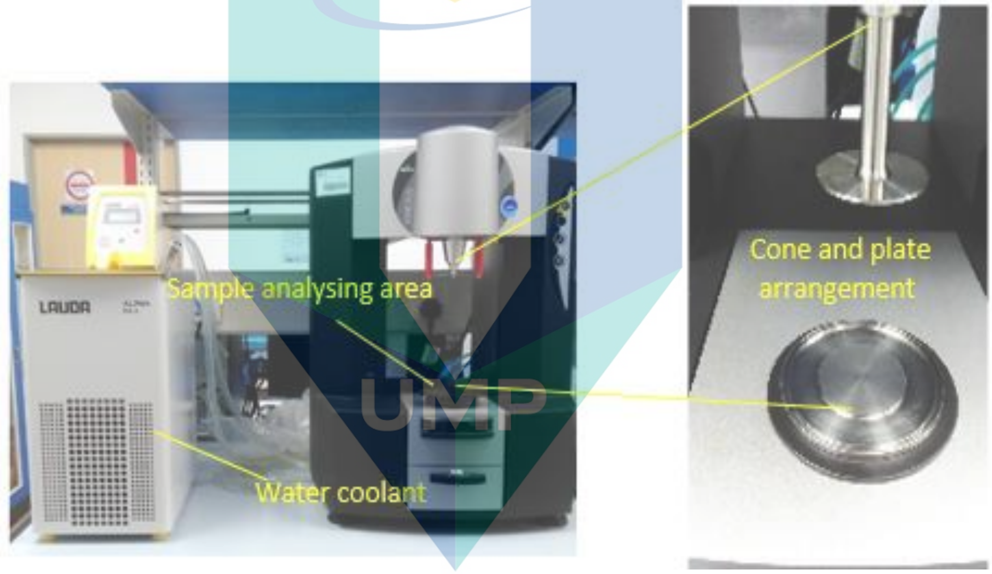

Figure 3.11 Rheometer Kinexus Lab+ (MAL 1135931), (a) cone and plate arrangement

3.4.5 Density measurement

Density of both pure PCM and nanoparticle-PCM composite samples are measured using a set up based on the Archimedes principle (ASTM C693), as shown in Figure 3.12. As the density of paraffin wax is less than water , it floats on the water. A sinker is used in this experiment to drown the samples. Mass of the sample and volume of water displaced is measured using the weighing scale. Distilled water is used in the experiment. Since the density of water is 1 g/cm^3, mass of the water displaced directly gives the volume of the sample. Finding the ratio between the mass and volume of the sample gives the density of the material. This can be obtained using Equation 3.2 as;

$$\rho_p = \frac{Ms+p-Ms}{Vs+p-Vs} \text{ g/cm}^3 \qquad 3.2$$

where ρ_p is density of paraffin wax, $Ms+p$ is mass of sinker+paraffin wax, Ms is mass of sinker, $Vs+p$ is volume of sinker+paraffin wax and, Vs is volume of the sinker.

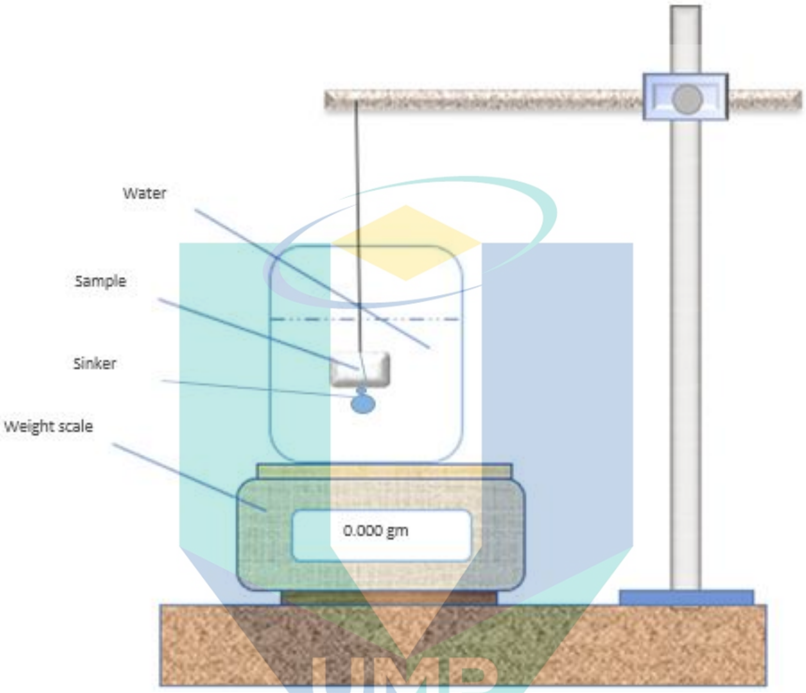

Figure 3.12 Experimental set up for density measurement of irregular shaped solid objects that floats on water

The experiment is conducted at room temperature for five pure PCM samples, fifteen nanoparticle-PCM composites and a sinker. For every sample, four pieces of different masses are selected. The sample is tied with the sinker using a thin thread then the reading in the weighing scale is noted in floating condition (Vs+p). Sample with sinker is then allowed to drop in the water then the reading is noted (Ms+p). Five times repeatability is maintained in the measurement for each sample; thus, for each thermal cycle, twenty readings are taken. The average value is considered for analysis. Since the standard deviation values are less than 2% then the measured values are acceptable.

3.5 Uncertainty analysis

Many factors affect accuracy of the measurement, namely calibration, sensitivity, human error while taking readings, observation, drift etc.. These unavoidable factors create uncertainty in measurements. Various parameters are measured manually in this study, such as void ratio, thermal conductivity and density. Other parameters such as latent heat capacity, melting and solidification temperature, viscosity are measured using standard instruments. Hence those parameters exhibit the uncertainty of the corresponding instruments. Uncertainty of instruments is mentioned in the respective sections in this chapter. Uncertainty in the parameters measured is less than one and is in the range of 0.0048 to 0.0191, 0.079 to 0.0088 and 0.0261 to 0.0431 in the void ratio, thermal conductivity and density respectively, and is listed in Table 3.6. Since the uncertainty values are less, error in the measurements is considered negligible.

Table 3.6 Uncertainty in the measured parameters

Parameters	**Uncertainty (standard deviation)**			
	PCM	**Al2O3-PCM**	**CuO-PCM**	**Hybrid-PCM**
Uncertainty in the measurement of Void ratio	0.0048	0.0078	0.0018	0.0191
Uncertainty in the measurement of thermal conductivity	0.0088	0.0085	0.0078	0.0079
Uncertainty in the measurement of density	0.0261	0.0342	0.0431	0.0327

3.6 Chapter summary

Specific instruments are used to measure the thermophysical properties of the samples to achieve the objectives mentioned in chapter 1. Methods adopted to analyse the data are also explained above. ImageJ software is used to measure the void ratio and is clearly explained in Section 3.2.2. Formulas are provided to calculate the void ratio and density of the samples. Five times repeatability is maintained in almost all the measurements. Experimental data collected are interpreted and analysed in Chapter 4.

CHAPTER 4

RESULTS AND DISCUSSION

Each section of this chapter presents results of material characterization of pure paraffin wax and nanoparticle-paraffin wax composites namely Al_2O_3–PCM, CuO–PCM and Al_2O_3+CuO–PCM after 1, 50, 100, 150 and 200 thermal cycles. Then, the results of pure and nanoparticle–Paraffin wax composites are analysed to study and compare the property degradation cycle-wise and sample-wise accordingly. Finally, the impact of voids on the number of thermal cycles and thermo-physical properties of all the samples are discussed in detail. The final section of this chapter validates the ideal PCM for thermal energy storage.

Thermo-physical properties of PCM and nanoparticle-PCM composites are investigated in this section. Material characterization of pure paraffin wax and nanoparticle-PCM composites are tested using the following devices as it is discussed in Chapter 3;

- Scanning Electron Microscope (SEM) is used to analyse formation of voids in the inner surface of the samples
- Differential Scanning Calorimeter (DSC) is used to investigate the melting and solidification temperature and latent heat capacity of the samples
- Thermogravimetric Analyser (TGA) is used to analyse thermal stability, thermal reliability and thermal degradation trend of the samples
- KD2- Pro Thermal Analyser is used to measure thermal conductivity of PCM and nanoparticle- PCM
- Rheometer (cone and plate arrangement) is used to investigate the viscosity of the samples in the temperature range of 65°C to 100°C

- Water displacement method using Archimedes principle is adopted to measure density of the samples

At least five times repeatability was maintained for each characterisation. Based on the results, thermophysical property degradation due to repeated thermal cycles is discussed based on void formation in the samples.

4.1 SEM analysis of PCM and nanoparticle-PCM composites

When the liquid phase is less dense than the solid, vapour bubbles or voids will be formed during solidification shrinkage. Void formation is not a preferable characteristic in latent heat material storage applications. Void formation has impacts on thermophysical properties; hence, affecting the storage performance of LHTESS. A detailed SEM analysis is carried out to investigate the impact of void formation in PCM and nanoparticle –PCM composite in the following section.

4.1.1 SEM analysis

SEM observation has shown void localization at the surface of samples. Some of the SEM images of C1PCM is shown in Figure 4.1. Void formations due to addition of Al_2O_3 nanoparticle after 200 thermal cycles is given in Figure 4.2. Void formations are marked in the images to show that CuO nanoparticle addition still resulted in void formation. SEM images of CuO-PCM after 100 thermal cycles is shown in Figure 4.3. Void formation is observed in all the hybrid-PCM samples. SEM images of C100 hybrid-PCM is shown in Figure 4.4. Void formation during the solidification shrinkage of pure PCM, Al_2O_3-PCM, CuO-PCM and Al_2O_3+CuO-PCM indicates that void formation is unpredictable and has to be analysed by quantifying them. Quantification of voids is explained in Section 3.3.2.

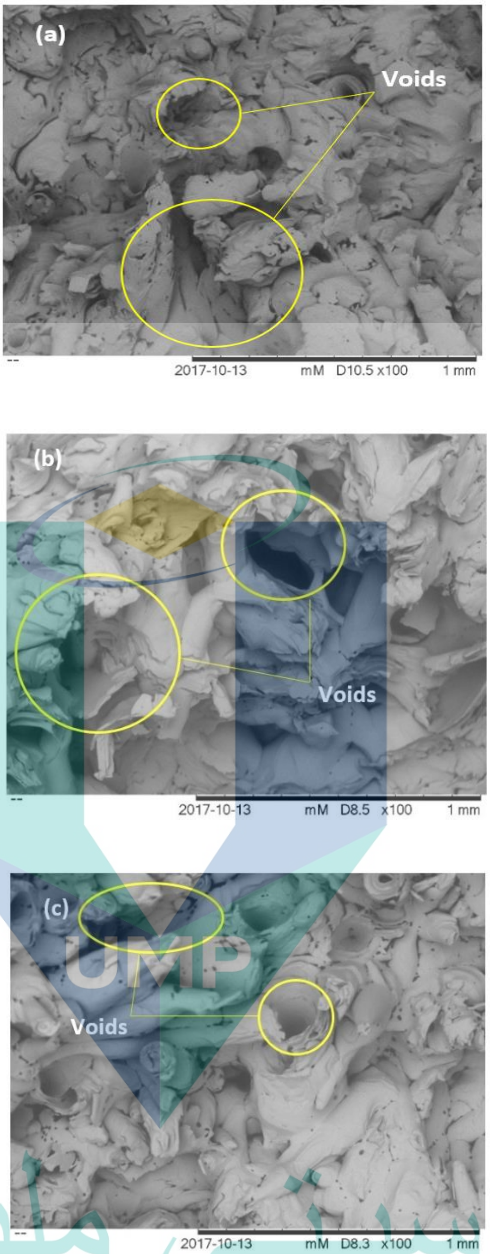

Figure 4.1 SEM pictures of C1PCM composite (a) bottom, (b) centre and (c) top with x100 magnification

A large number of small void formation is noted during solidification shrinkage of phase change materials by Sulfredge et al., (1992). These voids tend to move due to the temperature difference in the liquid and clog together to form larger voids. These voids move towards the centre of the cylinder to reduce the surface energy where the surface tension is low due to higher temperature. All the voids accumulated at the centre resulted in a single big void after final solidification. This void growth tendency depends on the pressure communication of the nearby voids. (Chow, 1992; Tagavi et al., 1990). This pressure is caused by the surface tension and has an inverse relation with the bubble radius in the liquid shrinkage. This pressure causes the liquid flow in direction of the axis, causing collapse of smaller voids and pushing towards the large voids (C. D. Sulfredge et al., 1992). If the pressure communication is good enough, the small voids does not originate or collapse to form big voids. Thus the void sizes increase. Void sizes are different and heterogeneous due to void growth (Chow, 1992).

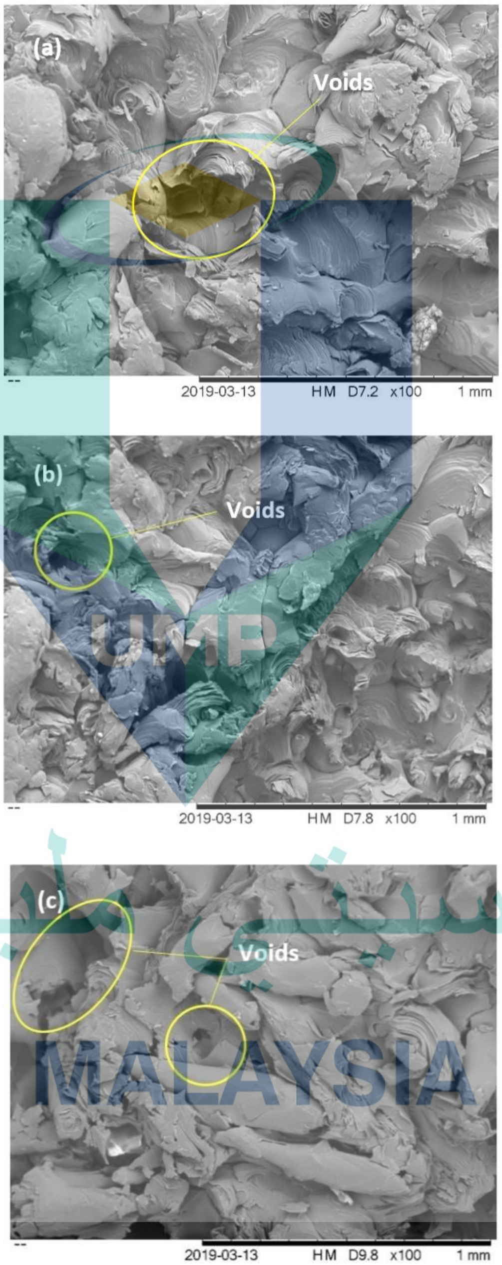

Figure 4.2 SEM pictures of C200 Al_2O_3-PCM composite (a) bottom, (b) centre and (c) top with x100 magnification

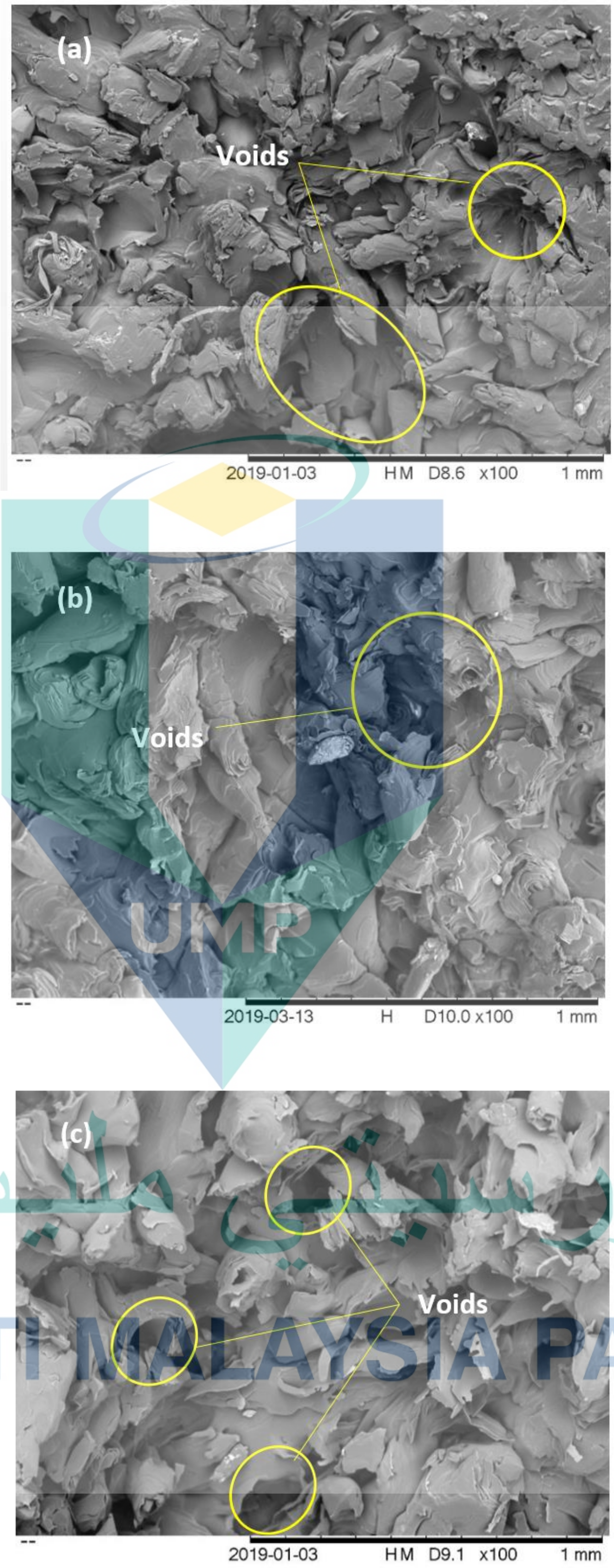

Figure 4.3 SEM pictures of C100 CuO-PCM composite (a) bottom, (b) centre and (c) top with x100 magnification

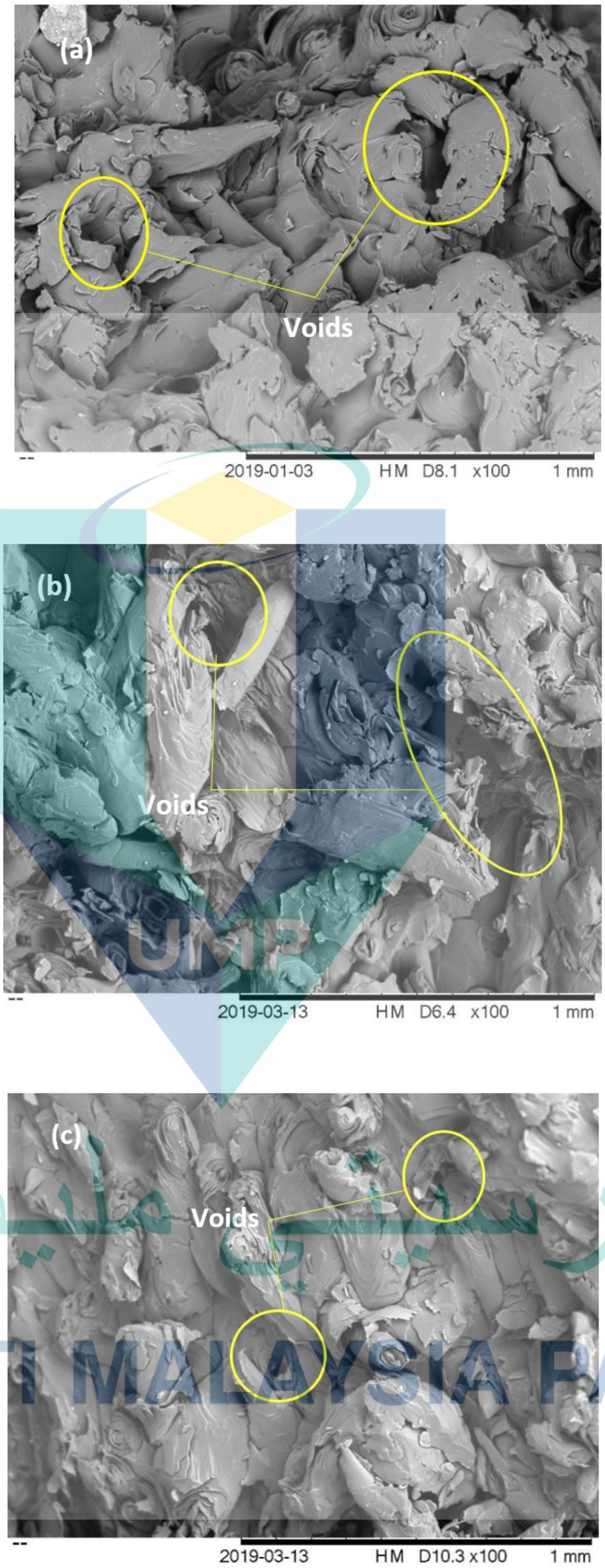

Figure 4.4 SEM pictures of C100 Al_2O_3+CuO-PCM composite (a) bottom, (b) centre and (c) top with x100 magnification

4.1.2 Quantification of voids

Binary pictures with original SEM images of the highest and lowest void ratios recorded in this study are given in Figure 4.5 and Figure 4.6. Porosity measurements of all PCM and nanoparticle-PCM composites are given in Table 4.1.

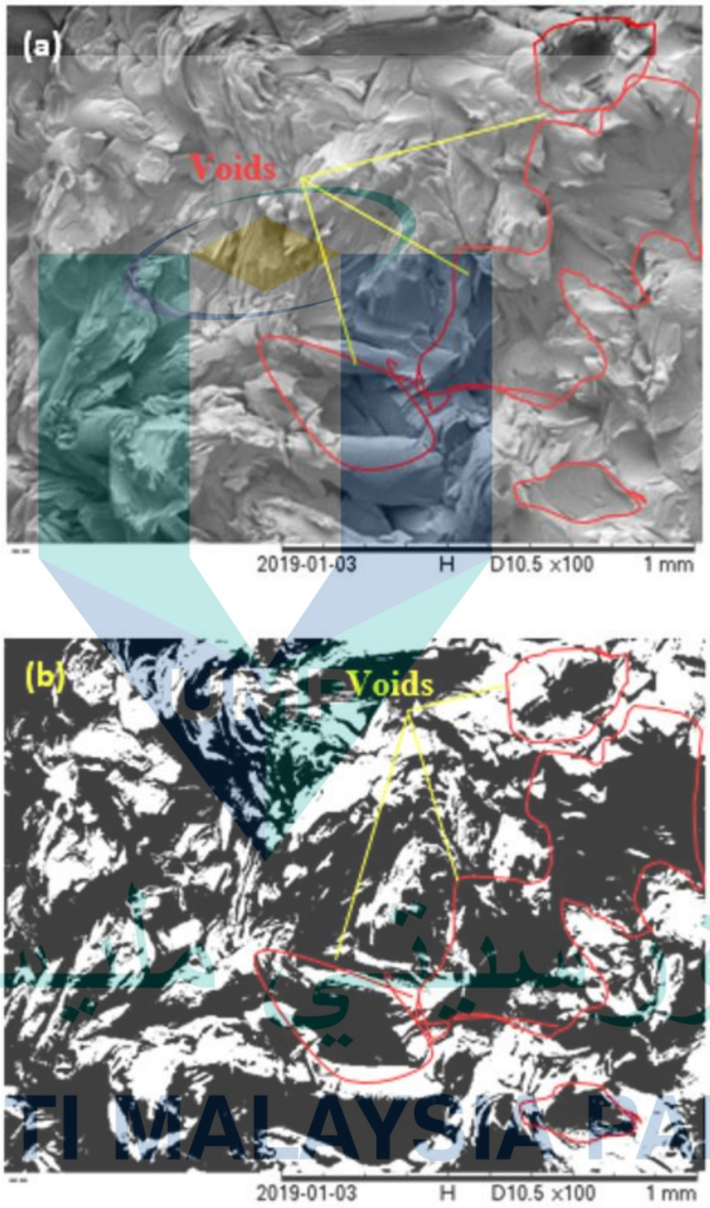

Figure 4.5 (a) original and (b) binary SEM pictures with x100 magnification of C200, Al_2O_3-PCM composite at the bottom with the highest void ratio (55.75%)

Table 4.1 Void ratio of the different samples at bottom, centre and top

Sample ID	Position	Void ratio (%)					Percentage of void variation C1-C200 (%)
		C1	C50	C100	C150	C200	
PCM	Bottom	46.00	44.70	33.02	39.41	51.33	11.58
	Centre	40.38	44.41	35.60	38.27	45.07	11.62
	Top	36.58	49.24	50.61	34.36	43.04	17.65
	Average	40.99	46.12	39.74	37.35	46.48	13.40
Al_2O_3-PCM	Bottom	44.24	41.44	44.65	37.51	55.75	26.03
	Centre	57.97	38.88	43.97	42.57	41.95	-27.64
	Top	37.40	45.98	50.28	40.79	37.29	-0.30
	Average	46.54	42.10	46.30	40.29	45.00	-3.31
Variation from PCM (%)		13.54	-8.71	16.50	7.89	-3.19	-
CuO-PCM	Bottom	37.87	39.28	45.44	41.80	44.27	16.91
	Centre	44.56	34.13	44.73	45.86	37.61	-15.60
	Top	44.84	51.34	36.13	44.82	45.00	0.35
	Average	42.42	41.58	42.10	44.16	40.89	-3.62
Variation from PCM (%)		3.51	-9.83	5.94	18.24	-12.03	-
Al_2O_3+CuO-PCM	Bottom	41.89	47.32	35.88	46.02	40.11	-4.25
	Centre	53.66	43.70	39.62	47.39	38.23	-28.76
	Top	52.52	44.88	50.10	53.81	44.91	-14.50
	Average	49.36	45.30	41.87	49.07	41.08	-16.77
Variation from PCM (%)		20.42	-1.78	5.35	31.40	-11.64	-

It is necessary to understand void formation and its distribution in the samples. To achieve this,

Step 1: void ratio changes are accounted from bottom to top in C1, C50, C100, C150 and C200 in the same category.

Step 2: void formation is compared between samples for all the thermal cycles in the same category.

Step 3: void ratio variation is calculated from C1 to C200 for all samples

Step 4: variation in the void ratio of nanoparticle–PCM and base PCM after 200 thermal cycles are calculated.

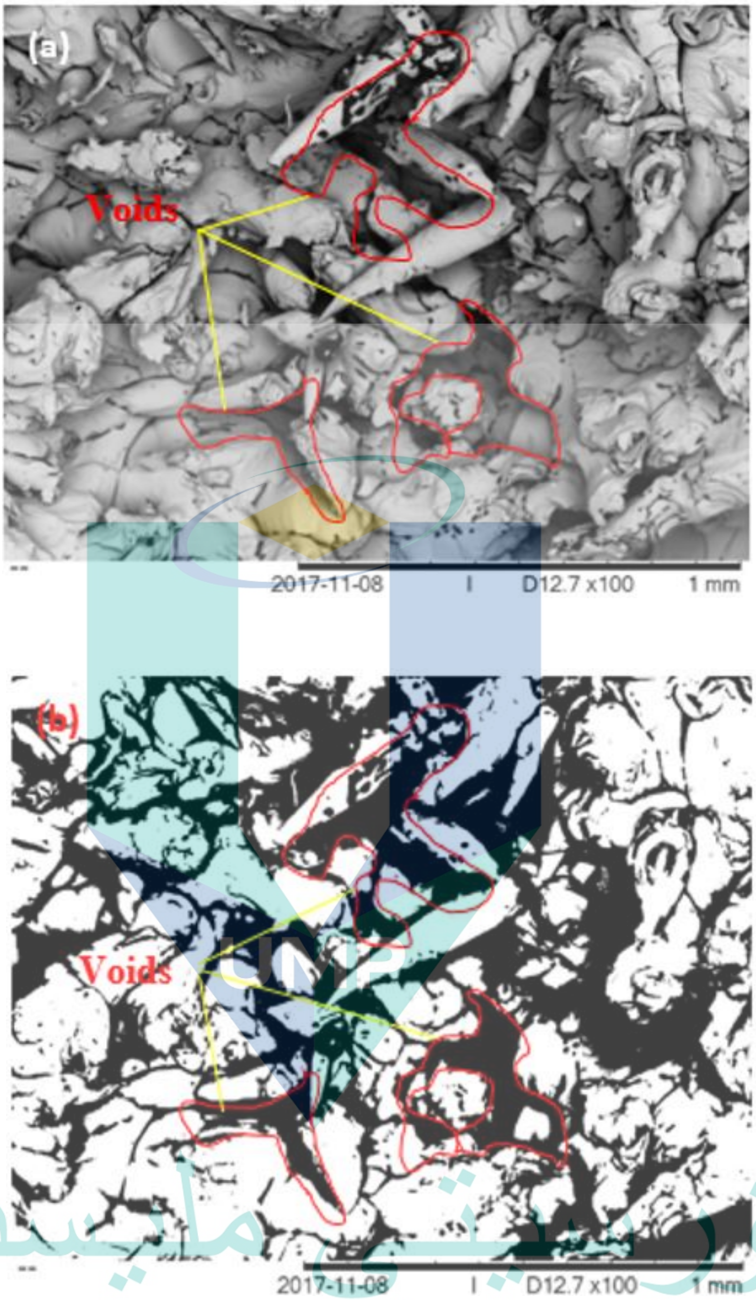

Figure 4.6 (a) original and (b) binary SEM pictures of with x100 magnification C100, PCM at the bottom with the lowest void ratio (33.02 %)

This analysis helps to obtain knowledge about the impact of void formation on thermo-physical properties of the PCM and nanoparticle PCM composites. The lowest and the highest void ratio values and percentage of void ratio swing (Cs) in each position for all the samples were tabulated in Table 4.2.

In pure paraffin wax, the void ratio variation from C1 to C200 is in the range of 33.02% to 51.33% at the bottom. At the centre and top, the range is between 35.60% to

45.07% and 34.36% to 50.61%, respectively. Figure 4.7 shows that in pure PCM, void ratio value is higher at C200 compared to C1 in all bottom, centre and top positions. The lowest and the highest value of void ratios are recorded at the bottom of C100 and C200. The swing in void ratio from the lowest to the highest value is 55.45% at the bottom. The void ratio swing from the lowest to the highest value at the bottom is higher compared to the top and the centre in the pure PCM.

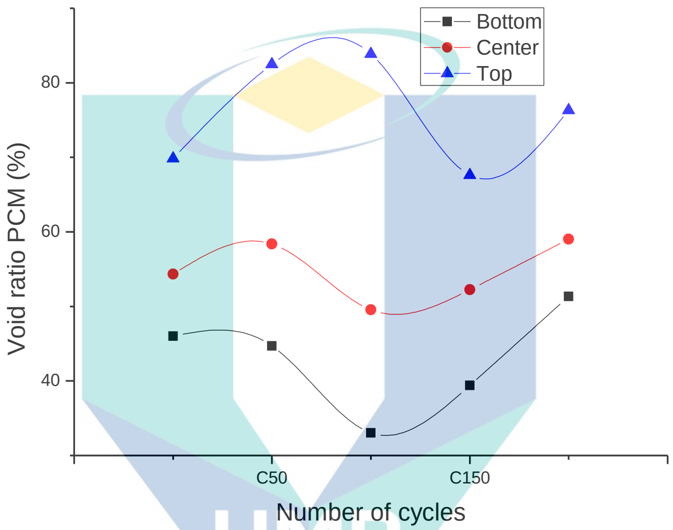

Figure 4.7 Void ratio of PCM samples against thermal cycles

In the Al_2O_3-PCM composite, void ratio variation within 200 thermal cycles is from 37.51% to 55.75% at the bottom, from 38.88% to 51.97% at the centre and from 36.13% to 51.34% at the top. The highest and the lowest void ratio values are recorded at the top of C200 and the centre of C1. After 200 thermal cycles, void ratio value has increased at the bottom but has decreased at the centre and the top compared to C1. The void ratio changes are shown in Figure 4.8. Percentage of difference in lowest to the highest void ratio value is 33.67% at the centre and 48.63% at the bottom. Al_2O_3 nanoparticle addition increased the void ratio at the bottom as compared to the top, while the highest value is recorded at the centre.

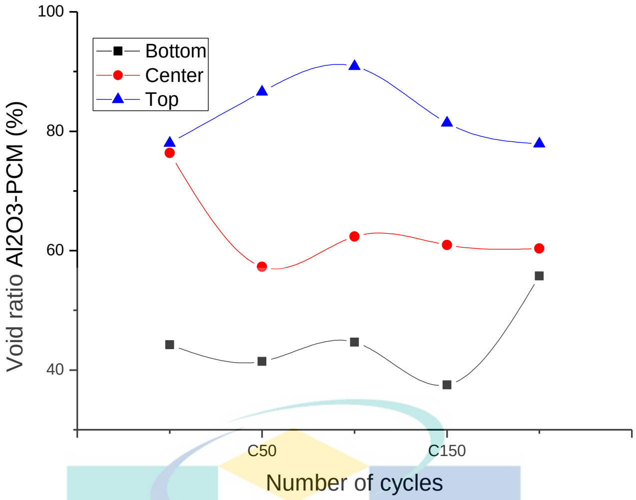

Figure 4.8 Void ratio of Al_2O_3-PCM samples against thermal cycles

In CuO-PCM composite, the lowest to the highest void ratio value has varied from 37.87% to 45.44% at the bottom. At the centre and top, the value varies from 34.13% to 45.86% and 36% to 51.34%, respectively. The highest and the lowest value of the void ratio is noted at the top and centre of C50. Void ratio value at C200 has decreased at the centre but has increased at the top and the bottom compared to C1. This trend is the same as that of Al_2O_3-PCM composite which is shown in Figure 4.9. Percentage of the highest to the lowest void ratio variation has a higher value at the top compared to the bottom and centre.

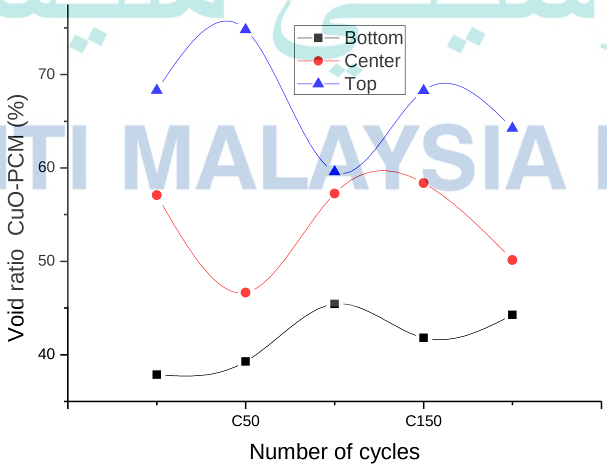

Figure 4.9 Void ratio of CuO-PCM samples against thermal cycles

In the hybrid-PCM composite, void ratio values varied from 35.88% to 47.32%, from 38.23% to 53.66% and from 44.58% to 53.81% at the bottom, centre and the top respectively. The lowest and highest void ratio values are recorded at the bottom of C100 and the top of C150. Figure 4.10 shows that void ratio has decreased after 200 thermal cycles in the top, centre and top with respect to C1. This result is contrary to pure PCM results. The highest value of void ratio swing is 40.37% at the centre, and the lowest is 19.90% at the top.

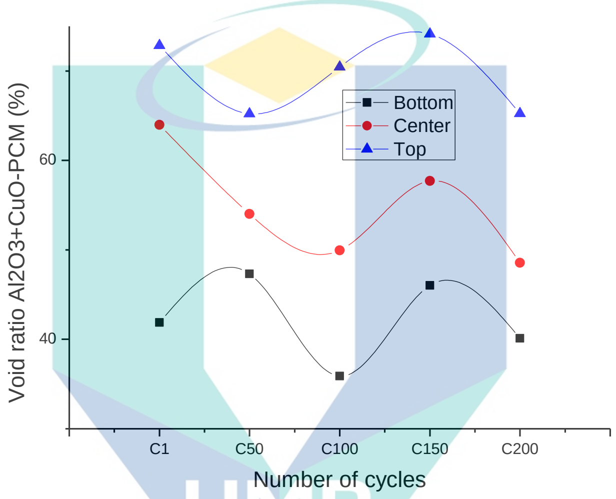

Figure 4.10 Void ratio of Al_2O_3+CuO-PCM samples against thermal cycles

Void ratio variation at the bottom of all the samples after 1, 50, 100, 150 and 200 thermal cycles are plotted in Figure 4.11. After 1 thermal cycle, the lowest and the highest void ratio value of 37.87% and 46% is observed at the bottom in CuO-PCM composite and pure PCM. At the same time, Al_2O_3+CuO-PCM and Al_2O_3-PCM have recorded the lowest and highest void ratio value of 40.11% and 55.75% after 200 thermal cycles. After 200 thermal cycles decline in void ratio value of 21.86% is noted only in hybrid-PCM composite.

The lowest value of 40.38% and the highest value of 57.97% is noted after 1 thermal cycle. After 200 thermal cycles the lowest and the highest values are obtained 37.61% and 45.07% in CuO-PCM and pure PCM. Void ratio changes at the centre for pure and Nanoparticle-PCM after many cycles are depicted in Figure 4.12. Graph in the figure shows that the void ratio value after C200 compared to C1 for all the nanoparticle-PCM composites show reduction except pure PCM. Percentage of increment in void ratio after C200 compared to C1 is 10.41%. Percentage of decline in void ratio after 200 thermal cycles in Al_2O_3-PCM , CuO-PCM and Al_2O_3+CuO-PCM compared to pure PCM is 6.92%, 16.55 and 15.18%, respectively.

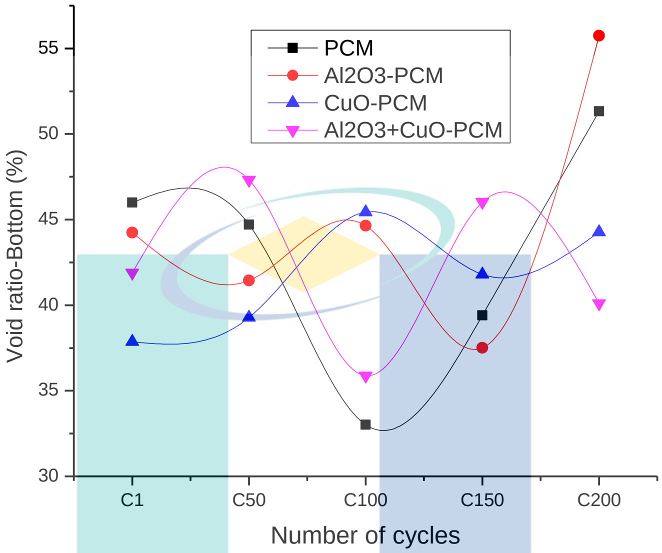

Figure 4.11 Void ratio at the bottom of all the samples against thermal cycles

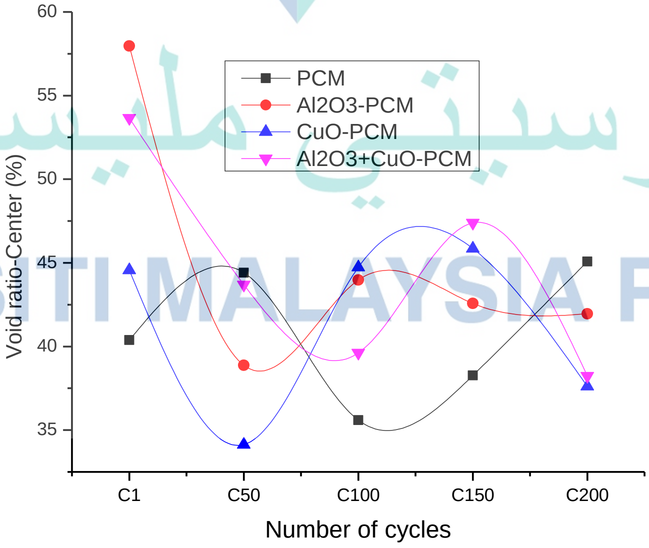

Figure 4.12 Void ratio at the center of all the samples against thermal cycles

The lowest and the highest value of void ratio variations of 36.58% and 52.52% after C1 is recorded in PCM and hybrid-PCM composite. After C200, void ratio value is the highest in CuO- PCM among all the samples. The highest void ratio value in CuO-PCM after C200 is 45.00%, which is 20.68% higher compared to the lowest void ratio obtained in Al_2O_3-PCM (37.29%). Figure 4.13 shows that in PCM, CuO-PCM and Al_2O_3+CuO-PCM have the void ratio value above 40% after C200 except for Al_2O_3-PCM.

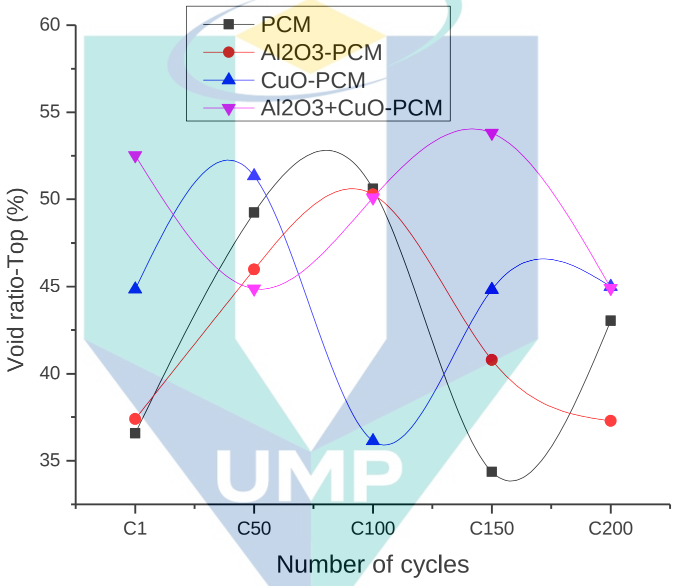

Figure 4.13 Void ratio at the top of all the samples against thermal cycles

Lowest void ratio of 40.99% is recorded in PCM and the highest value of 49.36% is found in hybrid-PCM after C1. After samples have gone 200 thermal cycles the highest void ratio value of 46.48% is noted in pure PCM. The percentage of decline in void ratio after C200 in Al_2O_3-PCM, CuO-PCM and Al_2O_3+CuO-PCM compared to base PCM is 3.18%, 12.03% and 11.64%, respectively.Figure 4.14 shows that the nanoparticle addition with base PCM has reduced the void ration after 200 thermal cycles.

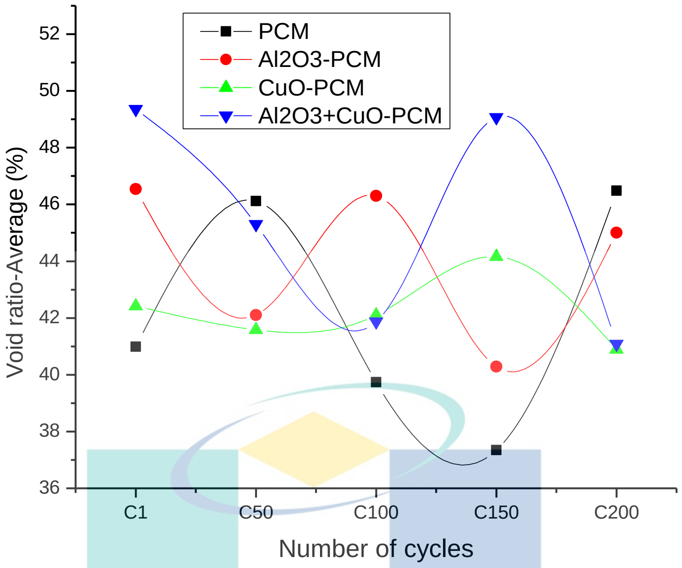

Figure 4.14 Average void ratio of all the samples against thermal cycles

This void ratio variation at the bottom, centre and the top resulted in vertical movement of bubbles due to temperature gradient. Young et al. (1959) have found that in bulk liquid, bubbles moved towards the warm region when placed in an intense temperature gradient field due to thermo-capillary forces (Hardy, 1979). The void ratio differs at different positions because voids are not frozen at the same height. This issue may be due to parameters such as temperature and liquid velocity at the solidification front. Some voids may have closed up at the same time other voids may have initiated if they are freezing from the top causing the spreading of many voids. If it is from the bottom, voids moved towards the top under gravity or centre due to zero gravity (Tagavi et al., 1990). Void location in the sample may be due to cooling temperature and cooling rate (Chala et al., 2014a). Since freezing is allowed freely at ambient temperature from the top voids are spread all over the sample. The cooling rate and the cooling temperature are not controlled in the solidification process.

Table 4.2 The lowest (*L*), the highest (*H*) and percentage of change in void ratio swing (C_s) values of all the samples

Position	**Void Ratio (%)**											
	PCM			**Al_2O_3-PCM**			**CuO-PCM**			**Al_2O_3+CuO-PCM**		
	L	**H**	**C_s (%)**	**L**	**H**	**C_s (%)**	**L**	**H**	**C_s (%)**	**L**	**H**	**C_s (%)**
Bottom	33.02	51.33	55.45	37.51	55.75	48.63	37.87	45.44	19.99	35.88	47.32	31.87
Center	35.60	45.07	26.60	38.88	51.97	49.10	34.13	45.86	34.37	38.23	53.66	40.37
Top	34.36	50.61	47.29	37.29	50.28	34.83	36.13	51.34	42.09	44.58	53.81	19.90

Figure 4.15 shows that void formation is higher at the top compared to the bottom and the centre in the pure PCM and CuO-PCM composite. This behaviour is reversed in Al_2O_3-PCM composite. Presence of Al_2O_3+CuO nanoparticles has shown greater void ratio variation at the centre. Average void ratio swing is decreased and maintained by the addition of CuO nanoparticles.

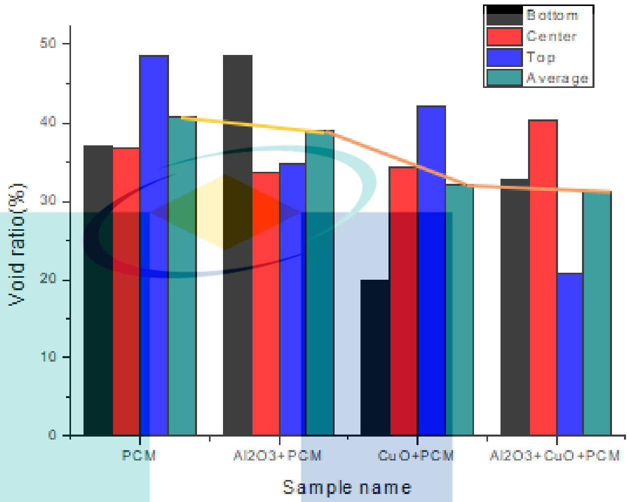

Figure 4.15 Void ratio in all the samples (C1-C200)

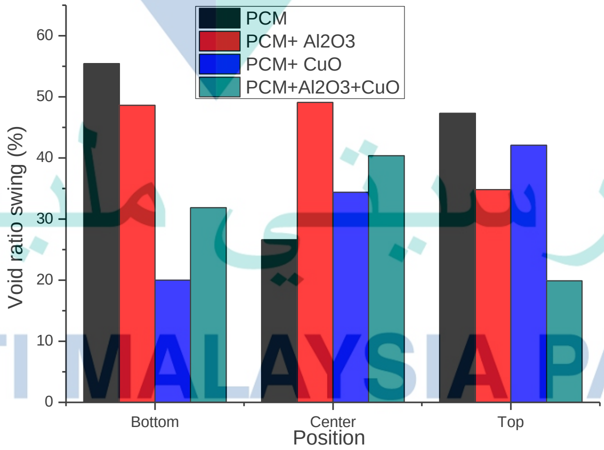

Figure 4.16 Void ratio swing in the samples

Percentage of void ratio swing from the lowest to the highest value is shown in Figure 4.16. The highest and the lowest void ratio swing are recorded at the bottom of pure PCM and at the top of Al_2O_3+CuO-PCM composite.

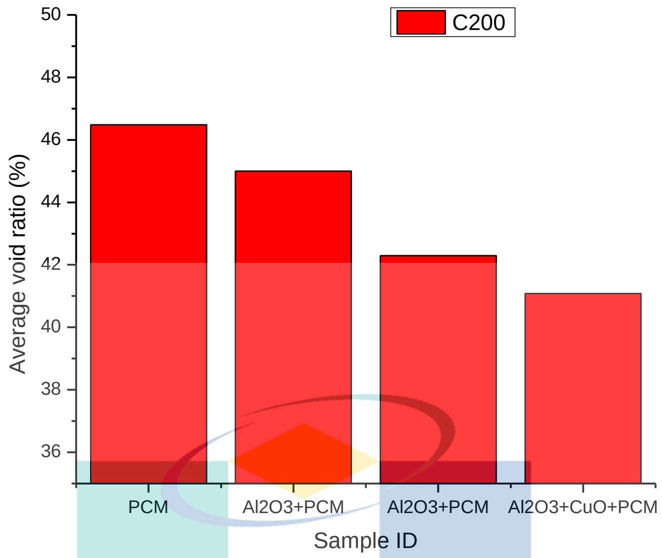

Figure 4.17 Average void ratio at C200 of all the samples

Figure 4.17 shows void formation in C200 of all the samples. At the end of 200 thermal cycles, void formation is reduced in nanoparticle composites compared to pure PCM. Changes in average void ratio compared to pure PCM after 200 thermal cycles in Al_2O_3-PCM, CuO-PCM and Al_2O_3+CuO-PCM composites are tabulated in Table 4.1. This value has changed by -3.19%, 12.03% and -11.61% in Al_2O_3-PCM, CuO-PCM and Al_2O_3+CuO-PCM composites, respectively.

Percentage of void ratio swing is reduced by addition of CuO and Al_2O_3+CuO nanoparticle. The percentage of changes in void ratio after 200 thermal cycles with respect to C1 is calculated for all the samples and plotted in the graph shown in Figure 4.18. The hybrid-PCM composite has recorded a nearly16.77% drop in voids ratio after the 200 thermal cycles compared to the average void formation after one cycle. The pure PCM has shown a 13.40% increase in void ratio after 200 thermal cycles. In both Al_2O_3-PCM and CuO-PCM, the percentage of void ratio has decreased by 3.31% and 3.62%. Hence, nanoparticle addition has decreased the void ratio after 200 thermal cycles. This reduction may be due to the higher heat capacity value of CuO and Al_2O_3 nanoparticles. These characteristics have slowed down the cooling process; hence the void formation is small due to reduction in the fast pulling of molecules or the movement of air bubbles. Among the four types of samples, a maximum decrease in the average void ratio is recorded by adding both Al_2O_3 and CuO nanoparticles together.

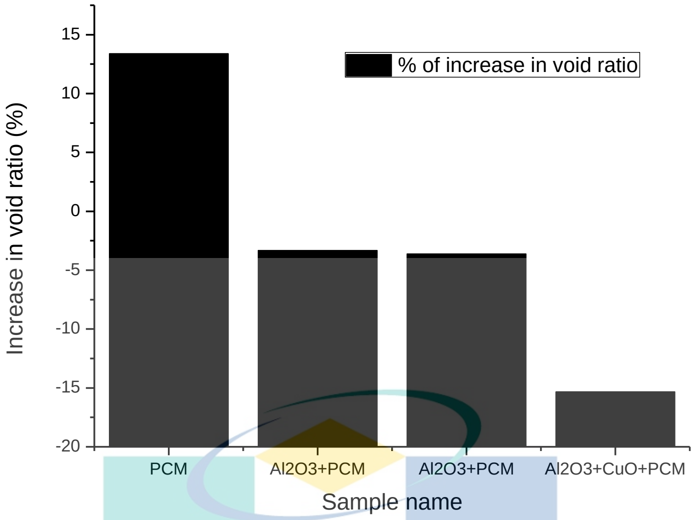

Figure 4.18 Percentage of increase in the void ratio of all the samples after 200 thermal cycles compared to C1.

4.1.3 Validation of methodology

In this research Scanning Electron Microscope is used to analyse void formation in PCM and nanoparticle-PCM composites. To quantify the voids, ImageJ software is used. This method of morphological study is validated with the help of two different paraffin wax samples of same mass. They are allowed to undergo 100 thermal cycles. The same methodology is adopted for repeated heating and cooling processes in the same atmospheric condition. Figure 4.19, (a) and (c) shows the SEM images of those two samples whereas (b) and (d) shows their corresponding binary images. The average void ratio values of two C100 paraffin wax samples are 40.29% and 39.74%. These void ratio values depicted in Figure 4.20 shows identical nature of the results. The standard deviation value is 0.3889, which is an acceptable value according to the standard deviation value index. Hence, using SEM to analyse the voids is a suitable methodology that could be adopted like other methods namely the optical microscope, Magnetic Resonance Imaging (MRI) and X-ray computed tomography. These methodologies are commonly used to study the gas voids in gelled crude oil (Chala et al., 2014b, 2015b) and void measurements in composites (Nikishkov et al., 2013).

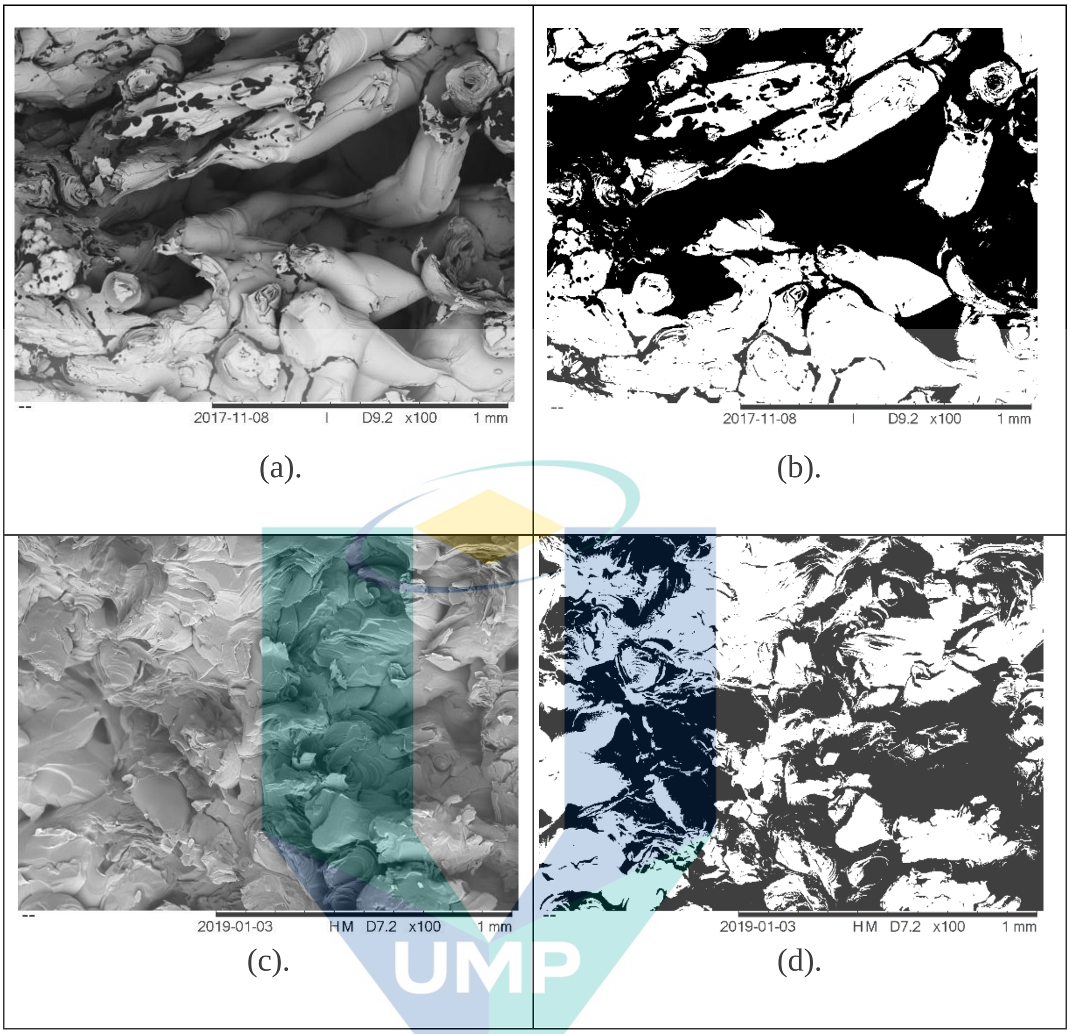

(a). (b).

(c). (d).

Figure 4.19 SEM image of sample1 (a), binary images of sample1 (b), SEM image of sample2 (c) and binary image of sample2 (d)

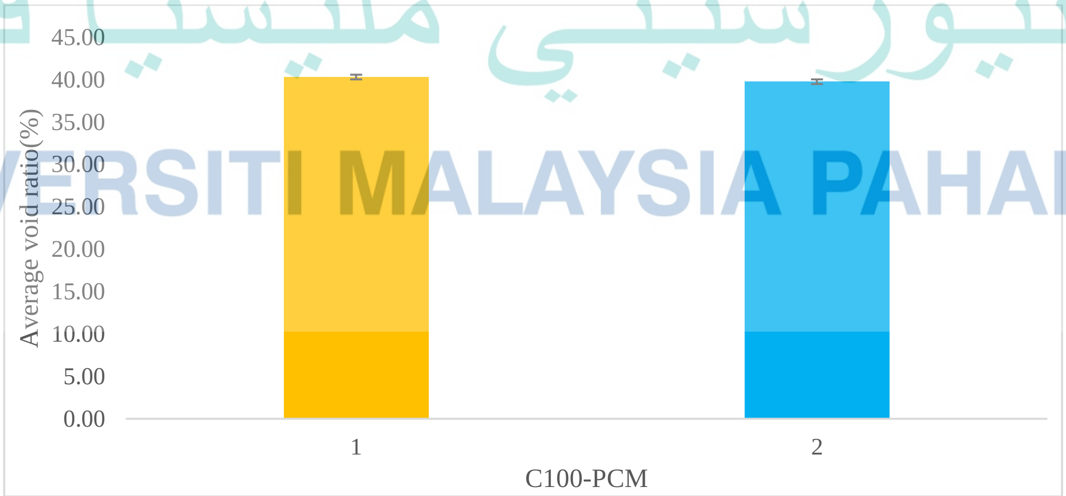

Figure 4.20 Average void ratio of two different samples of PCM after 100 thermal cycles

4.2 Thermal energy storage properties

DSC curves of heating (a) and cooling (b) of the PCM is shown in Figure 4.21. The heating graph shows that the highest melting temperature is observed at C150. The lowest and the highest solidification temperature is noted at C150 and C50, respectively, which is indicated in the cooling curve. DSC curves of heating (a) and cooling (b) of the Al_2O_3-PCM is shown in Figure 4.22. The heating curve of Al_2O_3-PCM indicates melting temperature variations against thermal cycles. On the other hand, cooling curve shows the highest and the lowest solidification temperature at C1 and C50. In Figure 4.23, heating (a) and cooling (b) of CuO-PCM is shown. Shift in the melting temperature due to repeated thermal cycling is observed in the heating curve and the highest and lowest solidification temperature is indicated in the cooling curve. Solidification temperature variation is clearly seen in the cooling graph. Figure 4.24 shows the DSC graph of both heating (a) and cooling (b) process of Hybrid-PCM. The lowest and the highest melting temperature is observed at C200 and C50 in the heating curve.Minimal variation in the solidification temperature is noted from the cooling graph. All the DSC curves show two peaks. The main peak and lower peak represent the solid-liquid and the solid-solid transitions, respectively.

Multiple relative peaks observed in the main peak in heating and cooling curves represent the melting and solidification points of the samples during different thermal cycles. Data extracted from the graph is discussed in the following sections in detail. Data of the onset temperature of melting (T_{onM}) and solidification (T_{onS}) offset temperature of melting (T_{offM}) and solidification (T_{offS}) and percentage of variation in T_{onM} and T_{offM} from C1 are tabulated in Table 4.3. Melting temperatures (T_M), solidification temperature (Ts), and percentage of variations after 200 thermal cycles are listed in Table 4.4.

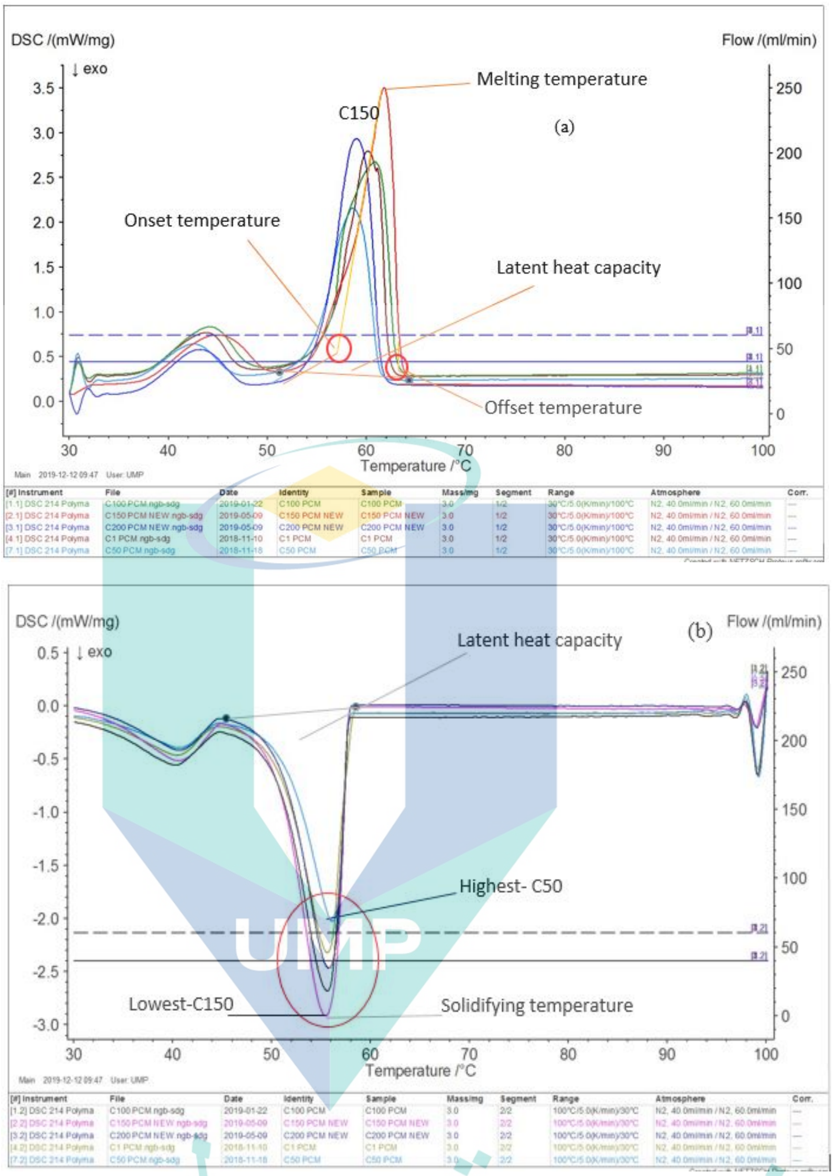

Figure 4.21 DSC- (a) heating and (b) cooling curves of PCM

In pure PCM, onset temperature for melting (T_{onM}) varies from 53.9°C to 56.9°C. By adding of Al_2O_3 nanoparticle, the highest value of T_{onM} has fallen to 56.1°C. A further reduction to 55.4°C is noted with the addition of CuO and Al_2O_3+CuO nanoparticles with base PCM. This shows that nanoparticle addition helps to start the melting process in nanoparticle-PCM composite earlier than pure PCM. This helps to reduce the loading time of the LHTESS. The melting process ended in the range of 61.3°C to 63.4°C in pure PCM. In Al_2O_3-PCM, CuO-PCM and Al_2O_3+CuO-PCM composites, the T_{offM} value varied from 61.4°C to 62.9°C, 61.8°C to 62.5°C and 61.8°C to 62.3°C, respectively. This range shows that melting is completed faster in nanoparticle-PCM composites compared to pure PCM.

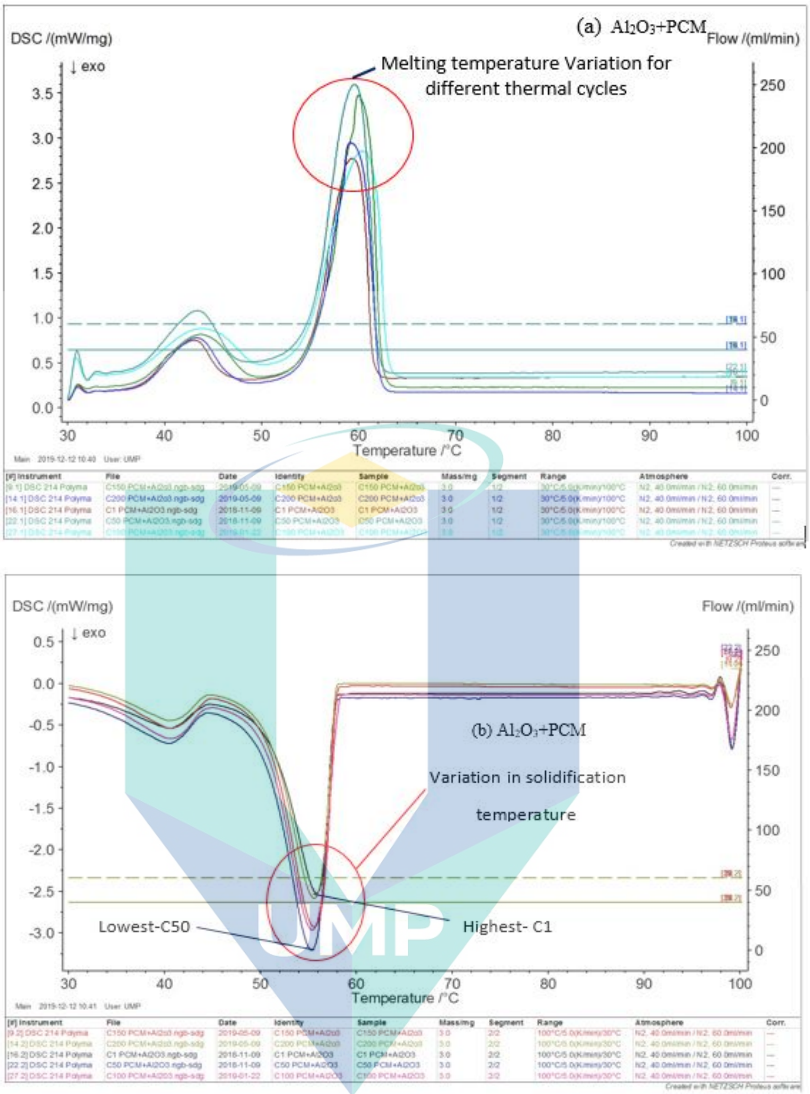

[#] Instrument	File	Date	Identity	Sample	Mass/mg	Segment	Range	Atmosphere	Corr.
[9.1] DSC 214 Polyma	C150 PCM+Al2o3.ngb-sdg	2019-05-09	C150 PCM+Al2o3	C150 PCM+Al2o3	3.0	1/2	30°C/5.0(K/min)/100°C	N2, 40.0ml/min / N2, 60.0ml/min	—
[14.1] DSC 214 Polyma	C200 PCM+Al2o3.ngb-sdg	2019-05-09	C200 PCM+Al2o3	C200 PCM+Al2o3	3.0	1/2	30°C/5.0(K/min)/100°C	N2, 40.0ml/min / N2, 60.0ml/min	—
[16.1] DSC 214 Polyma	C1 PCM+Al2O3.ngb-sdg	2018-11-09	C1 PCM+Al2O3	C1 PCM+Al2O3	3.0	1/2	30°C/5.0(K/min)/100°C	N2, 40.0ml/min / N2, 60.0ml/min	—
[22.1] DSC 214 Polyma	C50 PCM+Al2O3.ngb-sdg	2018-11-09	C50 PCM+Al2O3	C50 PCM+Al2O3	3.0	1/2	30°C/5.0(K/min)/100°C	N2, 40.0ml/min / N2, 60.0ml/min	—
[27.1] DSC 214 Polyma	C100 PCM+Al2O3.ngb-sdg	2019-01-22	C100 PCM+Al2O3	C100 PCM+Al2O3	3.0	1/2	30°C/5.0(K/min)/100°C	N2, 40.0ml/min / N2, 60.0ml/min	—

[#] Instrument	File	Date	Identity	Sample	Mass/mg	Segment	Range	Atmosphere	Corr.
[9.2] DSC 214 Polyma	C150 PCM+Al2o3.ngb-sdg	2019-05-09	C150 PCM+Al2o3	C150 PCM+Al2o3	3.0	2/2	100°C/5.0(K/min)/30°C	N2, 40.0ml/min / N2, 60.0ml/min	—
[14.2] DSC 214 Polyma	C200 PCM+Al2o3.ngb-sdg	2019-05-09	C200 PCM+Al2o3	C200 PCM+Al2o3	3.0	2/2	100°C/5.0(K/min)/30°C	N2, 40.0ml/min / N2, 60.0ml/min	—
[16.2] DSC 214 Polyma	C1 PCM+Al2O3.ngb-sdg	2018-11-09	C1 PCM+Al2O3	C1 PCM+Al2O3	3.0	2/2	100°C/5.0(K/min)/30°C	N2, 40.0ml/min / N2, 60.0ml/min	—
[22.2] DSC 214 Polyma	C50 PCM+Al2O3.ngb-sdg	2018-11-09	C50 PCM+Al2O3	C50 PCM+Al2O3	3.0	2/2	100°C/5.0(K/min)/30°C	N2, 40.0ml/min / N2, 60.0ml/min	—
[27.2] DSC 214 Polyma	C100 PCM+Al2O3.ngb-sdg	2019-01-22	C100 PCM+Al2O3	C100 PCM+Al2O3	3.0	2/2	100°C/5.0(K/min)/30°C	N2, 40.0ml/min / N2, 60.0ml/min	—

Figure 4.22 DSC- (a) heating (b) cooling curves of Al_2O_3-PCM

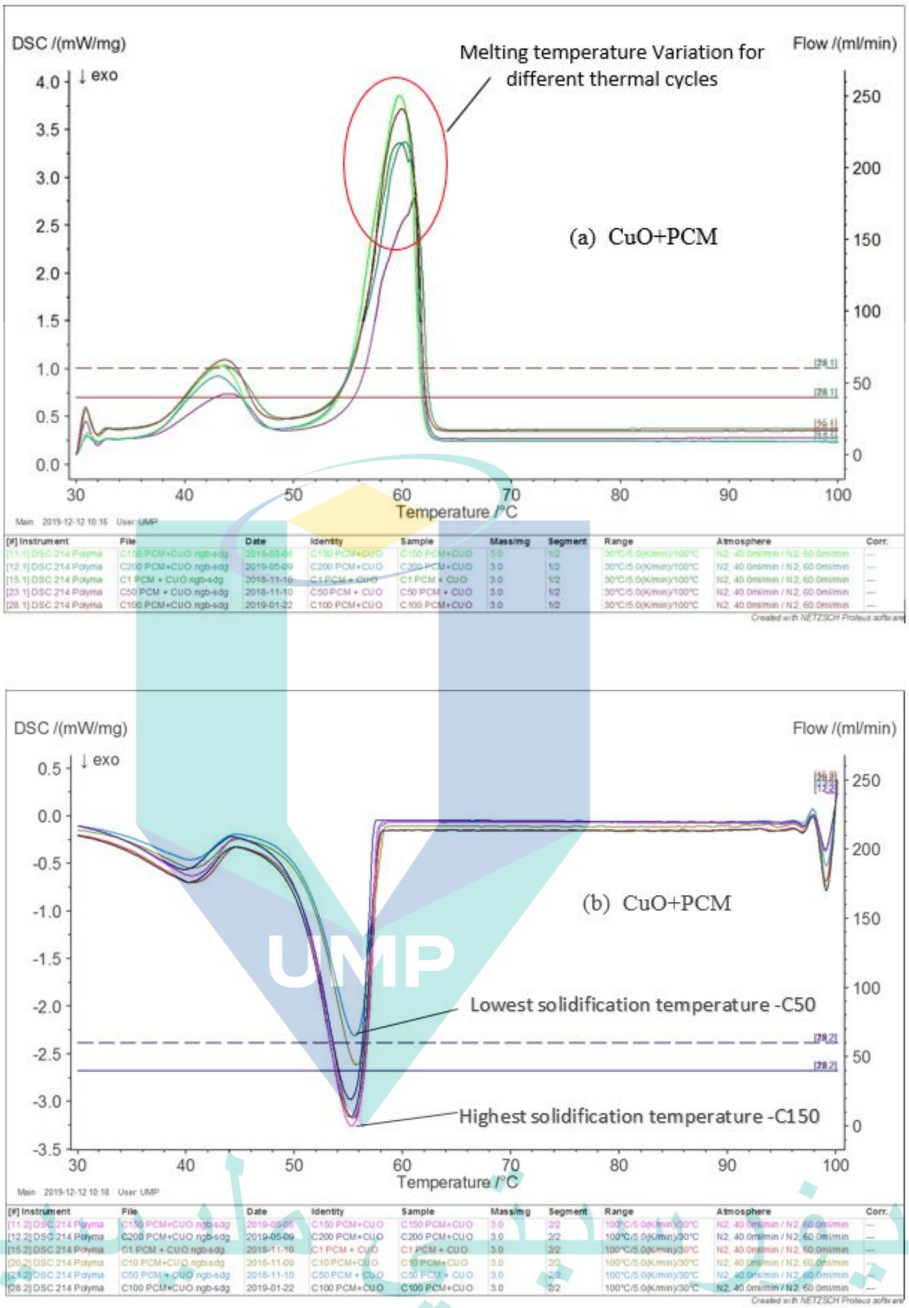

[#] Instrument	File	Date	Identity	Sample	Mass/mg	Segment	Range	Atmosphere	Corr.
[11.1] DSC 214 Polyma	C150 PCM+CUO.ngb-sdg	2019-05-08	C150 PCM+CUO	C150 PCM+CUO	3.0	1/2	30°C/5.0(K/min)/100°C	N2, 40.0ml/min / N2, 60.0ml/min	---
[12.1] DSC 214 Polyma	C200 PCM+CUO.ngb-sdg	2019-05-09	C200 PCM+CUO	C200 PCM+CUO	3.0	1/2	30°C/5.0(K/min)/100°C	N2, 40.0ml/min / N2, 60.0ml/min	---
[15.1] DSC 214 Polyma	C1 PCM + CUO.ngb-sdg	2018-11-10	C1 PCM + CUO	C1 PCM + CUO	3.0	1/2	30°C/5.0(K/min)/100°C	N2, 40.0ml/min / N2, 60.0ml/min	---
[23.1] DSC 214 Polyma	C50 PCM + CUO.ngb-sdg	2018-11-10	C50 PCM + CUO	C50 PCM + CUO	3.0	1/2	30°C/5.0(K/min)/100°C	N2, 40.0ml/min / N2, 60.0ml/min	---
[28.1] DSC 214 Polyma	C100 PCM+CUO.ngb-sdg	2019-01-22	C100 PCM+CUO	C100 PCM+CUO	3.0	1/2	30°C/5.0(K/min)/100°C	N2, 40.0ml/min / N2, 60.0ml/min	---

[#] Instrument	File	Date	Identity	Sample	Mass/mg	Segment	Range	Atmosphere	Corr.
[11.2] DSC 214 Polyma	C150 PCM+CUO.ngb-sdg	2019-05-08	C150 PCM+CUO	C150 PCM+CUO	3.0	2/2	100°C/5.0(K/min)/30°C	N2, 40.0ml/min / N2, 60.0ml/min	---
[12.2] DSC 214 Polyma	C200 PCM+CUO.ngb-sdg	2019-05-09	C200 PCM+CUO	C200 PCM+CUO	3.0	2/2	100°C/5.0(K/min)/30°C	N2, 40.0ml/min / N2, 60.0ml/min	---
[15.2] DSC 214 Polyma	C1 PCM + CUO.ngb-sdg	2018-11-10	C1 PCM + CUO	C1 PCM + CUO	3.0	2/2	100°C/5.0(K/min)/30°C	N2, 40.0ml/min / N2, 60.0ml/min	---
[20.2] DSC 214 Polyma	C10 PCM+CUO.ngb-sdg	2018-11-09	C10 PCM+CUO	C10 PCM+CUO	3.0	2/2	100°C/5.0(K/min)/30°C	N2, 40.0ml/min / N2, 60.0ml/min	---
[23.2] DSC 214 Polyma	C50 PCM + CUO.ngb-sdg	2018-11-10	C50 PCM + CUO	C50 PCM + CUO	3.0	2/2	100°C/5.0(K/min)/30°C	N2, 40.0ml/min / N2, 60.0ml/min	---
[28.2] DSC 214 Polyma	C100 PCM+CUO.ngb-sdg	2019-01-22	C100 PCM+CUO	C100 PCM+CUO	3.0	2/2	100°C/5.0(K/min)/30°C	N2, 40.0ml/min / N2, 60.0ml/min	---

Figure 4.23 DSC- (a) heating and (b) cooling curves of CuO-PCM

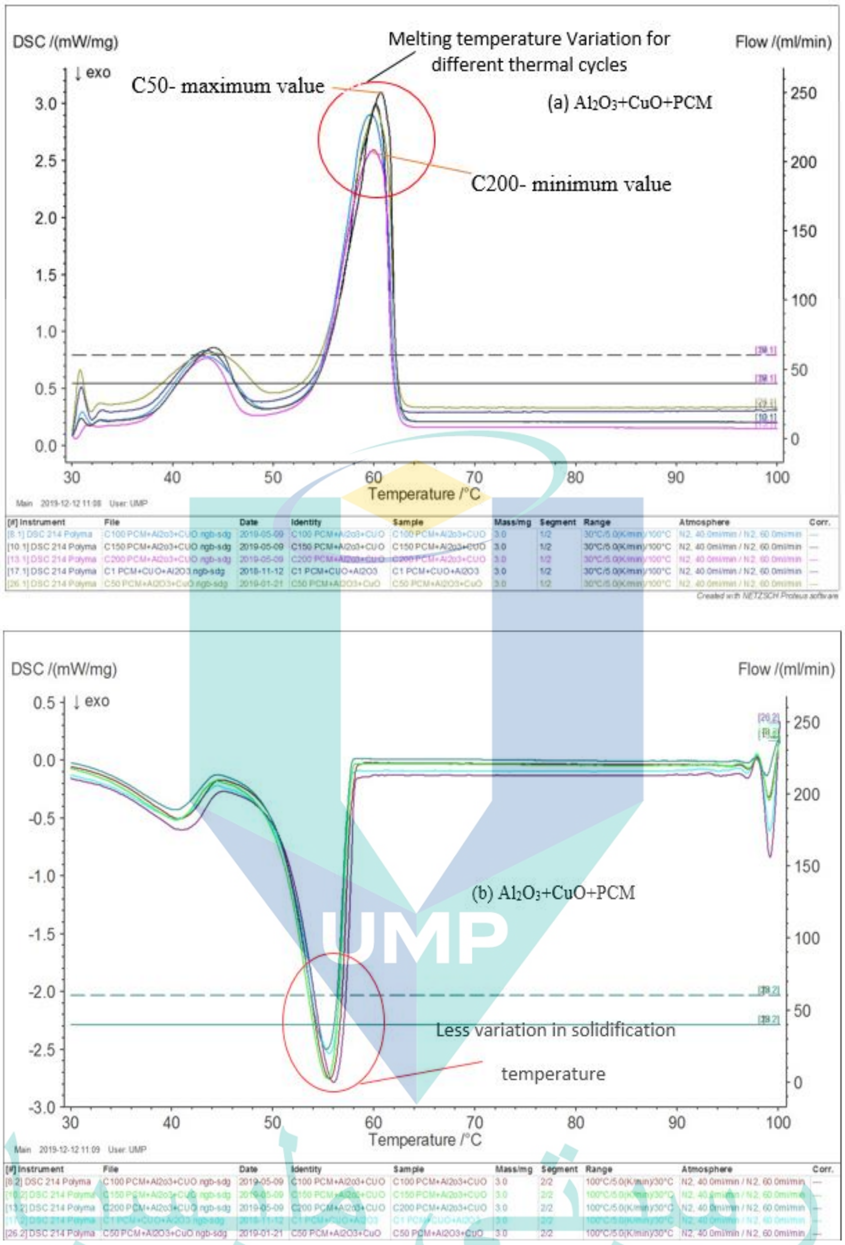

Figure 4.24 DSC- (a) heating and (b) cooling curve of Al_2O_3+CuO+PCM

4.2.1 Thermal reliability properties of pure and nanoparticle-PCM composites

Onset and offset temperatures are the two main factors that have impacted both loading and unloading in LHTESS. From Figure 4.25, onset temperature for melting (T_{onM}) of pure PCM fluctuates from C1 to C200. Minimum and maximum value of 53.9°C to 56.9°C is found in C50 and C150. By addition of Al_2O_3 nanoparticle, the highest value of T_{onM} fell to 56.1°C at C200 but this value is higher by 2.75% compared to the highest value of PCM at C200. The highest T_{onM} value of 55.4°C is noticed at C100 and C150 by addition of CuO and Al_2O_3+CuO nanoparticle with base PCM. Percentage of variation in T_{onM} in CuO-PCM and Al_2O_3+CuO-PCM is 0.55% and -1.83%.This fall in hybrid nanoparticle addition helps to start the melting process in hybrid-PCM composite earlier than pure PCM. This helps to reduce the loading time of LHTESS.

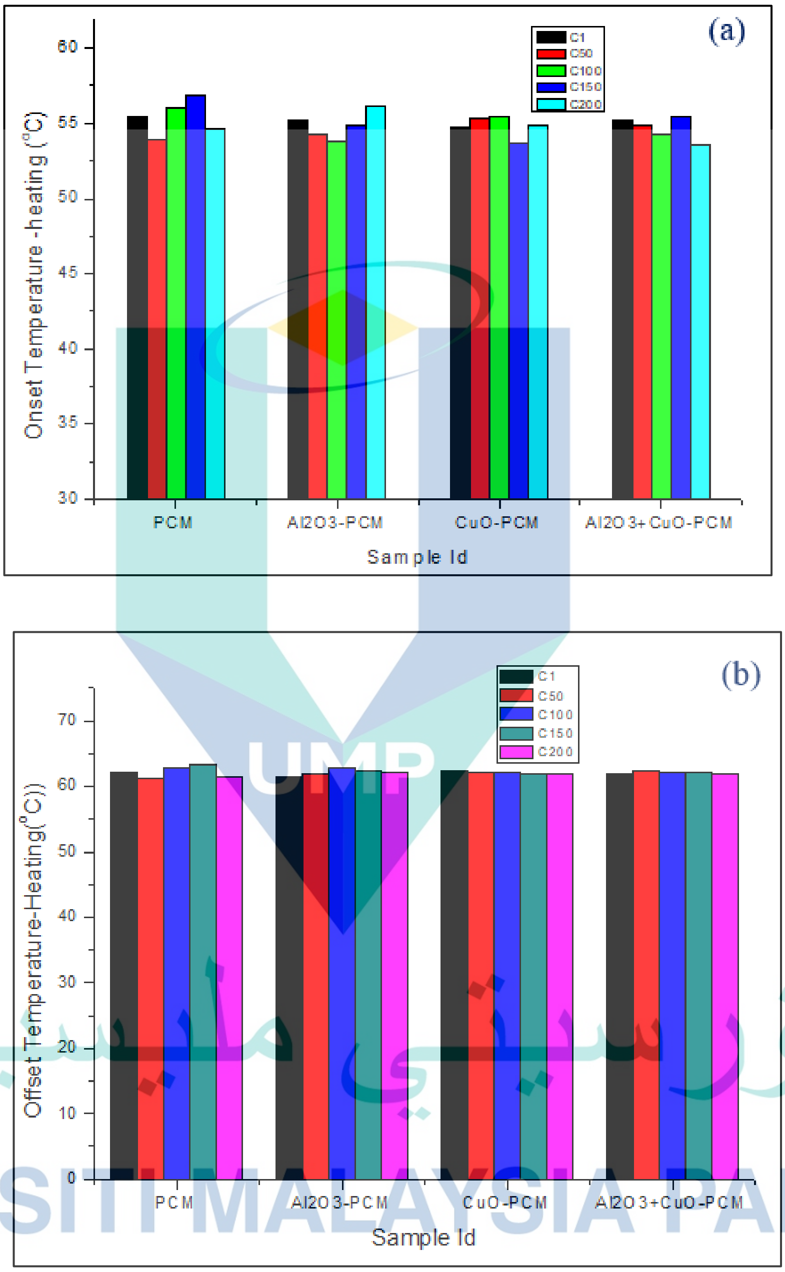

Figure 4.25 (a) onset and (b) offset temperature of samples while heating for C1, C50, C100, C150 and C200

Table 4.3 Onset, offset temperatures and loading, unloading times of samples

Sample name	**No. of thermal cycles**	**Heating (ºC)**		**Cooling (ºC)**	
		T_{onM}	T_{offM})	T_{onS}	T_{offS})
PCM	1	55.4	62.2	57.8	49.9
	50	53.9	61.3	57.8	50.8
	100	56.0	62.9	57.7	49.8
	150	56.9	63.4	57.8	49.7
	200	54.6	61.5	57.8	50.0
Variation (%)	1-200	-1.44	-1.13	0.0	0.20
Al_2O_3- PCM	1	55.2	61.4	57.8	50.1
	50	54.3	62.0	57.7	49.5
	100	53.8	62.9	58.0	49.6
	150	54.9	62.3	57.9	49.8
	200	56.1	62.1	57.9	49.8
Variation (%)	1-200	1.63	1.14	-0.17	-0.60
CuO- PCM	1	54.7	62.5	57.8	49.6
	50	55.3	62.1	57.9	49.9
	100	55.4	62.2	57.6	49.4
	150	53.7	61.8	57.7	49.6
	200	54.9	61.9	57.3	49.4
Variation (%)	1-200	0.37	-0.96	-0.87	-0.40
Al_2O_3 + CuO - PCM	1	55.2	61.8	57.6	49.8
	50	54.9	62.3	58.1	50.2
	100	54.3	62.2	57.8	49.9
	150	55.4	62.2	57.5	49.6
	200	53.6	62.0	57.6	49.5
Variation (%)	1-200	-2.90	0.32	0.0	-0.60

Melting process ended in the range of 61.3°C to 63.4°C in pure PCM. In Al_2O_3-PCM, CuO-PCM and Al_2O_3+CuO-PCM composites, T_{offM} value varies from 61.4°C to 62.9°C, 61.8°C to 62.5°C and 61.8°C to 62.3°C, respectively. This range shows that the melting process is completed faster in nanoparticle-PCM composites compared to pure PCM. T_{onM} and T_{offM} for the samples as depicted in Figure 4.25. This shows that there is a notable fluctuation in the onset temperature, whereas the fluctuation is less in the offset temperature during the heating process. The highest and the lowest values of percentage of variation in T_{onM} have also been noted in Al_2O_3-PCM composite (1.63%) and Al_2O_3+CuO-PCM (-2.90%) composite respectively. The lowest T_{offM} value is recorded in pure PCM (-1.13%), and the highest is found in Al_2O_3-PCM composite (1.14%). Variations in T_{onM} and T_{offM} are depicted in Figure 4.26.

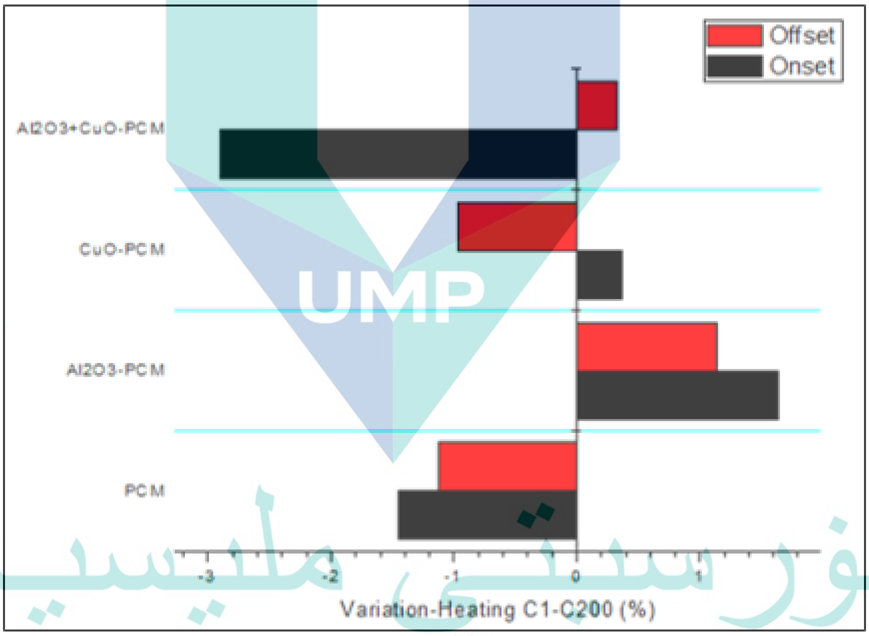

Figure 4.26 Variations in T_{onM} and T_{offM} for the samples

Onset and offset temperature for the cooling process of all the samples are plotted in Figure 4.27. In the process of cooling observed for 200 thermal cycles, solidification started in the range of 57.7°C to 57.8°C in pure PCM. This is the least variation in the onset temperature of solidification within 200 thermal cycles (0.1°C) in pure PCM. On the other hand, solidification ends in the range of 49.7°C to 50.8°C, which is the highest value among all the samples. The highest values of T_{onS} are 58°C, 57.9°C and 58.1°C in Al_2O_3-PCM, CuO-PCM and Al_2O_3+CuO-PCM composites, respectively.

Even though addition of nanoparticles increases the percentage of variation of T_{onS} at C200, with reference to C1 this value has decreased. The decrement was 0.2%, -0.6%, -0.4% and -0.6% in pure PCM, Al_2O_3-PCM, CuO-PCM and Al_2O_3+CuO-PCM, respectively. Thus, addition of nanoparticles reduces solidification onset temperature as the number of cycles have increased compared to pure PCM. If the solidification process starts earlier, then more stored heat energy could have been released from the material, and the super-cooling effect can be reduced.

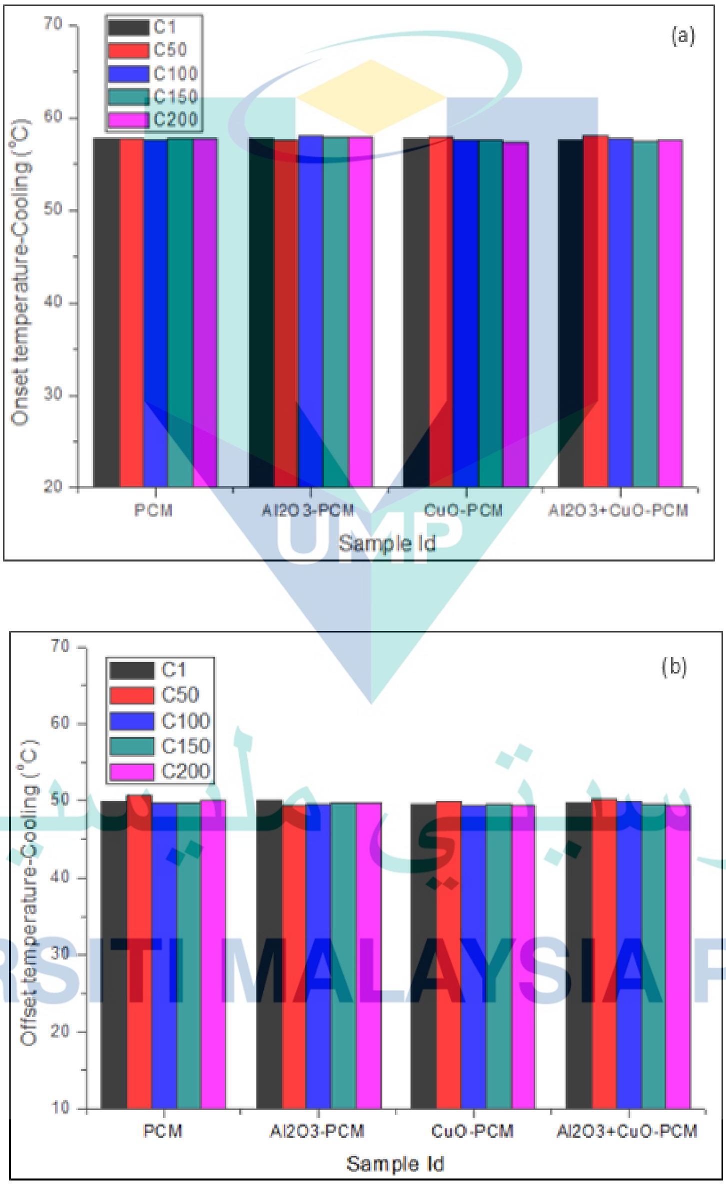

Figure 4.27 Onset and (b) Offset temperature of samples while cooling for C1,C50, C100, C150 and C200

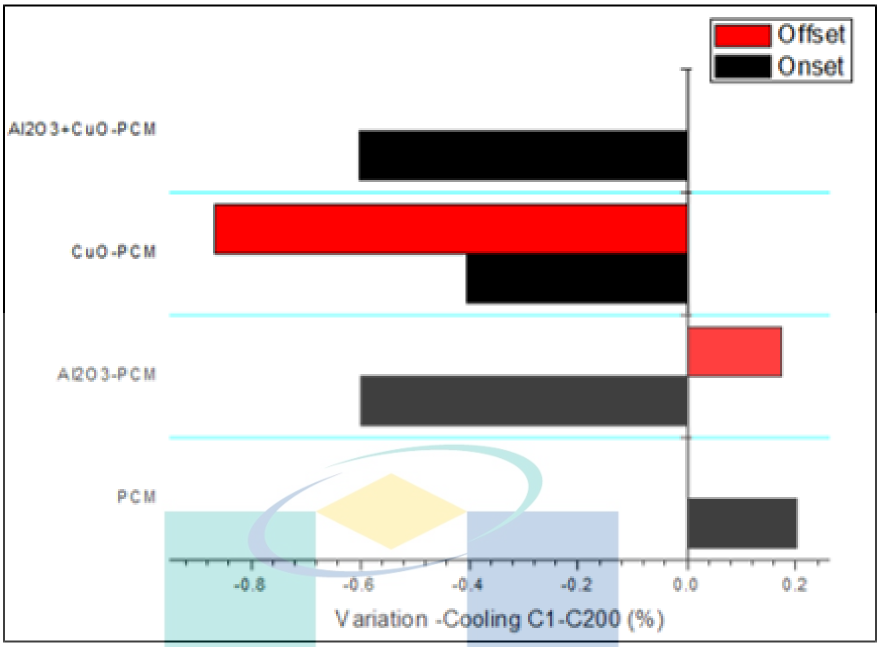

Figure 4.28 Variations (C1-C200) in T_{onS} and T_{offS} for the samples

Variations in T_{onS} and T_{offS} for the samples is as depicted in Figure 4.28. Variation in T_{offS} after 200 thermal cycles from C1 in Al_2O_3-PCM, CuO-PCM are 0.17% and -0.87% respectively. Whereas, pure PCM and Al_2O_3+CuO-PCM have shown 0.0% variation. Variation in the range of both onset and offset temperatures is less than 2% for all the samples except pure PCM. Addition of nanoparticle has less effect on T_{onS} and T_{offS}. This effect may be due to the settlement of nanoparticles during repeated heating. Solidification starts at a lower temperature in nanoparticle PCM compared to pure PCM due to the low resistance nature of nanoparticles (Mandal et al., 2019).

4.2.2 Melting and solidification temperature analysis

Melting and solidification temperatures are the two main parameters that affect efficiency of thermal energy storage system. Melting and solidifying temperatures of all the samples obtained from the DSC curve are tabulated in Table 4.4.

Table 4.4 Melting and solidification temperatures and enthalpy of the samples

Sample Name	**Cycle number**	**T_m (°C)**	**Change in T_m (°C) (50 cycles)**	**T_s (°C)**	**Change in T_s (°C) (50 cycles)**
PCM	1	60.0		55.5	
	50	58.5	-1.50	56.0	0.53
	100	61.0	2.48	55.5	-0.50
	150	62.0	1.02	55.5	0.00
	200	59.0	-3.00	56.0	0.49
Variation (%)	1-200	-1.67		0.94	
Al_2O_3-PCM	1	59.5		56.0	
	50	59.5	0.04	55.5	-0.47
	100	60.5	1.00	55.5	0.00
	150	60.0	-0.52	55.5	-0.02
	200	59.0	-0.99	55.5	0.01
Variation (%)	1-200	-0.81		-0.86	
CuO-PCM	1	59.5		55.5	
	50	61.0	1.47	55.5	-0.02
	100	60.0	-0.98	55.0	-0.50
	150	59.5	-0.47	55.5	0.53
	200	60.0	0.50	55.0	-0.50
Variation (%)	1-200	0.85		-0.88	
Al_2O_3+CuO-PCM	1	60.0		55.5	
	50	60.0	-0.02	56.0	0.48
	100	59.5	-0.48	55.5	-0.48
	150	60.5	1.00	55.5	0.00
	200	60.0	-0.50	55.5	0.00
Variation (%)	1-200	0.0		0.0	

The melting temperature range of pure PCM is between 58.52°C to 62.01°C. After 50, 100, 150 and 200 thermal cycles, the melting temperature value changes by -1.50°C, 2.48°C, 1.02°C, and -3.0°C, respectively. By addition of nanoparticle, the melting temperature value reduces and falls in the range of 59.01°C to 60.53°C, 59.5°C to 60.98°C, and 59.52°C to 60.52°C in Al_2O_3-PCM, CuO-PCM and Al_2O_3+CuO-PCM composites, respectively. There is no linear relationship found in the changes in T_m as the number of thermal cycles increased to 50, 100, 150 and 200 cycles. Nanoparticle addition reduces the melting temperature of the nanoparticle-PCM composites when compared to pure PCM. These results are in agreement with the work of Lin et al. , who worked on paraffin wax with CuO nanoparticles of a different mass fraction(S. C. Lin & Al-kayiem, 2016) (Mandal et al., 2019). The research of Kumar & Krishna on paraffin wax with Al_2O_3+CuO nanoparticles of different weight fraction (Kumar & Krishna, 2019) also shows similar results as this study. Figure 4.29 shows that temperature variation in pure PCM is higher compared to nanoparticle-PCMs. So, nanoparticle addition reduces the variation in melting temperature after 200 thermal cycles, and this value is negligible in Al_2O_3+CuO-PCM composite.

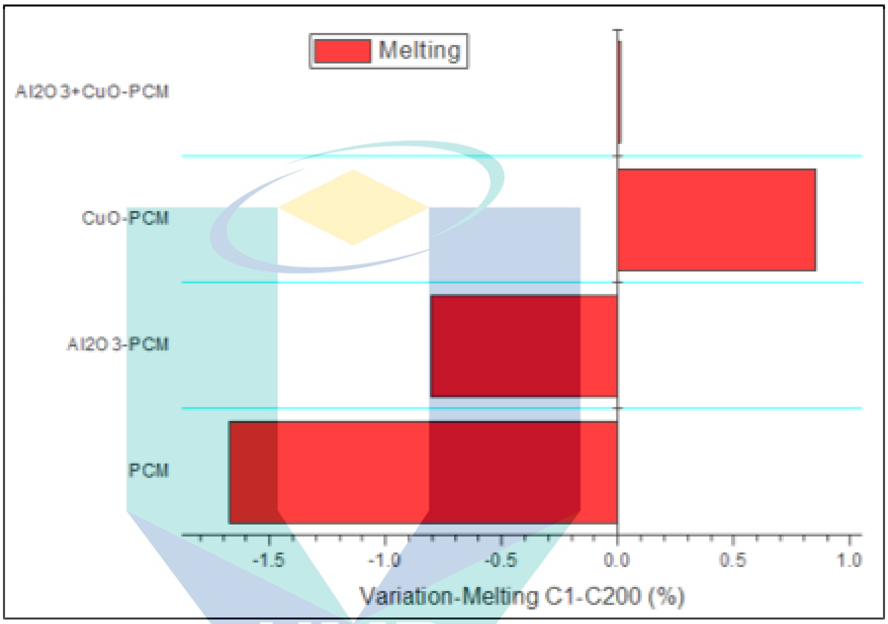

Figure 4.29 Variation in melting temperature of samples

Solidification temperature lies in the range of 55.50°C to 56.02°C, 55.51°C to 56, 55°C to 55.52°C and 55.52°C to 56°C in pure PCM, Al_2O_3-PCM, CuO-PCM and Al_2O3+ CuO-PCM composites respectively. According to this data, the solidification temperature of all the samples lies in the range of 55°C to 56°C only. From Table 4.4, solidification temperature changes after 50, 100, 150, 200 thermal cycles show a non-linear nature. The maximum to minimum value change for every 50 cycles in Ts are 0.53°C and -0.50°C respectively. After 100 cycles, there is no change in Ts.is observed in all the samples. Only after 200 thermal cycles in Al_2O_3+ CuO-PCM, the changes are observed. This change shows stability of the solidification process in the sample, even after repetitive cycling. Nanoparticle addition decreases the solidification temperature of base PCM. Nanoparticle PCM composites have low solidification temperature compared to the pure PCM. Figure 4.30 shows the percentage of variation (C1-C200) in the solidification of all the samples. The percentage of variation is negligible in Al_2O_{3+} CuO-PCM composite whereas there is less than 1% variation in all the other samples. These data are considered to have an insignificant effect on the performance characteristics of LHTESS.

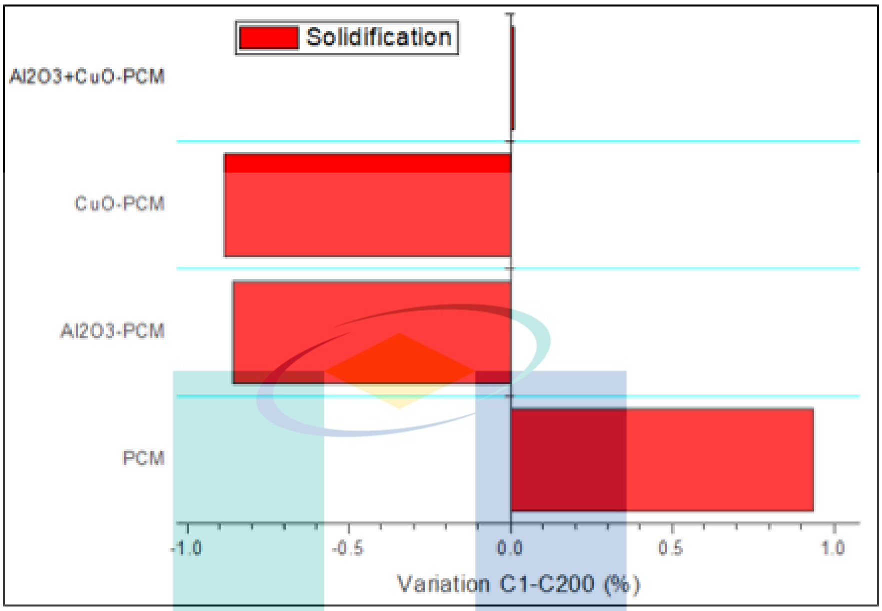

Figure 4.30 Variation in solidification temperature of samples

Melting and solidification temperatures have been reduced due to the addition of nanoparticle. These changes may be due to less heat resistance of the nanoparticles, and they behave as nucleation agent and cause the decrement in melting and solidification temperature (S. C. Lin & Al-kayiem, 2016; Mandal et al., 2019). Presence of defects as a result of solidification presents changes in melting temperature (Jiang et al., 2015). So, void formation may affect the melting and solidification process. Figure 4.31 reveals that melting and solidification temperature variations have a linear relationship with voids. In Al_2O_3+CuO-PCM composite, the void variations are very low compared to other samples. Hence, the variation in melting and solidification temperature is almost null. So, Al_2O3+CuO addition stabilizes the melting and solidification process without any temperature fluctuations. Thus, Al_2O_3-PCM and Al_2O_3+CuO-PCM composites show good stability in energy-releasing characteristics.

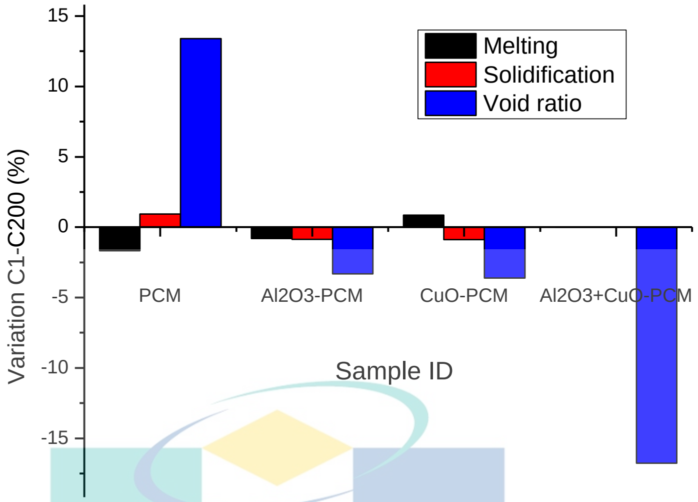

Figure 4.31 Percentage of variation (C1-C200) of voids and melting and solidification temperature

4.2.3 Thermal energy storage behaviour of pure and nano-PCM composites

Changes in the latent heat of paraffin wax as a result of variation of the thermal cycles are measured using DSC analysis. Solid-liquid melting peaks and liquid-solid solidification peaks are used to measure the melting and solidification latent heat values of samples, respectively (Zeng et al., 2016). Latent heat values of all the samples C1, C50, C100, C150 and C200 from DSC graph are depicted in Figure 4.32.

Latent heat value decreases from C1 to C50 and then increases after C50 till C150 in pure PCM and CuO-PCM composites. Whereas, latent heat value increases in Al_2O_3-PCM from C1 to C50 and then decreases till C200. In Al_2O_{3+} CuO-PCM composite latent heat value increases from C1 to C150, then decreases until C200. All the samples show decrement after 150 cycles. Thus, changes in latent heat value are non -linear due to the repetitive heating till 200 thermal cycles and this result is in agreement with Zang et al., (2017) who has worked on the thermal stability of paraffin wax till 10,000 accelerated thermal cycles (L. Zhang & Dong, 2017b).

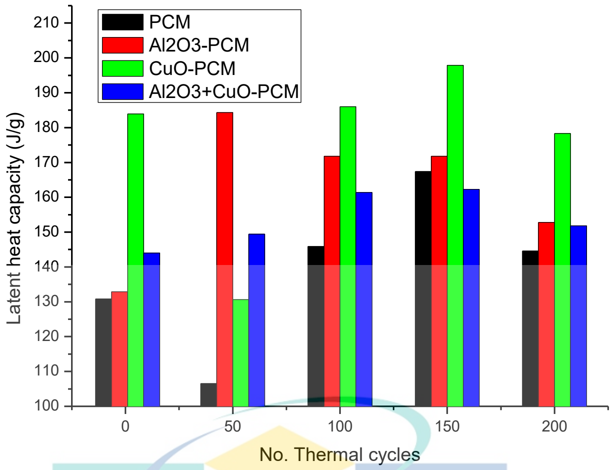

Figure 4.32 Latent heat value against the thermal cycles

This non-linear change may be due to the physicochemical changes that have taken place in the impurity and paraffin mixture during the phase change process (L. Zhang & Dong, 2017b). Moisture availability due to the absorption of moisture from the surrounding and purity of commercial-grade paraffin wax in the market is also a reason for fluctuations in latent heat value after many cycling (A. Sharma et al., 2002). The highest value of latent heat value of 167.4J/g is recorded at the 150th cycle, which is a 13.17% decline from the reference value.

The highest value of latent heat capacity is recorded as 184.3 J/g at C50, 197.9 J/g at C150 and 162.3 J /g at C150 in Al_2O_3-PCM, CuO-PCM and Al_2O_{3+}CuO-PCM composites, respectively. Al_2O_3 and CuO nanoparticle addition show an increment in latent heat capacity value compared to PCM. This result is in agreement with Colla et al. , (2016) who investigated nano-PCMs for energy storage and passive cooling. In this work, latent heat of RT20 (Rubitherm- paraffin wax with melting temperature of 20^{o}C) has increased by the addition of Al_2O_3 and carbon black nanoparticles separately (A. L. Colla et al., 2016). Results obtained by Prabhu and ValanArasu (2020) strengthen the findings in this study. TiO_2-Ag-paraffin wax composite shows an increment in thermal conductivity due to addition of nanoparticles (Prabhu & ValanArasu, 2020). These results are contrary to the results obtained by Jiang et al. , (2015). This research shows that latent heat value decreased by addition of Al_2O_3 nanoparticle (Jiang et al., 2015). Nourani et al., (2016) have concluded that Al_2O_3 nanoparticles (5%) addition with paraffin wax has no significant changes in latent heat capacity and phase change temperature which is contrary to the current research (Nourani et al., 2016). Changes in latent heat value for every 50 thermal cycles is tabulated in Table 4.5.

At C1, the latent heat capacity of melting (ΔH_m) shows an increment of 2.1 J/g, 53.1 J/g, and 13.2 J/g in Al_2O_3-PCM, CuO-PCM and Al_2O_{3+} CuO-PCM composites, respectively compared to C1 of PCM. However, this value increased to 8.2 J/g, 33.7 J/g and 7.2 J/g in the Al_2O_3-PCM, CuO-PCM and Al_2O_{3+} CuO-PCM composites, respectively after 200 thermal cycles. Thus, energy storage is higher in nanoparticle PCM composites compared to pure PCM even after 200 thermal cycles. Latent heat capacity value showed an increment of 5.67%, 21.7% and 5.0% by addition of Al_2O_3-PCM, CuO-PCM and Al_2O_{3+} CuO-PCM composites, respectively after C200. This increase in latent heat value of melting with the addition of nanoparticles is due to the interaction between base PCM molecules and nanoparticles (Nourani et al., 2016). This interaction may be due to carbon-hydrogen bonding arrangements in the structural lattice because of repeated heating and cooling process, dehydration property, aggregation property of organic material (N. H. Mohamed et al., 2017).

Latent heat capacity of melting changes after every 50 thermal cycles in the range of -24.3 J/g to 39.4 J/g, -12.5 J/g to 51.4 J/g, -53.3 J/g to 55.4 J/g in pure PCM, Al_2O_3-PCM and CuO-PCM composites respectively but it is only 10.5 J/g to 5.5 J/g in Al_2O_3+CuO-PCM composite. Thus, Al_2O_3+CuO-PCM composite shows fewer changes in ΔH_m for every 50 cycles. Hence, it is stable in the energy storing process. The percentage of variation from C1 to C200 during melting is 10.55%, 14.97%, -3.5% and 5.54% in PCM, Al_2O_3-PCM, CuO-PCM and Al_2O_3+CuO-PCM composites, respectively.

The latent heat capacity of cooling is smaller than heating except for C100 and C150 in PCM. The percentage of variation after 200 thermal cycles in latent heat of cooling is 10.7%, 13.81%, -3.85% and 7.43% in PCM, Al_2O_3-PCM, CuO-PCM and Al_2O_3+CuO-PCM composites, respectively. Figure 4.33 shows that the variation in latent heat of heating and cooling follows similar trend.

Table 4.5 Changes in latent heat value for heating and solidifying

Cycle No.	**Sample name**															
	PCM				**Al_2O_3-PCM**				**CuO-PCM**				**Al_2O_3+CuO-PCM**			
	ΔH_m (J/g)	**50 C ΔH_m (J/g)**	**ΔH_s (J/g)**	**50 C ΔH_s (J/g)**	**ΔH_m (J/g)**	**50 C H_m (J/g)**	**ΔH_s (J/g)**	**50C ΔH_s (J/g)**	**ΔH_m (J/g)**	**50 C ΔH_m (J/g)**	**ΔH_s (J/g)**	**50C ΔH_s (J/g)**	**ΔH_m (J/g)**	**50 ΔH_m (J/g**	**ΔH_s (J/g)**	**50C ΔH_s (J/g)**
C1	130.8		-127.1		132.9		-131.1		183.9		-179.2		144		-137.3	
C50	106.5	-24.3	-103.4	23.7	184.3	51.4	-177	-45.9	130.6	-53.3	-127.3	51.9	149.4	5.4	-149.6	-12.3
C100	145.9	39.4	-147.4	-44	171.8	-12.5	-169.6	7.4	186	55.4	-180.6	-53.3	161.4	12	-157.7	-8.1
C150	167.4	21.5	-172.7	-25.3	171.8	0	-169.4	0.2	197.9	11.9	-191.4	-10.8	162.3	0.9	-158.8	-1.1
C200	144.6	-22.8	-139.9	32.8	152.8	-19	-149.2	20.2	178.3	-19.6	-172.3	19.1	151.8	-10.5	-147.5	11.3
Variation C1-C200 (%)	10.55		10.07		14.97		13.81		-3.05		-3.85		5.42		7.43	

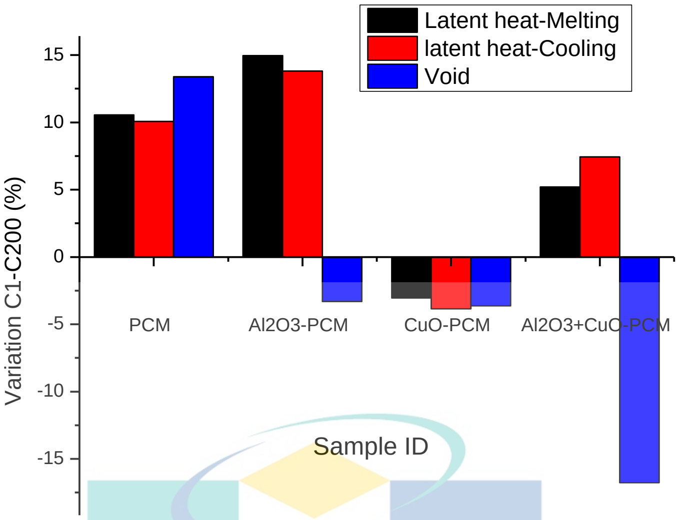

Figure 4.33 Variation in latent heat value for both heating and cooling with void ratio variation

Void ratio variation and latent heat capacity variation of melting and solidification have an inverse relationship in all the samples except for CuO-PCM composite. So, there is a decrease in void ratio and an increase in the latent heat capacity value after 200 thermal cycles in both the heating and cooling process. After 200 thermal cycles Al_2O_3, CuO and hybrid nanoparticle addition show an increment in the latent heat value from PCM by 5.6%, 23.3% and 7.21%, respectively. Even though there is an increase in latent heat value of nanoparticle- composite compared to base PCM, those values are lesser than the reference value of base PCM. Hence, the energy storing capacity of base PCM has improved with the addition of nanoparticles. This increment is because CuO and Al_2O_3 nanoparticles did not undergo melting or solidification process since their melting temperatures are far higher than the operating temperature of base PCM. Latent heat value changes for every 50 cycles shows the stability of Al_2O_3+CuO-PCM composites. Lower variation in latent heat capacity after 200 thermal cycles also shows that the composite is a promising thermal energy storage material in LHTES.

4.2.4 Energy storage time analysis

Among all the thermal storage properties discussed in this chapter, time taken to load and unload the heat energy in PCM is an important property to be analysed. This analysis helps to achieve efficient LHTES material. Thermal energy loading and unloading time is extracted from the DSC results. Since all the samples are heated with the same temperature rate, DSC data of the samples are used to measure the loading and unloading time of energy storage. The latent heat energy is stored during the melting process. Energy storing in PCM starts at onset temperature, and it ends at offset temperature. Difference between the starting time of melting (onset temperature) and ending time of melting (offset temperature) during the heating process gives the energy loading time. The time difference between starting and ending of solidification gives the energy unloading time. The energy loading time of all the samples is tabulated in Table 4.6.

The fastest and the slowest energy loading time is noted as 75 s and 87 s after 150 and 50 thermal cycles, respectively in PCM. In Al_2O_3-PCM, this value varies from 72 s to 111 s after the first and 100 cycles, respectively. The lowest value of 84 s; energy loading time is consistent in C50, C100 and C200. Whereas, 96 s is the highest value observed in C150. The calculated value of loading time for every fifty cycles varies, and it swings from 78 s (C1) to 99 s (C200). Thus, the loading time has shown no trend in all the samples and is shown in Figure 4.34. After 200 thermal cycles heat energy storage time is higher (99 s) in hybrid –PCM composite compared to other PCM and nanoparticle PCM composites.

Table 4.6 Energy loading time of the samples

Thermal cycle	**Energy loading time (sec)**			
	PCM	**Al_2O_3-PCM**	**CuO-PCM**	**Hybrid-PCM**
C1	81	75	93	78
C50	87	93	84	90
C100	84	111	84	96
C150	75	87	96	84
C200	84	72	84	99
Variation C1-C200 (%)	3.71	-4.00	-9.68	26.93

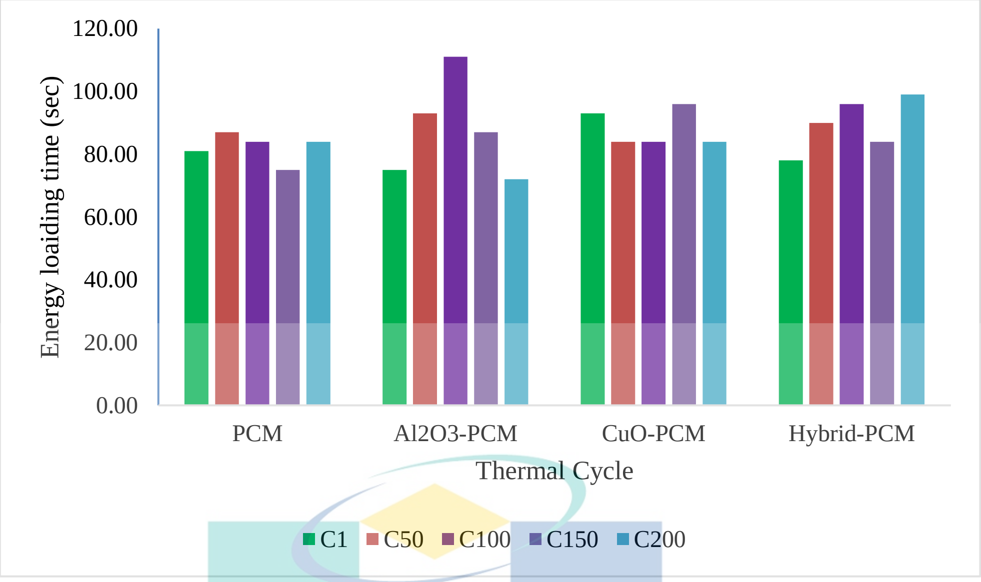

Figure 4.34 Energy loading time of all the samples

From Table 4.6 , both the lowest and the highest value of loading time among all the samples is 72 s and 111 s at C200 and C100 of Al_2O_3-PCM. The lowest and the highest swing of 14.3% and 49.4% in loading time is observed in CuO-PCM and Al_2O_3-PCM composites, respectively. Swing in the loading time of hybrid-PCM is higher (26.9%) compared to pure PCM (16%). The percentage of loading time variation after 200 thermal cycles with reference to C1 is 3.7%, -4.0%, -9.68% and 26.93% in PCM, Al_2O_3-PCM, CuO-PCM and hybrid-PCM, respectively. Highest variation indicates the longest time taken to store energy at C200 compared to C1. Compared to PCM, after 200 thermal cycles, loading time has varied by 14.29% and 17.86% in Al_2O_3-PCM and hybrid-PCM. There is no variation in CuO-PCM after 200 thermal cycles compared to PCM. Energy loading time variation and average void ratio variation for the samples are as depicted in Figure 4.35. Void ratio variation has an inverse relation with the loading time variation. Reduction in void ratio variation shows a negative impact on loading time. Energy storage time length has a notable impact on LHTESS performance.

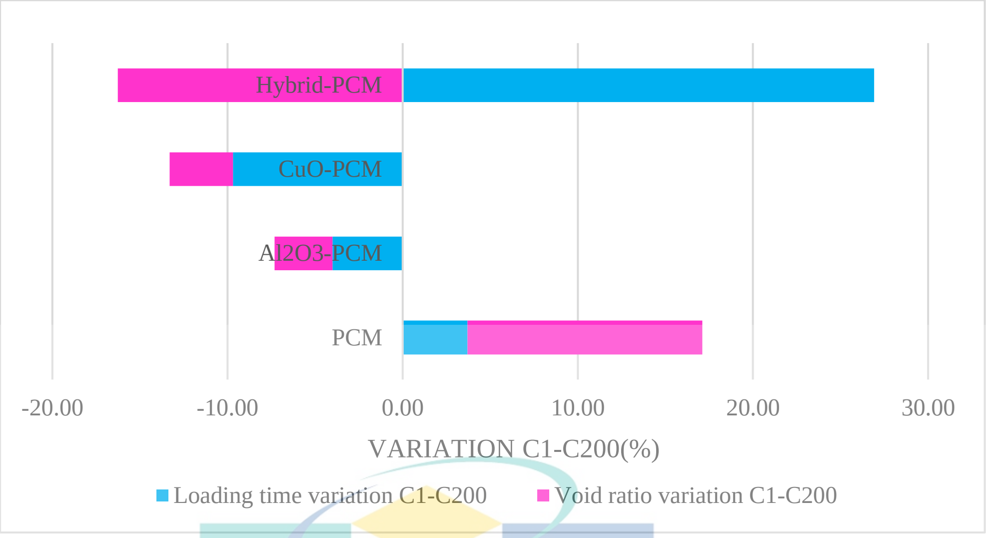

Figure 4.35 Variation of loading time and void ratio variation of samples

Time taken for heat energy unloading is calculated from the DSC data. The data is tabulated in Table 4.7. In PCM the lowest and the highest unloading time is 84 s in C50 and 96 sec in C100. In Al_2O_3-PCM composite, unloading time varies from 93 s in C1 to 102 sec in C100. The highest value of 102 s is observed in C100 of Al_2O_3 among all the samples. CuO nanoparticle addition has shown consistency in the lowest unloading time of 96 s in C50, C100 and C200 whereas the highest value is observed as 99 s in both C1 and C150. In hybrid-PCM, the lowest unloading time of 93 s is maintained till 100 thermal cycles from C1 and then has increased to 96 sec until 200 thermal cycles. Figure 4.36 shows the stability in the energy discharging time. In Pure PCM, Al_2O_3-PCM and CuO-PCM the trend is not seen, but the hybrid–PCM has shown an increasing trend. After 200 thermal cycles, all the nanoparticle-PCM composites have shown the same time for unloading (96 sec).

Table 4.7 Energy unloading time of the samples

Thermal cycle	**Energy unloading time (sec)**			
	PCM	**Al_2O_3-PCM**	**CuO-PCM**	**Hybrid-PCM**
C1	93	93	99	93
C50	84	96	96	93
C100	96	102	96	93
C150	93	99	99	96
C200	93	96	96	96
Variation C1-C200 (%)	0	3.2	-3.0	3.2

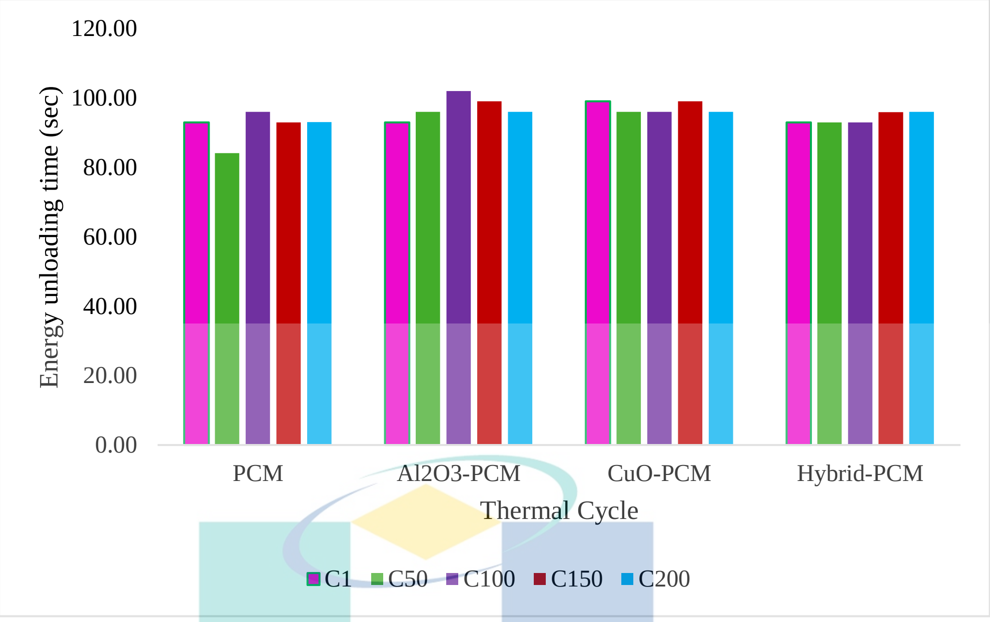

Figure 4.36 Energy unloading time of the samples

The unloading time swing from the lowest to the highest is 14.3%, 9.7%, 4.2% and 3.2% in PCM, Al_2O_3-PCM, CuO-PCM and hybrid-PCM composites, respectively. Less variation in hybrid-PCM shows stability in the duration of delivering heat energy. The percentage of unloading time variation from C1 to C200 is 3.2%, -3% and 3.2% in Al_2O_3-PCM, CuO-PCM and hybrid-PCM composites, respectively. However, there is no variation observed in PCM. After 200 thermal cycles, all the nanoparticle-PCM composites have shown the same increment of 3.2% in unloading time compared to pure PCM. This increment shows that the nanoparticle addition has helped to increase the heat supply time that is, the energy is stored longer time in the system, and longer time can be used. Average void variation and percentage of variation in the time of unloading after 200 cycles are plotted in Figure 4.37.

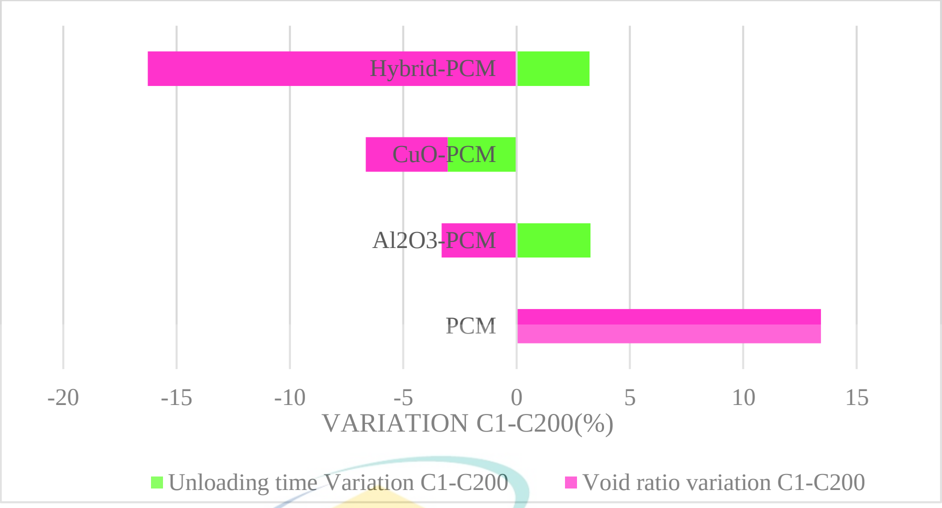

Figure 4.37 Void variation and unloading time variation of the samples

Variation in unloading time has an inverse relation with the void ratio variation. This is shown in Figure 4.37. If there is a less void variation, then longer time heat energy is stored in storage material. There is a strong inverse relation between variation in void ratio and unloading time in PCM and hybrid-PCM. Thus, nanoparticle addition has a positive impact on the unloading time.

4.3 Thermal stability analysis

Thermal stability of pure PCM and nanoparticle-PCM composites are investigated by finding the peak degradation points by using thermal gravimetric analysis (TGA). TGA and Differential Thermo Gravimetric Analysis (DTGA) curves for the pure PCM, Al_2O_3-PCM, CuO-PCM and Al_2O_3+CuO-PCM are as shown in Figure 4.38 and Figure 4.39. TGA curves shows that the weight loss occurs at different temperatures and is confirmed by DTGA curves. The TGA and DTGA curves have revealed that the paraffin wax degraded in one step.

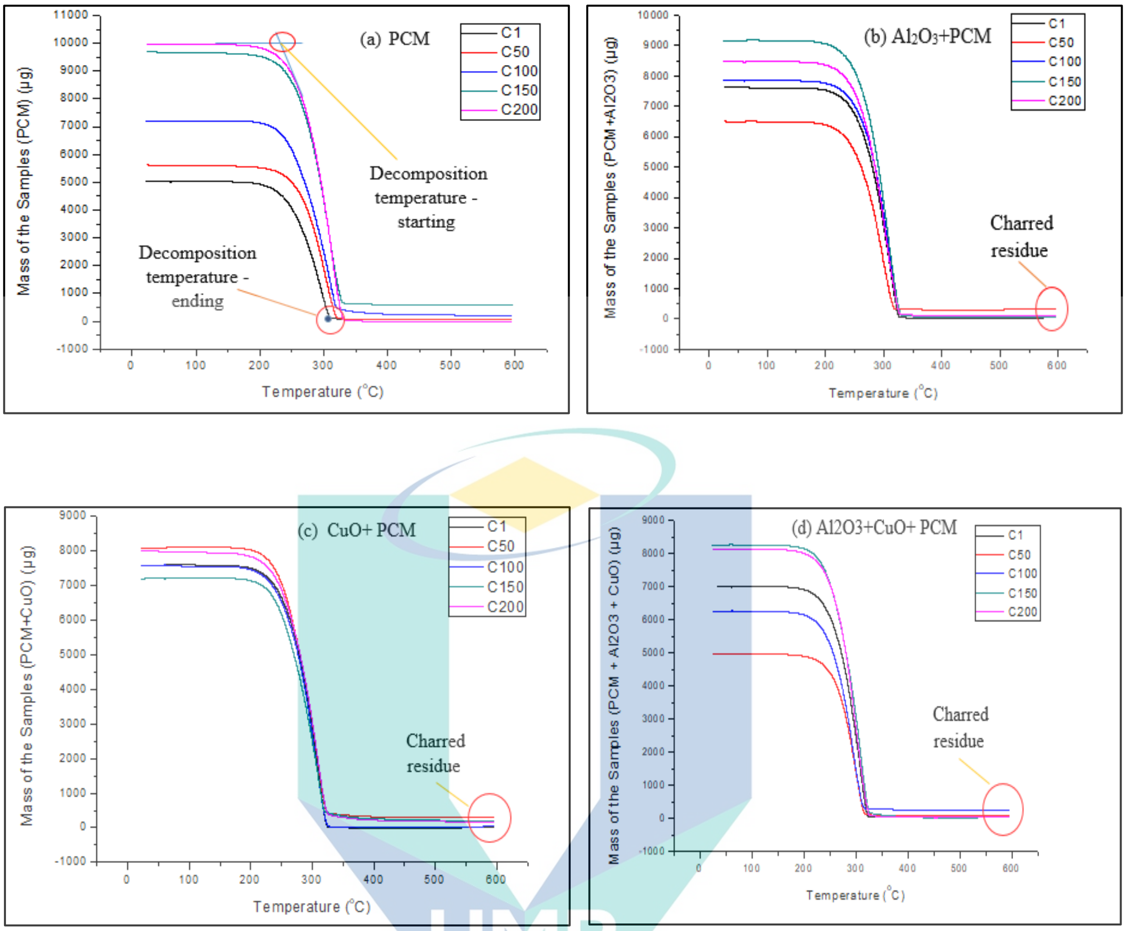

Figure 4.38 TGA curves of the samples (a) PCM, (b). Al_2O_3-PCM, (c). CuO-PCM, and (d). Al_2O_3+CuO-PCM composites

During TGA analysis, peak degradation started earlier at 99.6% mass after 200 thermal cycles in pure PCM. Compared to C1 of pure PCM, this drop was calculated at 1.6%. By addition of CuO and Al_2O_3 nanoparticle, this peak degradation is delayed by 4.5 % and 0.6% of mass difference after 200 thermal cycles. While by adding hybrid nanoparticles, the starting percentage of mass for peak degradation to start remained the same at C200 (98.9%) even though there is a slight fluctuation in C50 and C100. Mass reduction recorded at the stage of peak degradation in all the samples is attributed to removal of water or solvent. This highlights the presence of volatile substances (Jiang et al., 2015; S. C. Lin & Al-kayiem, 2016). Mass degradation from the peak temperature is due to oxidation. At high temperatures, C-H bond breaks and oxidised. The 5% weight loss temperature (*T-5%*), 50% weight loss temperature (*T-50%*), maximum decomposition temperature (*T- max*) and percentage of mass at which peak degradation starts and charred residue at 595^{o}c are listed in Table 4.8. The temperature at which 5% and 50% mass loss and *T-peak* of all the samples are depicted in the graph shown in Figure 4.40.

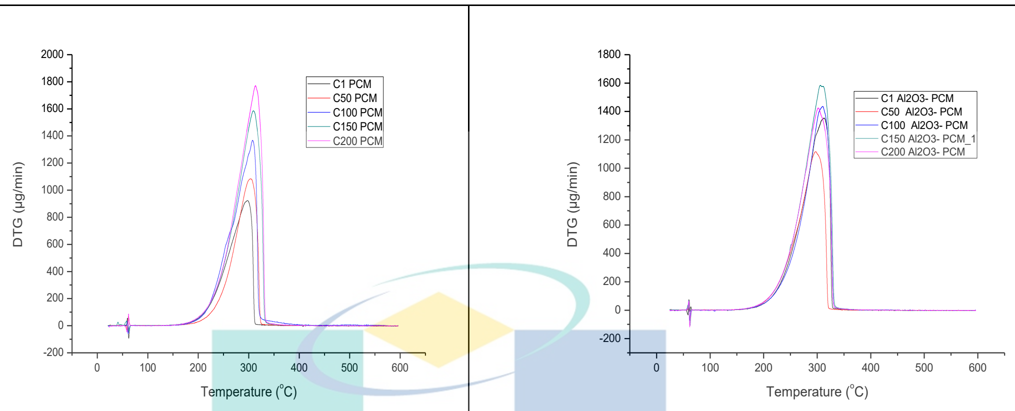

(a) PCM

(b) Al_2O_3-PCM

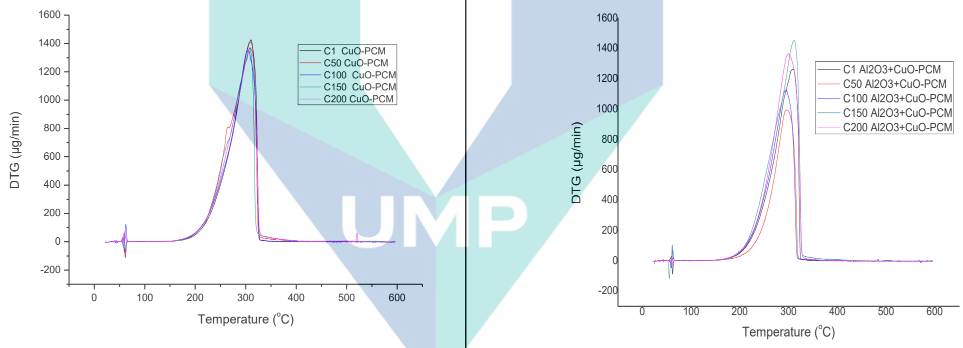

(c) CuO-PCM

(d) Al_2O_3+CuO-PCM

Figure 4.39 DTGA curves of (a). PCM, (b). Al_2O_3-PCM composites, (c). CuO-PCM composites, and (d). Al_2O_3+CuO-PCM composites

Table 4.8 Characteristic temperature and charred residue at 595°C of pure PCM and nanoparticle PCM composites

Sample name	**Thermal cycles**	***T- 5%* (°C)**	***T-50* (°C)**	**Charred residue (%)**	***T max* (°C)**	**Peak degradation starting mass (%)**
PCM	1	218.8	278.7	1.655	200.8	98.0
	50	228.4	290.3	1.196	245.5	91.4
	100	228.7	288.4	2.709	231.8	94.1
	150	229.3	296.3	6.263	239.1	92.8
	200	231.8	296.0	-0.049	182.0	99.6
Variation (%)	C1-C200	5.9	6.2	-103.0	-9.4	
Al_2O_3-PCM	1	229.4	293.3	0.578	192.7	98.9
	50	223.1	286.2	4.866	224.3	94.5
	100	231.5	295.8	1.241	208.9	98.2
	150	231.0	294.4	0.745	198.3	98.9
	200	228.9	292	1.291	206.4	98.3
Variation (%)	C1-C200	-0.2	-0.4	123.5	7.1	
CuO-PCM	1	228.7	292.1	0.030	175.9	99.7
	50	231.0	290.7	3.726	231.2	95.0
	100	225.0	290.3	0.510	205.4	98.0
	150	228.7	288.3	2.709	231.1	94.4
	200	223.3	291.4	2.131	222.5	95.2
Variation (%)	C1-C200	-2.4	-0.2	6914.2	26. 5	
Al_2O_3+ CuO PCM	1	227.2	290.0	1.014	196.6	98.9
	50	229.7	287.9	2.004	214.1	97.4
	100	222.2	283.5	4.309	223.5	94.7
	150	227.6	290.4	0.438	208	98.3
	200	226.4	289.3	0.445	193.7	98.9
Variation (%)	C1-C200	-0.4	-0.2	-56.1	-1.5	

Thermal stability of PCM was lower compared to other nanoparticle-PCM composites during the first cycle, but it showed increment after every cycle till 200 thermal cycles at 95% mass left. This stability improvement in terms of the temperature of 5.9%. At 50% mass left, the stability has shown fluctuations but get stable at higher cycles at 6.2%. Moreover, degradation starts at a lower temperature in C200 compared to C1 by 9.4%.

By addition of Al_2O_3 nanoparticles with base PCM, 95% of the mass left is observed at 229.4°C at thermal cycle C1 and 228.9°C at C200. This decrement in temperature is only by 0.2%. Fifty percent of the mass left is noted at 293.3°C in thermal cycle C1 and 292°C in C200. This temperature decline is only 0.4%. However, peak degradation temperature increased by 7.1%. The copper oxide nanoparticle addition has shown 2.4% and 2% decline in the degradation temperature for 95% and 50% mass left. The peak degradation temperature (*T-peak*) is increased to 26.5%. This shows the stability of CuO-PCM composite.

By addition of both Al_2O_3 and CuO nanoparticles together with base PCM, drop-in degradation temperature for 95% and 50% mass left is noted at 0.4% and 0.2% respectively at the end of 200 thermal cycles. At the same time, the T-peak value decreased by 1.5%. By addition of Al_2O_3, CuO and hybrid nanoparticles with base PCM peak degradation temperature (*T-Peak*) increased by 24.4°C, 40.5°C and 11.7°C, respectively compared to the pure PCM. This increment is calculated by comparing the peak degradation temperature of pure PCM after 200 thermal cycles. Compared to the hybrid--PCM composite and pure PCM, the nanoparticle addition has increased the thermal stability.

Charred residue percentage is unpredictable by thermal cycle wise and sample wise in all the samples studied but shows a higher amount of mass left for the nanoparticle composites compared to the pure PCM and hybrid-PCM composites. This mass left shows the thermal stability of hybrid-PCM composite even after 200 thermal cycles. The percentage of increment in charred residue at 595°C from C1 to C200 is plotted against the samples in Figure 4.41.

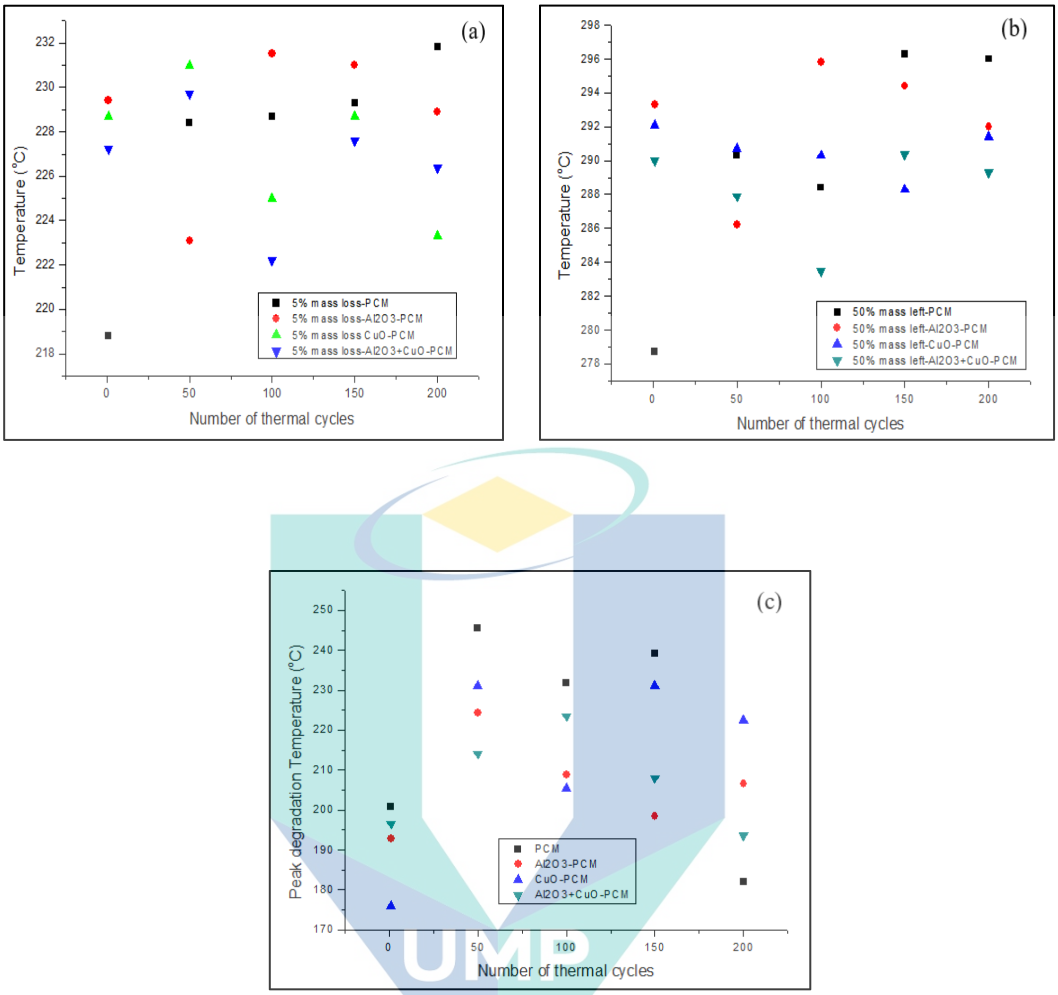

Figure 4.40 Mass left (a) 95%, (b) 50% and (c) *T-peak* after many cycles for all the samples

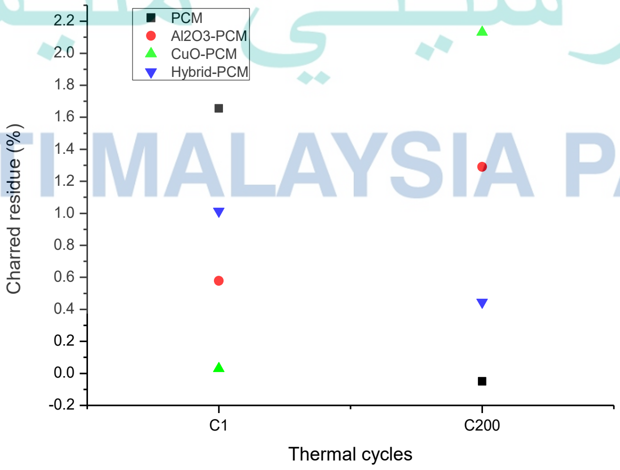

Figure 4.41 Percentage of charred residue at C1 and C200

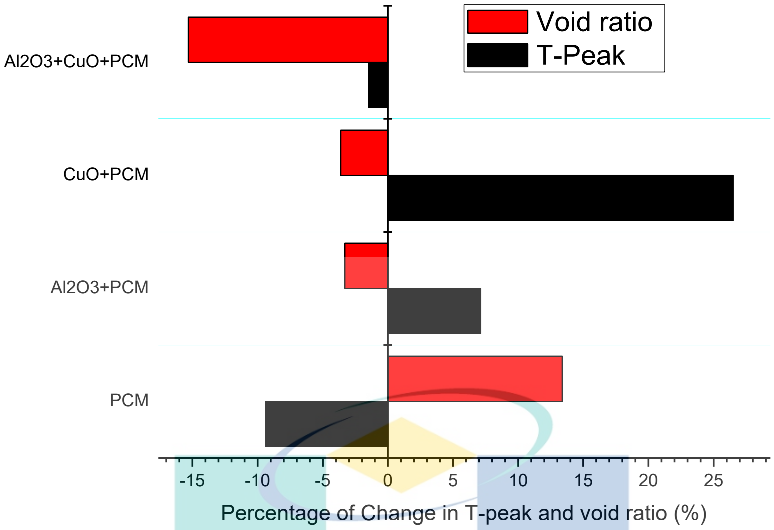

Figure 4.42 The percentage of change in *T-peak* and void ratio from C1 to C200 of all samples

The *T-peak* and void ratio value changes from C1 to C200 is calculated in percentage and plotted in Figure 4.42. The percentage of void ratio change has shown inverse relation with percentage of change in the *T-peak* value in CuO-PCM, Al_2O_3-PCM and pure PCM. This relation shows that thermal stability of the samples has an inverse relation with the void ratio in CuO-PCM and Al_2O_3-PCM. With pure PCM, the higher void ratio seems to have a negative effect on stability by reducing *T-peak*. Even though there is a reduction in the void ratio value in Al_2O_3+CuO-PCM, *T-peak* value has also reduced. This decline is lower compared to pure PCM. So, nanoparticle addition has increased the thermal stability of the base PCM compared to its pure PCM form.

4.4 Thermal conductivity analysis

Thermal conductivity plays a vital role in the energy storage rate of a thermal energy storage system. Thermal conductivity study helps to store heat energy in peak hours efficiently in LHTESS. Thermal conductivity data of pure and nanoparticle- PCM composites in the solid forms at different thermal cycles is tabulated in Table 4.9. The thermal conductivity of all samples is also depicted in Figure 4.43.

Table 4.9 Thermal conductivity data of pure and nanoparticle-PCM composites

Thermal cycle	**Thermal conductivity (W/(mK))**			
	PCM	**Al_2O_3-PCM**	**CuO-PCM**	**Al_2O_3+CuO-PCM**
1	0.252	0.243	0.214	0.298
50	0.34	0.275	0.346	0.291
100	0.313	0.278	0.27	0.288
150	0.276	0.285	0.273	0.278
200	0.258	0.262	0.27	0.272
Variation C1-C200 (%)	2.4	7.8	26.2	-8.7

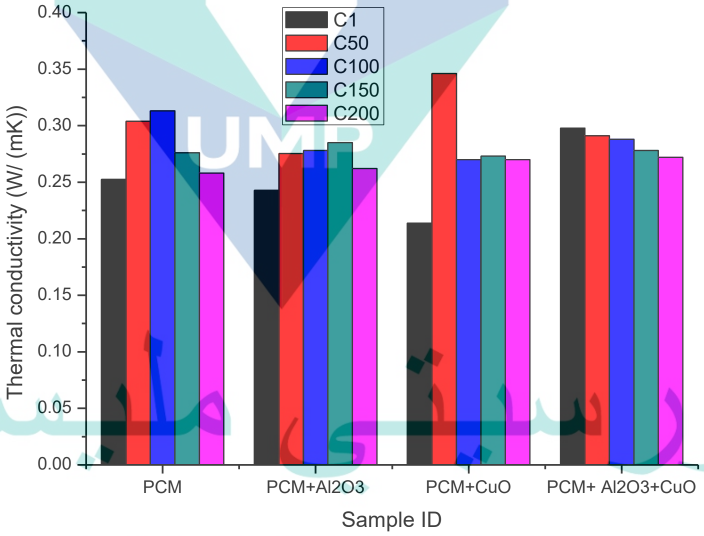

Figure 4.43 Thermal conductivity of Pure and nanoparticle-PCM composites

As depicted in Figure 4.43, it could be observed that the thermal conductivity of the pure PCM increased from C1 to C100 and then decreased till C200 but not less than C1. By adding Al_2O_3 nanoparticles, the thermal conductivity increased till C150 then decreased by 8.07% after 200 thermal cycles. CuO nanoparticle addition with base PCM has recorded an increment in the thermal conductivity at C50. After 50 thermal cycles, the thermal conductivity decreased till C200. When Al_2O_3 and CuO nanoparticles are added with base PCM in the form of hybrid, the thermal conductivity decreased by 2.35%, 1.03%, 3.47% and 2.16% for every 50 thermal cycles from C1 to C200. Thermal conductivity variation of nanoparticle-PCM composites from pure PCM is tabulated in Table 4.10. From the results, it is clear that aluminium oxide and copper oxide nanoparticle addition has resulted in degradation of thermal conductivity by 3.6% and 15.1% respectively after the first thermal cycle compared to C1 of the pure PCM. The hybrid nanoparticle addition, on the other hand, improved thermal conductivity by 18.3% after the first cycle. On the contrary, addition of aluminium oxide, copper oxide, and hybrid nanoparticles led to enhanced thermal conductivity by 1.6%, 4.7% and 5.4% respectively from base pure PCM after 200 thermal cycles.

Table 4.10 Thermal conductivity variation of nanoparticle-PCM composites compared to pure PCM

Thermal cycle	**Thermal conductivity Variation compared to PCM (%)**			
	PCM	**Al_2O_3-PCM**	**CuO-PCM**	**Al_2O_3+CuO-PCM**
1	-	-3.6	-15.1	18.3
50	-	-19.1	1.8	-14.4
100	-	-11.2	-13.7	- 8.0
150	-	3.3	-1.1	0.7
200	--	1.6	4.7	5.4

Colla et al., (2017) record a report on degradation of thermal conductivity after the addition of nanoparticle (L. Colla et al., 2017). The authors have tested RT20 (RUBITHERM-20- paraffin wax with melting temperature in the range of 20°C) and RT25 (RUBITHERM-25- paraffin wax with melting temperature in the range of 25°C) with 1% Al_2O_3 and 1% carbon black nanoparticles. The Al_2O_3 nanoparticle addition has penalised the thermal conductivity value by 7% and 8% whereas the carbon black nanoparticle addition has increased it by 24% and 35% for RT25 and RT20, respectively. Thermal conductivity of all the samples after 200 thermal cycles is depicted in

Figure 4.444 From the graph, it is clear that nanoparticle addition has improved the thermal conductivity compared to pure PCM after 200 thermal cycles.

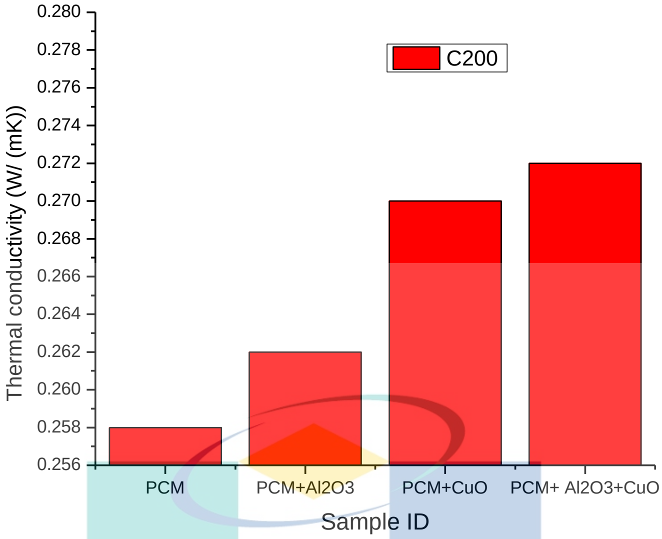

Figure 4.444 Thermal conductivity of all the samples (C200) after 200 thermal cycles.

The thermal conductivity and percentage of thermal conductivity variation (from C1 to C200) for all the samples are tabulated in Table 4.10, and the void ratio and thermal conductivity change after 200 thermal cycles are plotted Figure 4.45. The void ratio variation has an inverse relation with thermal conductivity variation in pure PCM, Al_2O_3-PCM composite and CuO-PCM composite. On the contrary, the thermal conductivity variation decreased with void ratio in hybrid-PCM. This behaviour may be due to the heat flowing (low resistance path) characteristics of solids attributed to atomic arrangements in the lattice because of void formation. Void ratio variation at the centre with respect to the thermal conductivity variation is depicted in Figure 4.46.

Percentage of change in void ratio at the centre and the percentage of thermal conductivity changes has an inverse relation in PCM and Al_2O_3-PCM composite but, in hybrid-PCM and CuO-PCM composites, it has shown direct relation. This result is due to the instrumental dependency on measuring way. In KD 2 pro, the tip of the props could reach only the centre part of the sample; hence at the centre heat may flow. Hence void ratio at the top and bottom have zero effect in thermal conductivity measurement. Most of the samples have behaved as pure PCM because of the possibility of settlement of nanoparticles due to repeated heating (L. Colla et al., 2017). After every heating process, samples remain in liquid form for a longer time during the solidification process, and this made the nanoparticles settle down hence leading to non-uniform distribution of nanoparticle in the base PCM (L. Colla et al., 2017). Compared to base PCM, hybrid-

PCM composite has shown enhancement in thermal conductivity due to chain-like structure formation (Kumar & Krishna, 2019)

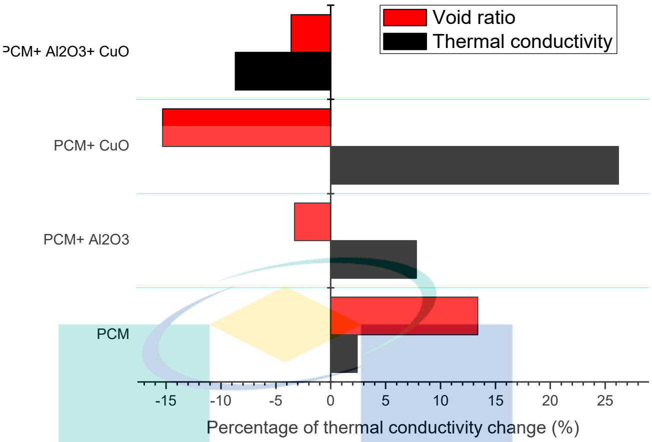

Figure 4.45 Variation in void ratio and thermal conductivity after 200 thermal cycles with reference to C1

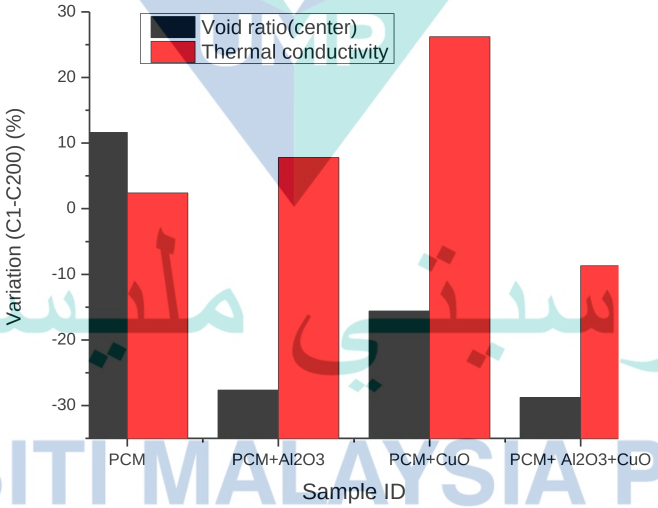

Figure 4.46 Void ratio variation at the centre and thermal conductivity variation for all the samples

4.5 Viscosity analysis

The measured viscosity values of paraffin wax samples are depicted in Figure 4.47. It is noted that the viscosity value decreased with an increase in temperature.

Besides, the graphs clearly illustrates that viscosity value has shown fluctuations within 200 thermal cycles. Viscosity value decline is recorded after 200 thermal cycles in all the nanoparticle-PCM composites. Viscosity at 65°C and 100°C is tabulated in Table 4.11. The viscosity changes are discussed at 65°C and 100°C. In this temperature range, only viscosity is measured.

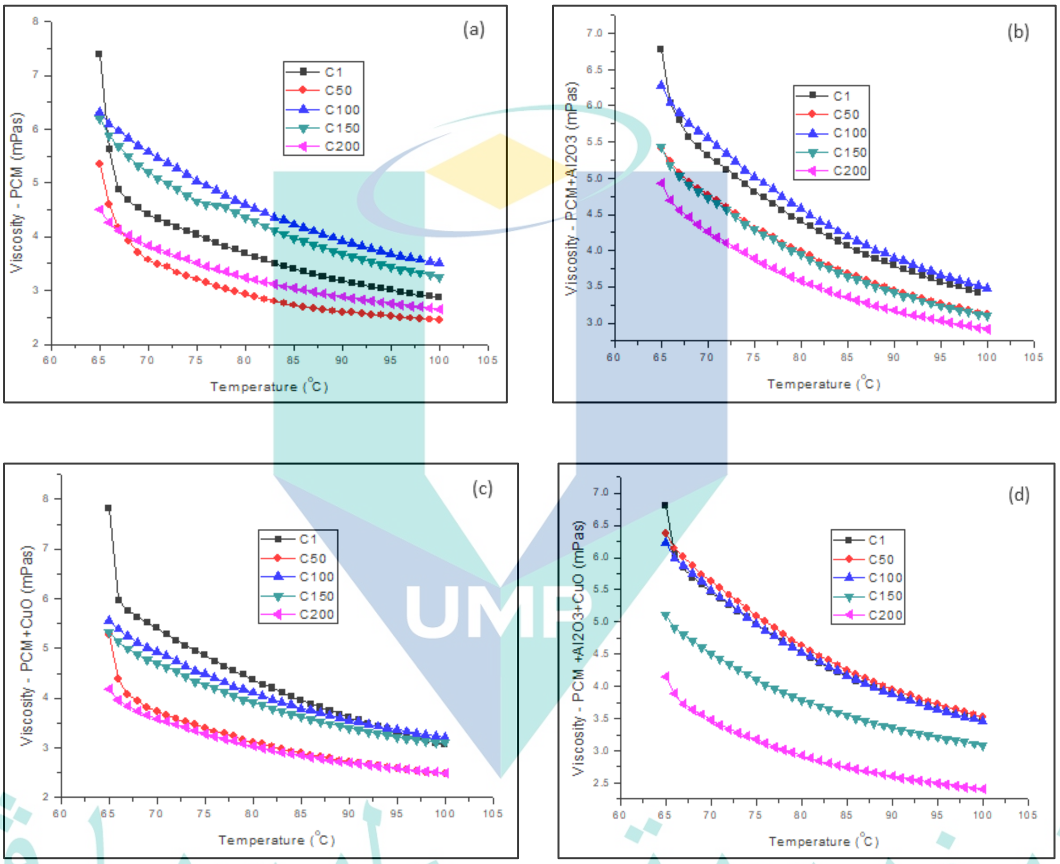

Figure 4.47 Measured viscosity values of (a) PCM, (b) Al_2O_3-PCM composites, (c) CuO-PCM composite and (d) Al_2O_3+CuO-PCM composites

At both temperatures, pure PCM and nanoparticle-PCM composites have shown viscosity reduction after 200 thermal cycles. The viscosity values have shown a variation of -39.18%, -27.36%, -46.50% and -39.06% for pure PCM, Al_2O_3-PCM, CuO-PCM and Al_2O_3+CuO-PCM, respectively. These percentages are the variation from C1 to C200 at 65°C. Percentage of variation at 100°C is recorded as -7.45%, -14.95%, -18.55% and -30.5% for Pure PCM, Al_2O_3-PCM, CuO-PCM and Al_2O_3+CuO-PCM, respectively. As the temperature increases, the viscosity decreases, but the value is higher in the nanoparticle-PCM composites. Reduction in viscosity of the samples has an effect on thermal conductivity. As the viscosity of material decreases, thermal conductivity is decreased. This affects the loading time of the thermal energy storage system. (Mossaz et al., 2015)

Percentage of viscosity variation after 200 thermal cycles with reference to C1 for all the samples at 65°C and 100°C is depicted in Figure 4.48. It is clear that at 65°C viscosity variation is lesser by adding CuO nanoparticles alone and together with Al_2O_3 nanoparticles compared to Al_2O_3 nanoparticles alone. However, at 100°C, Al_2O_3+CuO nanoparticles addition has shown very little variation compared to other samples. Viscosity variation in the samples at 100°C has followed the trend of the void ratio, which is shown in Figure 4.49.

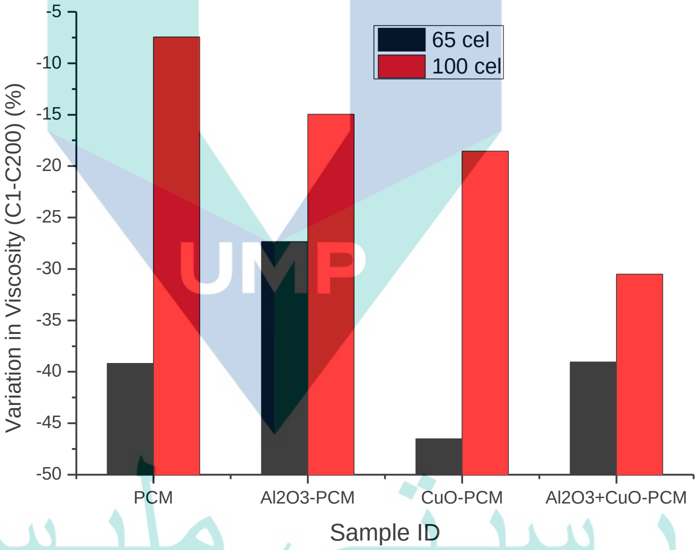

Figure 4.48 Viscosity variation of all the samples

In this study, viscosity values have exhibited inverse relation with the temperature, but it fluctuates and follows the void ratio trend with thermal cycles at any particular temperature below 100°C. This nature is due to the amount of voids formation and their movements. During viscosity measurement, shearing stress is applied, which may spread the voids. This may also be due to the kinetic property of gas inside the voids and uniform distribution of voids due to the upward convectional movement of particles upon absorbing heat energy.

Table 4.11 Viscosity of samples at different temperature

Sample type	**Temp. (°C)**	**Viscosity (mPas)**					**Variation**
		C1	**C50**	**C100**	**C150**	**C200**	**C1-C200 (%)**
PCM	65	7.401	5.341	6.326	6.190	4.501	-39.18
	100	2.865	2.447	3.503	3.255	2.652	-7.45
Al_2O_3-PCM	65	6.781	5.407	6.275	5.435	4.926	-27.36
	100	3.425	3.516	3.480	3.095	2.913	-14.95
CuO-PCM	65	7.823	5.284	5.567	5.332	4.186	-46.50
	100	3.054	3.118	3.206	3.116	2.488	-18.55
Al_2O_3+CuO-PCM	65	6.804	6.371	6.231	5.109	4.147	-39.06
	100	3.450	3.523	3.464	3.086	2.398	-30.51

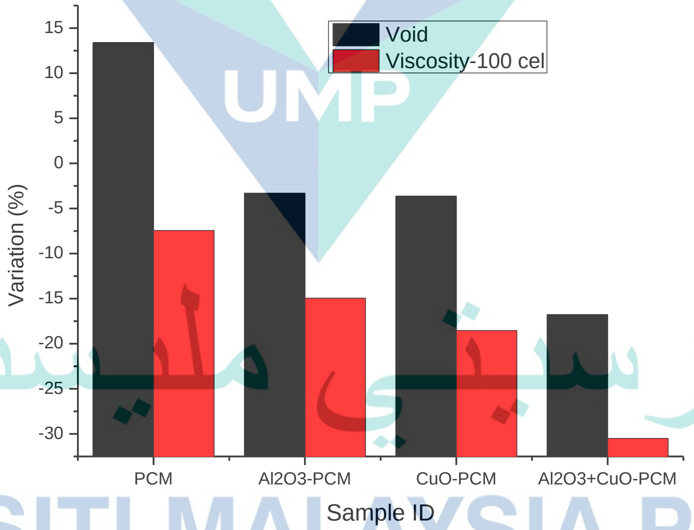

Figure 4.49 Viscosity variation at 100°C with void variation

4.6 Density analysis

Temperature and pressure are the two main factors that make changes in the state of the material, hence influencing the density. Measured density of the pure PCM, Al_2O_3-PCM, CuO-PCM and Al_2O_3+CuO-PCM composites is plotted in Figure 4.50. Except for the Al_2O_3+CuO-PCM composite, the density value of all the samples shown no distinctive trend. The values changes for every 50 cycles from C1 to C200 hence recording a fluctuated trend. On the contrary, the hybrid nanoparticle-PCM has shown a declining trend as the thermal cycle increases. The density of all the samples, percentage of variation in density value after 200 thermal cycles from C1 and density variation after 200 cycles with reference to the pure PCM for all the samples are listed in Table 4.12.

The variation in density after 200 thermal cycles of all the samples is plotted in Figure 4.51. After 200 thermal cycles, the density values of Al_2O_3-PCM, CuO-PCM and Al_2O_3+CuO-PCM have changed by -8.57%, 1.54% and 4.07%, respectively with reference to the pure PCM. With the reference of C1, the pure PCM, Al_2O_3-PCM, CuO-PCM and Al_2O_3+CuO-PCM has shown density declined by 15%, 24.04%, 15.14% and 13.54%, respectively. It was clear that density of the material has followed the same trend till C50 then continued with an inversely proportional trend to the void ratio.

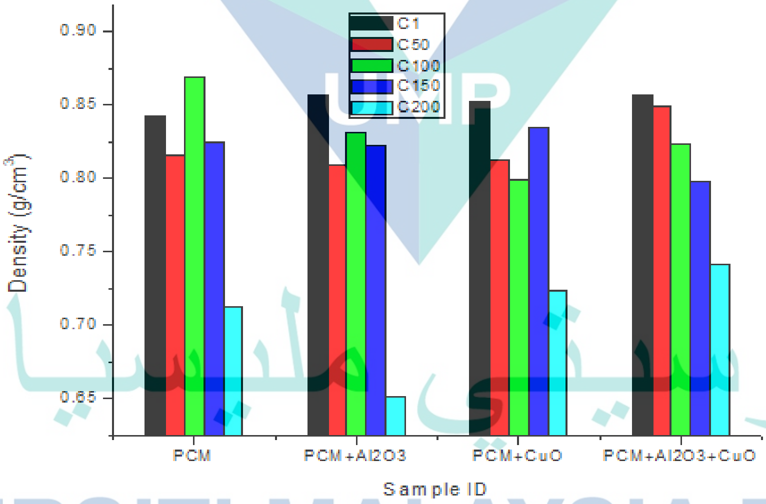

Figure 4.50 Density of all the samples

The external pressure due to void formation has pushed the molecules closer, making changes in their arrangement and increasing the density. By increasing temperature, the volume has increased, and thus the molecules moved apart causing reduction in density value (Shirai et al., 2011). As a result of heating, the volume has increased while voids being formed during solidification. The density value has decreased at the end of cycle 200 compared to other cycles.

Table 4.12 Density and density variation of all the samples

Samples	**Density (g/m^3)**					**Variation C1-C200 (%)**	**Variation from PCM C200(%)**
	C1	**C50**	**C100**	**C150**	**C200**		
PCM	0.842	0.816	0.869	0.825	0.712	-15.44	-
Al_2O_3-PCM	0.857	0.809	0.831	0.822	0.651	-24.04	-8.57
CuO-PCM	0.852	0.813	0.799	0.835	0.723	-15.14	1.54
Al_2O_3+CuO-PCM	0.857	0.849	0.823	0.798	0.741	-13.54	4.07

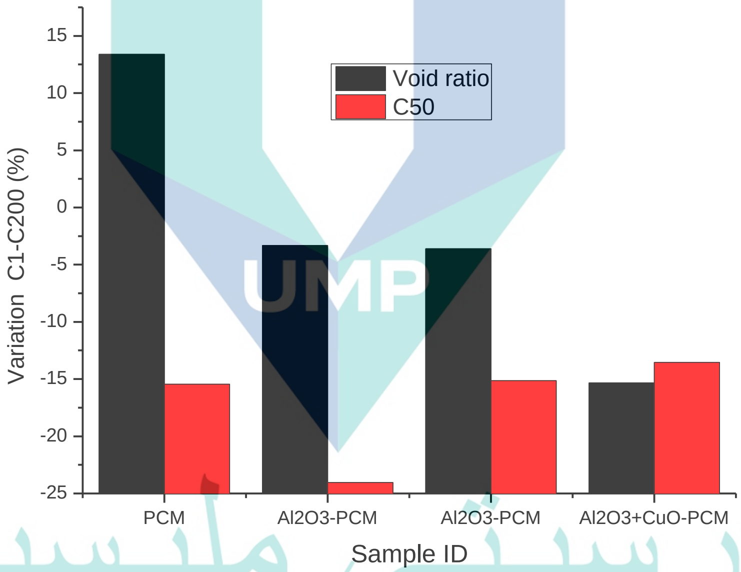

Figure 4.51 Density and void ratio variations

The density of nanoparticle PCM composites increased by 1.78%, 1.19% and 1.78% for Al_2O_3-PCM, CuO-PCM and Al_2O_3+CuO-PCM, respectively after the first thermal cycle. After 200 thermal cycles, CuO-PCM and Al_2O_3+CuO-PCM have shown improvement, but Al_2O_3 nanoparticle addition has shown a reduction by 8.57%. This result clears that CuO nanoparticle addition has improved the density. By analysing the relationship between density and thermal conductivity it shows that the thermal conductivity has increased with an increase in density. This could be identified by plotting density and thermal conductivity value after 200 thermal cycles, as shown in Figure 4.52

and Figure 4.53. Density measurement has shown an increasing trend except in Al_2O_3 – PCM. Even though the density value of Al_2O_3-PCM composite is less compared to other samples after200 thermal cycles, thermal conductivity value has increased like other samples. This may be due to the heterogeneous void distribution in the samples and settlement of nanoparticles due to repeated heating and cooling. However, the density of Al_2O_3+CuO-PCM is comparably high compared to the pure PCM; hence the thermal conductivity increment is recorded after 200 thermal cycles.

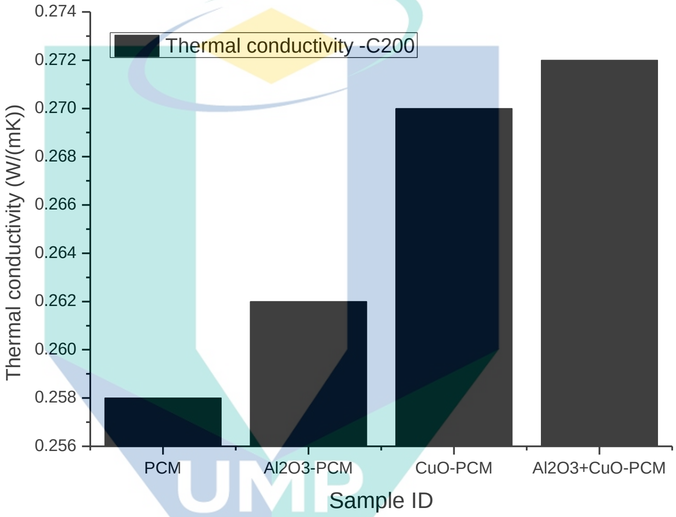

Figure 4.52 Thermal conductivity after C200

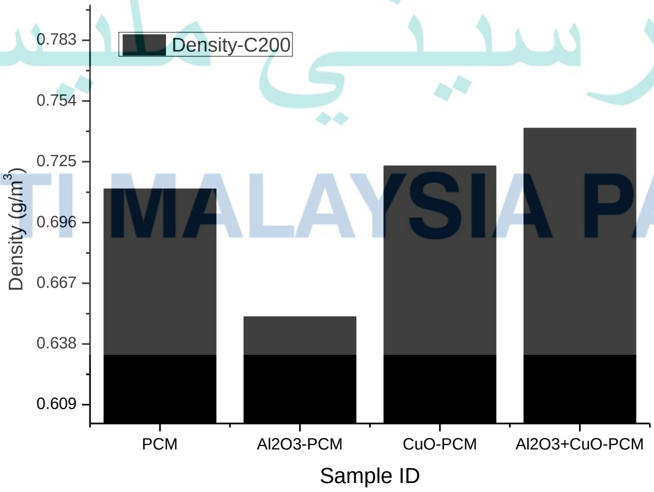

Figure 4.53 Density after C200

4.7 Chapter summary

Paraffin wax and nano-enhanced paraffin wax are tested to confirm long term thermal stability. .Al_2O_3 and CuO nanoparticles of 5 wt% and 2.5 wt% Al2O_3+2.5 wt% CuO are doped with the paraffin wax. Then, paraffin wax and nanoparticle-paraffin wax composites are made to undergo 1, 50, 100, 150 and 200 thermal cycles to study the stability of thermophysical properties. Voids are formed during solidification shrinkage. This naturally affects the thermo-physical properties of paraffin wax. Cyclic degradation of thermophysical properties on the basis of voids in the paraffin wax is investigated. Voids are heterogeneous in nature and show a cyclic trend when they are observed for every fifty cycles. The highest and the lowest void ratio value of 55.75%and 33.02% is found at the bottom of C200 Al_2O_3-PCM and C100 PCM, respectively.

Nanoparticle addition reduces void formation as the number of cycle increases. Hybrid nanoparticle addition reduces void formation in the base PCM. Percentage of variation after 200 thermal cycles from C1 is -16.77% with reference to PCM this value is -11.64% after 200 thermal cycles. Melting and solidification are stable in all nano enriched paraffin wax and the variation is 0% in Hybrid–PCM composite. The void formation is reduced, whereas latent heat capacity value is increased in nanoparticle-PCM composites compared to base PCM. Percentage of variation in latent heat value is lower by -3.05% and 5.52% in CuO-PCM and Hybrid-PCM, respectively. Al_2O_3-PCM, CuO-PCM and hybrid-PCM show 5.6%, 23.3% and 7.2% increment in latent heat value compared to PCM after 200 thermal cycles. Latent heat value has shown consistency for every fifty thermal cycles hence confirming the stability. Void variation has an inverse relation with the latent heat capacity value. Nano enriched PCMs starts to degrade at higher temperature as the number of thermal cycles increases. The void ratio has an inverse relation with all samples except hybrid-PCM and pure PCM. Thermal conductivity increment of 1.6%, 4.7% and 5.4% in Al_2O_3-PCM, CuO-PCM and hybrid-PCM compared to pure PCM at C200.

Nanoparticle addition has reduced the viscosity, and it has decreased with temperature. Viscosity drop of -46.5% is found in CuO-PCM at 100°C. This drop is the highest value compared to other samples. Viscosity and voids follow the same trend. Density of the nanoparticle-PCM composite has increased, and the highest is noted in CuO-PCM. Thermal conductivity increases with density. The void formation has a negative impact on thermophysical properties. By the addition of nanoparticles, this impact is reduced. Hybrid nanoparticle addition reduces the degradation of thermophysical properties in paraffin wax. Loading and unloading time improvement in nanoparticle-paraffin wax confirms the enhancement in storage performance.

CHAPTER 5

CONCLUSION

5.1 Conclusions

Heat energy, especially solar energy storage, is necessary to reduce energy-related problems and environmental issues in the world. Latent heat thermal energy storage utilizing paraffin wax is one of the promising ways of storing solar energy. Thermophysical properties of paraffin wax play an essential role in energy storing capacity. However, these properties degrade upon cyclic usage. Void formation during solidification shrinkage has a significant impact on thermophysical property degradation. This affects the lifetime duration of paraffin wax. Conclusions of this study are written according to the objectives below.

Objective 1 is to study the thermophysical property degradation due to repeated melting and solidification of PCM.The results have revealed that

- Void formation is found to be heterogeneous and it fluctuate
- Stable heat loading and unloading temperature is noted after 50 thermal cycles
- Thermal conductivity of solid paraffin wax has increased even after repeated thermal cycling
- Density after 200 thermal cycle is recorded as 0.712 g/m^3
- Viscosity value has decreased with the temperature

Objective 2 is to analyse the impact of thermophysical property degradation on the performance of thermal energy storage. To achieve the objectives, the thermophysical properties of paraffin wax are analysed based on void formation. The results have concluded that

- Void formation is hetrogeneous in nature and it fluctuates both position-wise and cycles wise in all the samples

- There are 25.17% and 33.7% of declination in the latent heat capacity and peak degradation temperature, respectively from C1 to C200. This declination has a negative impact on the storage performance of the thermal energy storage system
- Density has an inverse relation with the void ratio as the number of cycle increases
- Thermal conductivity increases with the thermal cycles by showing an increment of 12% after 200 thermal cycles
- Thermal conductivity follows the same trend as voids which shows sinusoidal nature. This nature reveals the fluctuations in storage performance

Objective 3 is to enhance the thermal storage performance of base PCM by incorporation of the nanoparticle. To achieve this objective, Al_2O_3, CuO and Al_2O_3+CuO nanoparticles are doped with paraffin wax to reduce the degradation in the thermophysical properties of the paraffin wax. Samples of nanoparticle-PCM composites are tested in the same way as that of pure paraffin wax. Results have found that

- The void ratio has shown fluctuation in all the samples as the number of thermal cycles increases
- Reduction in the void formation is noted as 3.31%, 3.62% and 16.77% in the Al_2O_3-PCM, CuO-PCM and Al_2O_3+CuO-PCM composites, respectively
- Melting and solidification process is stable in the hybrid-PCM composite compared to the other samples
- Latent heat capacity value of melting and solidification has shown an inverse relation with the void ratio. Latent heat value of melting has increased by 5.67%, 21.7% and 5.0% in Al_2O_3-PCM, CuO-PCM and Al_2O_3+CuO-PCM composites, respectively with reference to pure PCM. In cooling, the increment in this value is 6.65%, 23.16% and 5.43% in Al_2O_3-PCM, CuO-PCM and Al_2O_3+CuO-PCM composites, respectively
- Stability in the latent heat capacity of a hybrid-PCM composite is observed for every fifty thermal cycles and is found consistent

- The degradation of base PCM is reduced by the addition of nanoparticles. *T-peak* value has increased to 13.4%, 22.25% and 6.43% from PCM by the addition of Al_2O_3, CuO and hybrid nanoparticles, respectively

- Thermal conductivity of all the nanoparticle-PCM composites has increased, and the highest value recorded is in the hybrid-PCM (5.4%)

- Thermal stability and thermal conductivity has an inverse relation with the void ratio

- Minimum viscosity variation (C1-C200) of -30.51% is noted in hybrid-PCM composites at 100°C

- Density has an inverse relation with the void ratio. At C200, the highest value of 4.07% increment is recorded in the density of hybrid- PCM composite

- Nanoparticle addition has stabilized the loading and unloading process by decreasing and increasing the energy storage and releasing time

Finally, the addition of Al_2O_3 and CuO nanoparticle with the base PCM, respectively have shown improvement in latent heat and peak degradation temperature, thermophysical property stability is achieved better in the hybrid-PCM composite. This stability is observed by noticing the consistency in changes of latent heat value for every 50 thermal cycles and all the property variations after 200 thermal cycles.

5.2 Recommendations

i. Due to time limitations, the experiment is conducted until 200 thermal cycles only. Fluctuations identified in the void formation and its effect on thermophysical properties requiresthis study to be extended by increasing the number of thermal cycles. Instead of 200 atleast 400 thermal cycles are recommended to confirm the stability in thermophysical properties of PCM

ii. Another concept is adopting a different ratio for the addition of the nanoparticles. In this study, to get the hybrid-PCM composite, the ratio of 50% of Al_2O_3 + 50% of CuO nanoparticle combination is added with base PCM. It is recommended to adopt the different percentage of combination of Al_2O_3 and CuO nanoparticles with base PCM to get a hybrid-PCM composite for future studies

iii. Paraffin waxes are promising thermal energy storage materials. So, it is also recommended for different metal oxide and carbon-based nanoparticles doping with paraffin wax to study the improvement of thermophysical properties due to repeated thermal cycling

iv. In this study, the nanoparticle settlement is noticed. To ensure the homogeneous dispersion of nanoparticles and to maintain the long-term stability inhomogeneity, addition of surfactant is recommended

REFERENCES

Abdulrahman, R. S., Ibrahim, F. A., & Dakhil, S. F. (2019). Development of paraffin wax as phase change material based latent heat storage in heat exchanger. *Applied Thermal Engineering*, *150*(October 2018), 193–199. https://doi.org/10.1016/j.applthermaleng.2018.12.149

Abedin, A. H., & Rosen, M. A. (2011). *A Critical Review of Thermochemical Energy Storage Systems*. 42–46.

Abhat, A. (1983). *Low temperature latent heat thermal energy storage: Heat storage*. *10*(4), 313–332.

Agarwal, A., & Sarviya, R. M. (2017a). An experimental investigation of shell and tube latent heat storage for solar dryer using paraffin wax as heat storage material. *Engineering Science and Technology, an International Journal*, *4*(1), 779–789. https://doi.org/10.1016/j.matpr.2017.01.086

Agarwal, A., & Sarviya, R. M. (2017b). ScienceDirect Characterization of Commercial Grade Paraffin wax as Latent Heat Storage material for Solar dryers. *Materials Today: Proceedings*, *4*(2), 779–789. https://doi.org/10.1016/j.matpr.2017.01.086

Agyenim, F. (2010). *A review of materials , heat transfer and phase change problem formulation for latent heat thermal energy storage systems (LHTESS). February*. https://doi.org/10.1016/j.rser.2009.10.015

Agyenim, F., Hewitt, N., Eames, P., & Smyth, M. (2010). *A review of materials , heat transfer and phase change problem formulation for latent heat thermal energy storage systems (LHTESS). 14*, 615–628. https://doi.org/10.1016/j.rser.2009.10.015

Akeiber, H. J., Wahid, M. A., Hussen, H. M., & Mohammad, A. T. (2016). A newly composed paraffin encapsulated prototype roof structure for efficient thermal management in hot climate. *Energy*, *104*, 99–106. https://doi.org/10.1016/j.energy.2016.03.131

Ali, A. H., Ibrahim, S. I., Jawad, Q. A., Jawad, R. S., & Chaichan, M. T. (2019). Effect of nanomaterial addition on the thermophysical properties of Iraqi paraffin wax. *Case Studies in Thermal Engineering*, *15*(August), 100537. https://doi.org/10.1016/j.csite.2019.100537

Ali, M. A., Fayaz, Viegas, R. F., Shyam Kumar, M. B., Kannapiran, R. K., & Feroskhan, M. (2019). Enhancement of heat transfer in paraffin wax PCM using nano graphene composite for industrial helmets. *Journal of Energy Storage*, *26*(May), 100982. https://doi.org/10.1016/j.est.2019.100982

Alper, A., & Oguz, O. (2016). The role of renewable energy consumption in economic growth : Evidence from asymmetric causality. *Renewable and Sustainable Energy Reviews*, *60*, 953–959. https://doi.org/10.1016/j.rser.2016.01.123

Alva, G., Liu, L., Huang, X., & Fang, G. (2017). Thermal energy storage materials and systems for solar energy applications. *Renewable and Sustainable Energy Reviews*, *68*(August 2016), 693–706. https://doi.org/10.1016/j.rser.2016.10.021

André, L., Abanades, S., & Flamant, G. (2016). Screening of thermochemical systems based on solid-gas reversible reactions for high temperature solar thermal energy storage. *Renewable and Sustainable Energy Reviews*, *64*, 703–715. https://doi.org/10.1016/j.rser.2016.06.043

Babapoor, A., & Karimi, G. (2015a). *Thermal properties measurement and heat storage analysis of paraf fi nnanoparticles composites phase change material : Comparison and optimization*. *90*. https://doi.org/10.1016/j.applthermaleng.2015.07.083

Babapoor, A., & Karimi, G. (2015b). Thermal properties measurement and heat storage analysis of paraf fi nnanoparticles composites phase change material : Comparison and optimization. *Applied Thermal Engineering*, *90*, 945–951. https://doi.org/10.1016/j.applthermaleng.2015.07.083

Behl, R. K., Chhibar, R. N., Jain, S., Bahl, V. P., & Bassam, N. El. (2010). “Renewable” energy sources and their limitations. In *Topics in Safety, Risk, Reliability and Quality* (Vol. 16). https://doi.org/10.1007/978-90-481-8667-9_4

Belessiotis, G. V., Papadokostaki, K. G., Favvas, E. P., Efthimiadou, E. K., & Karellas, S. (2018). Preparation and investigation of distinct and shape stable paraffin/SiO2 composite PCM nanospheres. *Energy Conversion and Management*, *168*(January), 382–394. https://doi.org/10.1016/j.enconman.2018.04.059

Buckman, J., Bankole, S. A., Zihms, S., Lewis, H., Couples, G., & Corbett, P. W. M. (2017). Quantifying porosity through automated image collection and batch image processing: Case study of three carbonates and an aragonite cemented sandstone. *Geosciences (Switzerland)*, *7*(3). https://doi.org/10.3390/geosciences7030070

Cabeza, L. F., Castell, A., Barreneche, C., De Gracia, A., & Fernández, A. I. (2011). Materials used as PCM in thermal energy storage in buildings: A review. *Renewable and Sustainable Energy Reviews*, *15*(3), 1675–1695. https://doi.org/10.1016/j.rser.2010.11.018

Cabeza, L.F;, ., Castell, A., Barreneche, C., de Gracia, A., & Fernández, A. I. (2011). Materials used as PCM in thermal energy storage in buildings: A review. *Renewable and Sustainable Energy Reviews*, *15*(3), 1675–1695. https://doi.org/10.1016/j.rser.2010.11.018

Cárdenas, B., & León, N. (2013). High temperature latent heat thermal energy storage : Phase change materials , design considerations and performance enhancement techniques. *Renewable and Sustainable Energy Reviews*, *27*, 724–737. https://doi.org/10.1016/j.rser.2013.07.028

Chala, G. T., Sulaiman, S. A., Japper-Jaafar, A., Kamil Wan Abdullah, W. A., & Mior Mokhtar, M. M. (2014a). Gas void formation in statically cooled waxy crude oil. *International Journal of Thermal Sciences*, *86*, 41–47. https://doi.org/10.1016/j.ijthermalsci.2014.06.034

Chala, G. T., Sulaiman, S. A., Japper-Jaafar, A., Kamil Wan Abdullah, W. A., & Mior Mokhtar, M. M. (2014b). Gas void formation in statically cooled waxy crude oil. *International Journal of Thermal Sciences*, *86*, 41–47. https://doi.org/10.1016/j.ijthermalsci.2014.06.034

Chala, G. T., Sulaiman, S. A., Japper-Jaafar, A., & Wan Abdullah, W. A. K. (2015a). Impacts of Cooling Rates on Voids in Waxy Crude Oil under Quiescent Cooling Mode. *Applied Mechanics and Materials*, *799–800*(October), 62–66. https://doi.org/10.4028/www.scientific.net/amm.799-800.62

Chala, G. T., Sulaiman, S. A., Japper-Jaafar, A., & Wan Abdullah, W. A. K. (2015b). Impacts of Cooling Rates on Voids in Waxy Crude Oil under Quiescent Cooling Mode. *Applied Mechanics and Materials*, *799–800*(October), 62–66. https://doi.org/10.4028/www.scientific.net/amm.799-800.62

Chow, L. C. (1992). *Void Formation in Radial Solidification of Cylinders*. *114*(February 1992).

Colla, A. L., Fedele, L., Mancin, S., Danza, L., Colla, L., Fedele, L., Mancin, S., Danza, L., & Manca, O. (2016). Nano-PCMs for enhanced energy storage and passive cooling applications. *Applied Thermal Engineering*. https://doi.org/10.1016/j.applthermaleng.2016.03.161

Colla, L., Fedele, L., Mancin, S., Danza, L., & Manca, O. (2017). Nano-PCMs for enhanced energy storage and passive cooling applications. *Applied Thermal Engineering*, *110*, 584–589. https://doi.org/10.1016/j.applthermaleng.2016.03.161

Dheep, G. R., & Sreekumar, A. (2018). Investigation on thermal reliability and corrosion characteristics of glutaric acid as an organic phase change material for solar thermal energy storage applications. *Applied Thermal Engineering*, *129*, 1189–1196. https://doi.org/10.1016/j.applthermaleng.2017.10.133

Diaz, P. M. (2016). *Analysis and Comparison of different types of Thermal Energy Storage Systems : A Review Analysis and Comparison of different types of Thermal Energy Storage Systems : A Review*. *February*. https://doi.org/10.18831/james.in/2016011004

Drahansky, M., Paridah, M. ., Moradbak, A., Mohamed, A. ., Owolabi, F. abdulwahab taiwo, Asniza, M., & Abdul Khalid, S. H. . (2016). We are IntechOpen , the world ' s leading publisher of Open Access books Built by scientists , for scientists TOP 1 %. *Intech*, *i*(tourism), 13. https://doi.org/http://dx.doi.org/10.5772/57353

Economic Planning Unit. (2017). *Malaysia Sustainable Development Goals -Voluntary National Review 2017*. https://sustainabledevelopment.un.org/content/documents/15881Malaysia.pdf

Fan, L. W., Fang, X., Wang, X., Zeng, Y., Xiao, Y. Q., Yu, Z. T., Xu, X., Hu, Y. C., & Cen, K. F. (2013). Effects of various carbon nanofillers on the thermal conductivity and energy storage properties of paraffin-based nanocomposite phase change materials. *Applied Energy*, *110*, 163–172. https://doi.org/10.1016/j.apenergy.2013.04.043

Fan, Y. F., Zhang, X. X., Wang, X. C., Li, J., & Zhu, Q. B. (2004). *Super-cooling prevention of microencapsulated phase change material*. *413*(November 2003), 1–6. https://doi.org/10.1016/j.tca.2003.11.006

Farid, M. M., Khudhair, A. M., Ali, S., & Razack, K. (2004). *A review on phase change energy storage : materials and applications*. *45*, 1597–1615. https://doi.org/10.1016/j.enconman.2003.09.015

Fauzi, H., Metselaar, H. S. C., Mahlia, T. M. I., Silakhori, M., & Ong, H. C. (2015). Thermal characteristic reliability of fatty acid binary mixtures as phase change materials (PCMs) for thermal energy storage applications. *Applied Thermal Engineering*, *80*, 127–131. https://doi.org/10.1016/j.applthermaleng.2015.01.047

Feczkó, T., Trif, L., & Horák, D. (2016). *Latent heat storage by silica-coated polymer beads containing organic phase change materials*. http://real.mtak.hu/44973/1/Feczko_et_al_2016_silica_coated_polymer_beads_REAL_u.pdf

Goia, F., & Boccaleri, E. (2016a). Physical-chemical properties evolution and thermal properties reliability of a paraffin wax under solar radiation exposure in a real-scale PCM window system. *Energy & Buildings*. https://doi.org/10.1016/j.enbuild.2016.03.007

Goia, F., & Boccaleri, E. (2016b). Physical – chemical properties evolution and thermal properties reliability of a paraffin wax under solar radiation exposure in a real-scale PCM window system. *Energy & Buildings*, *119*, 41–50. https://doi.org/10.1016/j.enbuild.2016.03.007

Guillot, S., Faik, A., Rakhmatullin, A., Lambert, J., Veron, E., Echegut, P., Bessada, C., Calvet, N., & Py, X. (2012). *Corrosion effects between molten salts and thermal storage material for concentrated solar power plants*. *94*, 174–181. https://doi.org/10.1016/j.apenergy.2011.12.057

Gulfam, R., Zhang, P., & Meng, Z. (2019). *Advanced thermal systems driven by paraffin-based phase change materials-A review*. https://doi.org/10.1016/j.apenergy.2019.01.114

Gunjo, D. G., Jena, S. R., Mahanta, P., & Robi, P. S. (2018). Melting enhancement of a latent heat storage with dispersed Cu, CuO and Al2O3 nanoparticles for solar thermal application. *Renewable Energy*, *121*, 652–665. https://doi.org/10.1016/j.renene.2018.01.013

Haines, T. J., Neilson, J. E., Healy, D., Michie, E. A. H., & Aplin, A. C. (2015). The impact of carbonate texture on the quantification of total porosity by image analysis. *Computers and Geosciences*, *85*, 112–125. https://doi.org/10.1016/j.cageo.2015.08.016

Hale, D. V, Hoover, M. J., & Neill, M. J. O. (1971). *PHASE CHANGE MATERIALS HANDBOOK by NASA Contractor Report NASA CR-51363*. 232.

Hardy, S. C. (1979). The motion of bubbles in a vertical temperature gradient. *Journal of Colloid And Interface Science*, *69*(1), 157–162. https://doi.org/10.1016/0021-9797(79)90090-0

He, Z., Wang, X., Du, X., Amjad, M., Yang, L., & Xu, C. (2019). Experiments on comparative performance of water thermocline storage tank with and without encapsulated paraffin wax packed bed. *Applied Thermal Engineering*, *147*(July 2018), 188–197. https://doi.org/10.1016/j.applthermaleng.2018.10.051

Himran, S., Suwono, A., & Mansoori, G. A. (1994). Characterization of Alkanes and Paraffin Waxes for Application as Phase Change Energy Storage Medium. *Energy Sources*, *16*(1), 117–128. https://doi.org/10.1080/00908319408909065

Hosseini, M. J., Rahimi, M., & Bahrampoury, R. (2014). Experimental and computational evolution of a shell and tube heat exchanger as a PCM thermal storage system ☆. *International Communications in Heat and Mass Transfer*, *50*, 128–136. https://doi.org/10.1016/j.icheatmasstransfer.2013.11.008

Jiang, X., Luo, R., Peng, F., Fang, Y., Akiyama, T., & Wang, S. (2015). Synthesis, characterization and thermal properties of paraffin microcapsules modified with nano-Al2O3. *Applied Energy*, *137*, 731–737. https://doi.org/10.1016/j.apenergy.2014.09.028

Jin, Y., Wan, Q., & Ding, Y. (2015). PCMs heat transfer performance enhancement with expanded graphite and its thermal stability. *Procedia Engineering*, *102*, 1877–1884. https://doi.org/10.1016/j.proeng.2015.01.326

Kabbara, M., Groulx, D., & Joseph, A. (2016). Experimental investigations of a latent heat energy storage unit using finned tubes. *Applied Thermal Engineering*, *101*, 601–611. https://doi.org/10.1016/j.applthermaleng.2015.12.080

Karaipekli, A., & Sari, A. (2010). Preparation, thermal properties and thermal reliability of eutectic mixtures of fatty acids/expanded vermiculite as novel form-stable composites for energy storage. *Journal of Industrial and Engineering Chemistry*, *16*(5), 767–773. https://doi.org/10.1016/j.jiec.2010.07.003

Karaman, S., Karaipekli, A., Sarı, A., & Bic, A. (2011). *Solar Energy Materials & Solar Cells Polyethylene glycol (PEG)/ diatomite composite as a novel form-stable phase change material for thermal energy storage*. *95*, 1647–1653. https://doi.org/10.1016/j.solmat.2011.01.022

Karthik, M., Faik, A., & D'Aguanno, B. (2017a). Graphite foam as interpenetrating matrices for phase change paraffin wax: A candidate composite for low temperature thermal energy storage. *Solar Energy Materials and Solar Cells*, *172*(April), 324–334. https://doi.org/10.1016/j.solmat.2017.08.004

Karthik, M., Faik, A., & D'Aguanno, B. (2017b). Graphite foam as interpenetrating matrices for phase change paraffin wax: A candidate composite for low temperature thermal energy storage. *Solar Energy Materials and Solar Cells*, *172*(August), 324–334. https://doi.org/10.1016/j.solmat.2017.08.004

Kenisarin, M., Mahkamov, K., Kahwash, F., & Makhkamova, I. (2019). Enhancing thermal conductivity of paraffin wax 53–57 °C using expanded graphite. *Solar Energy Materials and Solar Cells*, *200*(June), 110026. https://doi.org/10.1016/j.solmat.2019.110026

Kenisarin, Murat, & Mahkamov, K. (2016). Solar Energy Materials & Solar Cells Salt hydrates as latent heat storage materials : Thermophysical properties and costs. *Solar Energy Materials and Solar Cells*, *145*, 255–286. https://doi.org/10.1016/j.solmat.2015.10.029

Khan, Z., & Ahmad Khan, Z. (2018). Experimental and numerical investigations of nano-additives enhanced paraffin in a shell-and-tube heat exchanger: A comparative study. *Applied Thermal Engineering*, *143*(April), 777–790. https://doi.org/10.1016/j.applthermaleng.2018.07.141

Khan, Z., Khan, Z., & Ghafoor, A. (2016). A review of performance enhancement of PCM based latent heat storage system within the context of materials , thermal stability and compatibility. *Energy Conversion and Management*, *115*, 132–158. https://doi.org/10.1016/j.enconman.2016.02.045

Kibria, M. A., Anisur, M. R., Mahfuz, M. H., Saidur, R., & Metselaar, I. H. S. C. (2015). A review on thermophysical properties of nanoparticle dispersed phase change materials. *Energy Conversion and Management*, *95*, 69–89. https://doi.org/10.1016/j.enconman.2015.02.028

Kim, S., Moon, H., & Kim, J. (2015). Thermal characterizations of the paraffin wax/low density polyethylene blends as a solid fuel. *Thermochimica Acta*, *613*, 9–16. https://doi.org/10.1016/j.tca.2015.05.016

Kukreja. (2009). *Conservation Energy Future*. Renewable Energy. http://www.conserve-energy-future.com

Kumar, M. S., & Krishna, V. M. (2019). Experimental investigation on performance of hybrid PCM's on addition of nano particles in thermal energy storage. *Materials Today: Proceedings*, *17*, 271–276. https://doi.org/10.1016/j.matpr.2019.06.430

Kurnia, J. C., Sasmito, A. P., & Ping, S. I. (2017). Investigation of Heat Transfer on a Rotating Latent Heat Energy Storage. *Energy Procedia*, *105*, 4173–4178. https://doi.org/10.1016/j.egypro.2017.03.887

Lane, G. A. (1980). Low temperature heat storage with phase change materials. *International Journal of Ambient Energy*, *1*(3), 155–168. https://doi.org/10.1080/01430750.1980.9675731

Li, G. (2015). Energy and exergy performance assessments for latent heat thermal energy storage systems. *Renewable and Sustainable Energy Reviews*, *51*, 926–954. https://doi.org/10.1016/j.rser.2015.06.052

Li, G. (2016). Sensible heat thermal storage energy and exergy performance evaluations. *Renewable and Sustainable Energy Reviews*, *53*, 897–923. https://doi.org/10.1016/j.rser.2015.09.006

Li, M. (2013). A nano-graphite / paraffin phase change material with high thermal conductivity. *APPLIED ENERGY*, *106*, 25–30. https://doi.org/10.1016/j.apenergy.2013.01.031

Liang, W., Wang, L., Zhu, H., Pan, Y., Zhu, Z., Sun, H., Ma, C., & Li, A. (2018). Enhanced thermal conductivity of phase change material nanocomposites based on MnO 2 nanowires and nanotubes for energy storage. *Solar Energy Materials and Solar Cells*, *180*(September 2017), 158–167. https://doi.org/10.1016/j.solmat.2018.03.005

Likhachev, V., & Vladimir Likhachev. (2012). *Energy revolution XXX1 century*. Energy Revolution. XXI Century. Reset. https://russiancouncil.ru/en/analytics-and-comments/analytics/energy-revolution-xxi-century-reset/

Lin, S. C., & Al-kayiem, H. H. (2016). ScienceDirect Evaluation of copper nanoparticles – Paraffin wax compositions for solar thermal energy storage. *Solar Energy*, *132*, 267–278. https://doi.org/10.1016/j.solener.2016.03.004

Lin, Y., Jia, Y., Alva, G., & Fang, G. (2018). Review on thermal conductivity enhancement , thermal properties and applications of phase change materials in thermal energy storage. *Renewable and Sustainable Energy Reviews*, *82*(October 2017), 2730–2742. https://doi.org/10.1016/j.rser.2017.10.002

Liu, B., Yang, J., Zhang, Z., Yang, J., & Li, D. (2018). A phase change microactuator based on paraffin wax/expanded graphite/nickel particle composite with induction heating. *Sensors and Actuators, A: Physical*, *275*, 129–136. https://doi.org/10.1016/j.sna.2018.04.006

Liu, K., Ostadhassan, M., Gentzis, T., & Fowler, H. (2019). Image analysis of the pore structures: An intensive study for Middle Bakken. *Journal of Natural Gas Science and Engineering*, *61*(August 2018), 32–45. https://doi.org/10.1016/j.jngse.2018.11.008

Liu, Lifang, Chen, J., Qu, Y., Xu, T., Wu, H., Huang, G., Zhou, X., & Yang, L. (2019). A foamed cement blocks with paraffin/expanded graphite composite phase change solar thermal absorption material. *Solar Energy Materials and Solar Cells*, *200*(June), 110038. https://doi.org/10.1016/j.solmat.2019.110038

Liu, Lifang, Qu, Y., Xu, T., Chen, J., Wu, H., Huang, G., Zhou, X., & Yang, L. (2019). Experimental study on preparation of a novel foamed cement with paraffin/ expanded graphite composite phase change thermal energy storage material. *Energy Procedia*, *158*, 4799–4804. https://doi.org/10.1016/j.egypro.2019.01.717

Liu, Lingkun, Su, D., Tang, Y., & Fang, G. (2016). *Thermal conductivity enhancement of phase change materials for thermal energy storage : A review*. *62*, 305–317. https://doi.org/10.1016/j.rser.2016.04.057

Liu, M., Gomez, J. C., Turchi, C. S., Tay, N. H. S., Saman, W., & Bruno, F. (2015). Solar Energy Materials & Solar Cells Determination of thermo-physical properties and stability testing of high-temperature phase-change materials for CSP applications. *Solar Energy Materials and Solar Cells*, *139*, 81–87. https://doi.org/10.1016/j.solmat.2015.03.014

Liu, M., Saman, W., & Bruno, F. (2012). Review on storage materials and thermal performance enhancement techniques for high temperature phase change thermal storage systems. *Renewable and Sustainable Energy Reviews*, *16*(4), 2118–2132. https://doi.org/10.1016/j.rser.2012.01.020

Long, Z., & Jiankai, D. (2017). Experimental study on the thermal stability of a paraffin mixture with up to 10 , 000 thermal cycles. *Thermal Science and Engineering Progress*, *1*, 78–87. https://doi.org/10.1016/j.tsep.2017.02.005

Lorsch, H. G., Kauffman, K. W., & Denton, J. C. (1975). Thermal energy storage for solar heating and off-peak air conditioning. *Energy Conversion*, *15*(1–2), 1–8. https://doi.org/10.1016/0013-7480(75)90002-9

Mandal, S. K., Kumar, S., Singh, P. K., Mishra, S. K., Bishwakarma, H., Choudhry, N. P., Nayak, R. K., & Das, A. K. (2019). Performance investigation of CuO-paraffin wax nanocomposite in solar water heater during night. *Thermochimica Acta*, *671*(July 2018), 36–42. https://doi.org/10.1016/j.tca.2018.11.003

Mengjie, S., Man, W. A. N., Swapnil, D., Dongmei, P. A. N., & Ning, M. A. O. (2017). ScienceDirect ScienceDirect Thermal stability of organic binary PCMs for energy storage Assessing feasibility of using the temperature function for a long-term district heat demand forecast. *Energy Procedia*, *142*, 3287–3294. https://doi.org/10.1016/j.egypro.2017.12.459

Mohamed, N. H., Soliman, F. S., El, H., & Moustfa, Y. M. (2017). Thermal conductivity enhancement of treated petroleum waxes , as phase change material , by α nano alumina : Energy storage. *Renewable and Sustainable Energy Reviews*, *70*(November 2016), 1052–1058. https://doi.org/10.1016/j.rser.2016.12.009

Mohamed, S. A., Al-sulaiman, F. A., Ibrahim, N. I., Zahir, H., Al-ahmed, A., Saidur, R., Y, B. S., & Sahin, A. Z. (2016). *A review on current status and challenges of inorganic phase change materials for thermal energy storage systems*. *February*. https://doi.org/10.1016/j.rser.2016.12.012

Morcos, V. H. (1990). *Investigation of a Latent Heat Thermal*. *7*(2), 197–202.

Mossaz, S., Gruss, J. A., Ferrouillat, S., Skrzypski, J., Getto, D., Poncelet, O., & Berne, P. (2015). Experimental study on the influence of nanoparticle PCM slurry for high temperature on convective heat transfer and energetic performance in a circular tube under imposed heat flux. *Applied Thermal Engineering*, *81*, 388–398. https://doi.org/10.1016/j.applthermaleng.2015.01.028

Nikishkov, Y., Airoldi, L., & Makeev, A. (2013). Measurement of voids in composites by X-ray Computed Tomography. *Composites Science and Technology*, *89*, 89–97. https://doi.org/10.1016/j.compscitech.2013.09.019

Nourani, M., Hamdami, N., Keramat, J., & Moheb, A. (2016). Thermal behavior of paraf fi n-nano-Al 2 O 3 stabilized by sodium stearoyl lactylate as a stable phase change material with high thermal conductivity. *Renewable Energy*, *88*, 474–482. https://doi.org/10.1016/j.renene.2015.11.043

Ojike, O., & Okonkwo, W. I. (2019). Study of a passive solar air heater using palm oil and paraffin as storage media. *Case Studies in Thermal Engineering*, *14*(April), 100454. https://doi.org/10.1016/j.csite.2019.100454

Owolabi, A. L., Al-kayiem, H. H., & Baheta, A. T. (2016). Nanoadditives induced enhancement of the thermal properties of paraffin-based nanocomposites for thermal energy storage. *Solar Energy*, *135*, 644–653. https://doi.org/10.1016/j.solener.2016.06.008

Padmanabhan.P.V, & Murthy Krishna.M.V. (1986). Outward phase change in a cylindrical annulus with axial fins on the inner tube. *International Journal of Heat and Mass Transfer*, *29*(12), 1855–1868. http://ac.els-cdn.com/0017931086900049/1-s2.0-0017931086900049-main.pdf?_tid=d7e59684-155b-11e7-94f0-00000aab0f26&acdnat=1490887166_3fb48ebf82018a68e3b5c474483f38c5

Pal, Y., & Ravikumar, V. (2019). Mechanical Characterization of Paraffin-Based Hybrid Rocket Fuels. *Materials Today: Proceedings*, *16*, 939–948. https://doi.org/10.1016/j.matpr.2019.05.180

Pereira, J., & Eames, P. (2016). Thermal energy storage for low and medium temperature applications using phase change materials – A review. *Applied Energy*, *177*, 227–238. https://doi.org/10.1016/j.apenergy.2016.05.097

Pielichowska, K., & Pielichowski, K. (2014). Progress in Materials Science. *Journal of Progression in Material Science*, *65*, 67–123. https://doi.org/10.1016/j.pmatsci.2014.03.005

Prabhu, B., & ValanArasu, A. (2020). Stability analysis of TiO2–Ag nanocomposite particles dispersed paraffin wax as energy storage material for solar thermal systems. *Renewable Energy*, *152*, 358–367. https://doi.org/10.1016/j.renene.2020.01.043

Putra, N., Hakim, I. I., Erwin, F. P., Abdullah, N. A., Ariantara, B., Amin, M., Mahlia, T. M. I., & Kusrini, E. (2019). Development of a novel thermoelectric module based device for thermal stability measurement of phase change materials. *Journal of Energy Storage*, *22*(December 2018), 331–335. https://doi.org/10.1016/j.est.2019.02.030

Rabienataj, A. A., Jourabian, M., & Farhadi, M. (2016). Melting and solidification of PCM enhanced by radial conductive fins and nanoparticles in cylindrical annulus. *Energy Conversion and Management*, *118*, 253–263. https://doi.org/10.1016/j.enconman.2016.04.016

Rathod, M. K., & Banerjee, J. (2013). Thermal stability of phase change materials used in latent heat energy storage systems : A review. *Renewable and Sustainable Energy Reviews*, *18*, 246–258. https://doi.org/10.1016/j.rser.2012.10.022

Reinhard, S., Verhagen, J., Wolters, W., & Ruben, R. (2017). Water-food-energy nexus. *Wageningen Economic Research*. https://library.wur.nl/WebQuery/wurpubs/fulltext/424551

Reyes, A., Henríquez-Vargas, L., Aravena, R., & Sepúlveda, F. (2015). Experimental analysis, modeling and simulation of a solar energy accumulator with paraffin wax as PCM. *Energy Conversion and Management*, *105*, 189–196. https://doi.org/10.1016/j.enconman.2015.07.068

Reyes, A., Henríquez-Vargas, L., Vásquez, J., Pailahueque, N., & Aguilar, G. (2020). Analysis of a laboratory scale thermal energy accumulator using two-phases heterogeneous paraffin wax-water mixtures. *Renewable Energy*, *145*, 41–51. https://doi.org/10.1016/j.renene.2019.06.007

Reyes, Alejandro, Negrete, D., Mahn, A., & Sepúlveda, F. (2014). Design and evaluation of a heat exchanger that uses paraffin wax and recycled materials as solar energy accumulator. *Energy Conversion and Management*, *88*, 391–398. https://doi.org/10.1016/j.enconman.2014.08.032

Sahan, N., & Paksoy, H. O. (2014). Thermal enhancement of paraffin as a phase change material with nanomagnetite. *Solar Energy Materials and Solar Cells*, *126*, 56–61. https://doi.org/10.1016/j.solmat.2014.03.018

Said, A., Salah, A., & Abdel Fattah, G. (2018). Thermo-optic switching properties of paraffin-wax hosting carbon fillers. *Journal of Energy Storage*, *19*(February), 260–271. https://doi.org/10.1016/j.est.2018.07.016

Salomoni, V. A., Majorana, C. E., Giannuzzi, G. M., Miliozzi, A., Di, R., Girardi, F., Mele, D., & Lucentini, M. (2014). ScienceDirect Thermal storage of sensible heat using concrete modules in solar power plants. *Solar Energy*, *103*, 303–315. https://doi.org/10.1016/j.solener.2014.02.022

Sami, S., & Etesami, N. (2017). Improving thermal characteristics and stability of phase change material containing TiO 2 nanoparticles after thermal cycles for energy storage. *Applied Thermal Engineering*, *124*, 346–352. https://doi.org/10.1016/j.applthermaleng.2017.06.023

Sari, A., & Karaipekli, A. (2008a). Preparation, thermal properties and thermal reliability of capric acid/expanded perlite composite for thermal energy storage. *Materials Chemistry and Physics*, *109*(2–3), 459–464. https://doi.org/10.1016/j.matchemphys.2007.12.016

Sari, A., & Karaipekli, A. (2008b). Preparation and thermal properties of capric acid/palmitic acid eutectic mixture as a phase change energy storage material. *Materials Letters*, *62*(6–7), 903–906. https://doi.org/10.1016/j.matlet.2007.07.025

Sari, A., & Karaipekli, A. (2009). Preparation, thermal properties and thermal reliability of palmitic acid/expanded graphite composite as form-stable PCM for thermal energy storage. *Solar Energy Materials and Solar Cells*, *93*(5), 571–576. https://doi.org/10.1016/j.solmat.2008.11.057

Sari, A., Karaipekli, A., & Alkan, C. (2009). Preparation, characterization and thermal properties of lauric acid/expanded perlite as novel form-stable composite phase change material. *Chemical Engineering Journal*, *155*(3), 899–904. https://doi.org/10.1016/j.cej.2009.09.005

Sarier, N., & Onder, E. (2012). Thermochimica Acta Organic phase change materials and their textile applications : An overview. *Thermochimica Acta*, *540*, 7–60. https://doi.org/10.1016/j.tca.2012.04.013

Schneider, C. A., Rasband, W. S., & Eliceiri, K. W. (2012). NIH Image to ImageJ: 25 years of image analysis. *Nature Methods*, *9*(7), 671–675. https://doi.org/10.1038/nmeth.2089

Senthil, R., Sundaram, P., & Kumar, M. (2018). Experimental investigation on packed bed thermal energy storage using paraffin wax for concentrated solar collector. *Materials Today: Proceedings*, *5*(2), 8916–8922. https://doi.org/10.1016/j.matpr.2017.12.326

Shahan. (2014). *Clean Technica*. Solar Power. https://cleantechnica.com/solar-power/

Shaikh, S., & Lafdi, K. (2010). C/C composite, carbon nanotube and paraffin wax hybrid systems for the thermal control of pulsed power in electronics. *Carbon*, *48*(3), 813–824. https://doi.org/10.1016/j.carbon.2009.10.034

Sharma, A., Sharma, S. D., & Buddhi, D. (2002). *Accelerated thermal cycle test of acetamide , stearic acid and paraffin wax for solar thermal latent heat storage applications*. *43*, 1923–1930.

Sharma, A., Tyagi, V. V, Chen, C. R., & Buddhi, D. (2009). *Review on thermal energy storage with phase change materials and applications*. *13*, 318–345. https://doi.org/10.1016/j.rser.2007.10.005

Sharma, R. K., Ganesan, P., Tyagi, V. V., & Mahlia, T. M. I. (2016). Accelerated thermal cycle and chemical stability testing of polyethylene glycol (PEG) 6000 for solar thermal energy storage. *Solar Energy Materials and Solar Cells*, *147*, 235–239. https://doi.org/10.1016/j.solmat.2015.12.023

Sharma, R.K, Ganesan, P., Tyagi, V. V, Metselaar, H. S. C., & Sandaran, S. C. (2015). Developments in organic solid – liquid phase change materials and their applications in thermal energy storage. *Energy Conversion and Management*, *95*, 193–228. https://doi.org/10.1016/j.enconman.2015.01.084

Sharma, Ravi Kumar. (2016). *Reliability Testing and Heat Transfer Enhancement of Organic Phase Change Materials Ravi Kumar Sharma a Thesis Submitted in Fulfillment of the Requirements for the Award of the Degree of Doctor of Philosophy Faculty of Engineering University of Malaya*.

Shirai, H., Ikeda, M., & Tanno, K. (2011). Factors affecting the density and specific surface area (Blaine Value) of fly ash from pulverized coal combustion. *Energy and Fuels*, *25*(12), 5700–5706. https://doi.org/10.1021/ef201071e

Shukla, A., Buddhi, D., & Sawhney, R. L. (2008). *Thermal cycling test of few selected inorganic and organic phase change materials*. *33*, 2606–2614. https://doi.org/10.1016/j.renene.2008.02.026

Silakhori, M., Naghavi, M. S., Simon, H., Metselaar, C., Meurah, T., Mahlia, I., Fauzi, H., & Mehrali, M. (2013). *Accelerated Thermal Cycling Test of Microencapsulated Paraffin Wax/Polyaniline Made by Simple Preparation Method for Solar Thermal Energy Storage*. 1608–1620. https://doi.org/10.3390/ma6051608

Sulfredge, C. D., Chow, L. C., & Tagavi, K. A. (1992). Solidification void formation in tubes: Role of liquid shrinkage and bubble nucleation. *Experimental Heat Transfer*, *5*(3), 147–160. https://doi.org/10.1080/08916159208946438

Sulfredge, C. D., Chow, L. C., & Tagavi, K. A. (1993). Void formation in unidirectional freezing from above. *Experimental Heat Transfer*, *6*(1), 1–16. https://doi.org/10.1080/08916159208945366

Sulfredge, C.D;, Chow, L. C., & Tagavi, K. A. (1993). Void formation in unidirectional freezing from above. *Experimental Heat Transfer*, *6*(1), 1–16. https://doi.org/10.1080/08916159208945366

Sulfredge, C.D;, CL.Chow;, & KA.Tagavi. (1990). *Experimental Heat Transfer : A Journal of Thermal Energy Generation , Transport , Storage , and Conversion HEAT TRANSFER CHARACTERISTICS OF WATER FLOWING THROUGH MICROCHANNELS*. *November 2013*, 37–41. https://doi.org/10.1080/08916159408946485

SunilRaj, B. A., & Eswaramoorthy, M. (2019). Experimental study on hybrid natural circulation type solar air heater with paraffin wax based thermal storage. *Materials Today: Proceedings*, *xxxx*. https://doi.org/10.1016/j.matpr.2019.06.381

Tagavi, K., Chow, L. C., & Solaiappan, O. (1990). Void formation in unidirectional solidification. *Experimental Heat Transfer*, *3*(3), 239–255. https://doi.org/10.1080/08916159008946388

Tang, Y., Alva, G., Huang, X., Su, D., Liu, L., & Fang, G. (2016). *Thermal properties and morphologies of MA – SA eutectics / CNTs as composite PCMs in thermal energy storage*. *127*, 603–610. https://doi.org/10.1016/j.enbuild.2016.06.031

Tiskatine, R., Eddemani, A., Gourdo, L., Abnay, B., Ihlal, A., Aharoune, A., & Bouirden, L. (2016). Experimental evaluation of thermo-mechanical performances of candidate rocks for use in high temperature thermal storage. *Applied Energy*, *171*, 243–255. https://doi.org/10.1016/j.apenergy.2016.03.061

Veale, K., Adali, S., Pitot, J., & Bemont, C. (2018). The structural properties of paraffin wax based hybrid rocket fuels with aluminium particles. *Acta Astronautica*, *151*(July), 864–873. https://doi.org/10.1016/j.actaastro.2018.07.042

Velraj, R., Seeniraj, R. V., Hafner, B., Faber, C., & Schwarzer, K. (1999). Heat transfer enhancement in a latent heat storage system. *Solar Energy*, *65*(3), 171–180. https://doi.org/10.1016/S0038-092X(98)00128-5

Wang, C., Lin, T., Li, N., & Zheng, H. (2016). Heat transfer enhancement of phase change composite material: Copper foam/paraffin. *Renewable Energy*, *96*, 960–965. https://doi.org/10.1016/j.renene.2016.04.039

Wang, J., Xie, H., Guo, Z., Guan, L., & Li, Y. (2014). Improved thermal properties of paraffin wax by the addition of TiO2 nanoparticles. *Applied Thermal Engineering*, *73*(2), 1541–1547. https://doi.org/10.1016/j.applthermaleng.2014.05.078

Wang, Z., Qiu, F., Yang, W., & Zhao, X. (2015). Applications of solar water heating system with phase change material. *Renewable and Sustainable Energy Reviews*, *52*, 645–652. https://doi.org/10.1016/j.rser.2015.07.184

Wen, R., Zhang, X., Huang, Z., Fang, M., Liu, Y., Wu, X., Min, X., Gao, W., & Huang, S. (2018). Preparation and thermal properties of fatty acid/diatomite form-stable composite phase change material for thermal energy storage. *Solar Energy Materials and Solar Cells*, *178*(January), 273–279. https://doi.org/10.1016/j.solmat.2018.01.032

World Energy Council. (2018). World Energy Issues Monitor: Perspectives on The Grand Energy Transition. In *World Energy Council*. https://doi.org/10.1109/ICECE.2006.355300

Xiang, J., & Drzal, L. T. (2011). Investigation of exfoliated graphite nanoplatelets (xGnP) in improving thermal conductivity of paraffin wax-based phase change material. *Solar Energy Materials and Solar Cells*, *95*(7), 1811–1818. https://doi.org/10.1016/j.solmat.2011.01.048

Xu, B., Ma, H., Lu, Z., & Li, Z. (2015). Paraffin/expanded vermiculite composite phase change material as aggregate for developing lightweight thermal energy storage cement-based composites. *Applied Energy*, *160*, 358–367. https://doi.org/10.1016/j.apenergy.2015.09.069

Yang, L., Cao, X., Zhang, N., Xiang, B., Zhang, Z., & Qian, B. (2019). Thermal reliability of typical fatty acids as phase change materials based on 10,000 accelerated thermal cycles. *Sustainable Cities and Society*, *46*(April 2018), 101380. https://doi.org/10.1016/j.scs.2018.12.008

Yu, S., Jeong, S., Chung, O., & Kim, S. (2014). Solar Energy Materials & Solar Cells Bio-based PCM / carbon nanomaterials composites with enhanced thermal conductivity. *Solar Energy Materials and Solar Cells*, *120*, 549–554. https://doi.org/10.1016/j.solmat.2013.09.037

Zalba, B., Marín, J. M., Cabeza, L. F., & Mehling, H. (2003). Review on thermal energy storage with phase change: materials, heat transfer analysis and applications. *Applied Thermal Engineering*, *23*(3), 251–283. https://doi.org/10.1016/S1359-4311(02)00192-8

Zeng, J., Xuan, Y., & Duan, H. (2016). Solar Energy Materials & Solar Cells Tin-silica-silver composite nanoparticles for medium-to-high temperature volumetric absorption solar collectors. *Solar Energy Materials and Solar Cells*, *157*, 930–936. https://doi.org/10.1016/j.solmat.2016.08.012

Zhang, K., Han, B., & Yu, X. (2012). Electrically conductive carbon nanofiber/paraffin wax composites for electric thermal storage. *Energy Conversion and Management*, *64*, 62–67. https://doi.org/10.1016/j.enconman.2012.06.021

Zhang, L., & Dong, J. (2017a). Experimental study on the thermal stability of a paraffin mixture with up to 10,000 thermal cycles. *Thermal Science and Engineering Progress*, *1*, 78–87. https://doi.org/10.1016/j.tsep.2017.02.005

Zhang, L., & Dong, J. (2017b). Experimental study on the thermal stability of a paraffin mixture with up to 10,000 thermal cycles. *Thermal Science and Engineering Progress*, *1*, 78–87. https://doi.org/10.1016/j.tsep.2017.02.005

Zhang, Q., Wang, H., Ling, Z., Fang, X., & Zhang, Z. (2015). RT100/expand graphite composite phase change material with excellent structure stability, photo-thermal performance and good thermal reliability. *Solar Energy Materials and Solar Cells*, *140*, 158–166. https://doi.org/10.1016/j.solmat.2015.04.008

Zoundi, Z. (2016). CO2 emissions , renewable energy and the Environmental Kuznets Curve , a panel cointegration approach. *Renewable and Sustainable Energy Reviews*, *February*, 0–1. https://doi.org/10.1016/j.rser.2016.10.018